NOTICE

AVIS

The quality of this microform is heavily dependent upon the quality of the original thesis submitted for microfilming. Every effort has been made to ensure the highest quality of reproduction possible.

If pages are missing, contact the university which granted the degree.

Some pages may have indistinct print especially if the original pages were typed with a poor typewriter ribbon or if the university sent us an inferior photocopy.

Previously copyrighted materials (journal articles, published tests, etc.) are not filmed.

Reproduction in full or in part of this microform is governed by the Canadian Copyright Act. R.S.C. 1970, c. C-30.

La qualité de cette microforme dépend grandement de la qualité de la thèse soumise au microfilmage. Nous avons tout fait pour assurer une qualité supérieure de reproduction.

S'il manque des pages, veuillez communiquer avec l'université qui a conféré le grade.

La qualité d'impression de certaines pages peut laisser à désirer, surtout si les pages originales ont été dactylographiées à l'aide d'un ruban usé ou si l'université nous a fait parvenir une photocopie de qualité inférieure.

Les documents qui font déjà l'objet d'un droit d'auteur (articles de revue, tests publiés, etc.) ne sont pas microfilmés.

La reproduction, même partielle, de cette microforme est soumise à la Loi canadienne sur le droit d'auteur, SRC 1970, c. C-30.

Canada

INTERCALATION AND DISTRIBUTION OF SILVER IN THE TRANSITION METAL DICHALCOGENIDE 2T-TiS$_2$

by

Dayakanthi Kaluarachchi

B.Sc. (Hon.) University of Sri Lanka, Vidyodaya Campus, 1977

M.Sc. Simon Fraser University, 1983

THESIS SUBMITTED IN PARTIAL FULFILLMENT OF

THE REQUIREMENTS FOR THE DEGREE OF

DOCTOR OF PHILOSOPHY

in the Department

of

Physics

© Dayakanthi Kaluarachchi 1987

SIMON FRASER UNIVERSITY

July, 1987

APPROVAL

Name: Dayakanthi Kaluarachchi

Degree: Doctor of Philosophy

Title of Thesis: Intercalation and distribution of silver in the transition metal dichalcogenide 1T-TiS$_2$

Examining Committee:

    Chairperson: Dr. D.H. Boal

Dr. Robert F. Frindt
Senior Supervisor

Dr. George Kirczenow

Dr. Albert E. Curzon

Dr. Bretislav Heinrich

Dr. Manfred H. Jericho
External Examiner
Professor
Department of Physics
University of Dalhousie, Halifax. Nova Scotia.

Date Approved: <u>July 27, 1987</u>

PARTIAL COPYRIGHT LICENSE

I hereby grant to Simon Fraser University the right to lend my thesis, project or extended essay (the title of which is shown below) to users of the Simon Fraser University Library, and to make partial or single copies only for such users or in response to a request from the library of any other university, or other educational institution, on its own behalf or for one of its users. I further agree that permission for multiple copying of this work for scholarly purposes may be granted by me or the Dean of Graduate Studies. It is understood that copying or publication of this work for financial gain shall not be allowed without my written permission.

Title of Thesis/Project/Extended Essay

Intercalation and Distribution of Silver in

the Transition Metal Dichalcogenide 1T-TiS$_2$

Author:

(signature)

Dayakanthi KALUARACHCHI

(name)

14th Aug '87

(date)

Author: Dayakanthi Kaluarachchi
Title of Thesis: Intercalation and Distribution of Silver
In the Transition Metal Dichalcogenide 1T-TiS₂
Senior Supervisor: Prof. R. F. Frindt

ABSTRACT

The intercalation and motion of silver (Ag) in partially intercalated titanium disulphide (TiS$_2$) crystals were studied using a scanning Auger electron microscope with ion sputtering, a scanning electron microscope with an x-ray fluorescence attachment, an optical microscope and radioactive tracers. The x-ray fluorescence results indicated a rapid conversion of stage 1 Ag into stage 2 Ag at room temperature and a stationary behavior of the stage 2 Ag after the stage conversion was completed. The radioactive tracer results showed that stage 2 Ag was mobile during the stage 1 to stage 2 conversion and also when a crystal was being intercalated. The motion of stage 2 Ag in the bulk of a crystal was observed only when stage 1 was present in the crystal.

Auger analysis with ion sputtering yielded the 3-dimensional distribution of Ag in a partially intercalated stage 2 crystal. Ag was observed to be intercalated across the crystal surface region while the bulk was intercalated only for a short distance, indicating that the Ag has a high rate of motion near the crystal surface. A stage 2 region with a high Ag concentration was observed to be unstable near the crystal surface.

Dedicated to my dear parents.

ACKNOWLEDGEMENTS

I wish to express my sincere gratitude to my senior supervisor Professor R.F. Frindt for his valuable guidance and encouragement during the course of this research.

My special thanks are due to Per Joensen for his kind concern shown in numerous ways throughout the period of this research. His willing assistance, valuable advice and moral support given me without any reservation are deeply appreciated.

My thanks are due to the members of my supervisory committee, Professor G. Kirczenow for his encouragement and valuable discussions on theoretical aspects; the director of Surface Science Laboratory Dr.B. Heinrich for helpful discussions and advice on Auger analysis; and Professor A.E. Curzon for useful discussions and suggestions, especially for SEM work. I wish to express my gratitude to Professor M.H. Jericho for sparing his valuable time to act as the external examiner.

Thanks are also due to Ken Urquhart for computer programming. Sylvia Wessel and Per Joensen are thanked for correcting grammar in the manuscript.

The financial assistance from my supervisor, Professor R.F. Frindt through a research grant from the Natural Sciences and Engineering Research Council of Canada along with the

My thanks are due to all members of the Physics Department; faculty, research, technical and secretarial staff and fellow students for their friendly cooperation.

Finally, I wish to thank my husband, Ranjith; for the unfailing support he gave me in every way possible, including typing, correcting and helping me in the preparation of the manuscript.

TABLE OF CONTENTS

List of Tables

List of Figures

CHAPTER 1

INTRODUCTION

1.1 Layered compounds

1.1.1 Structure

Much experimental and theoretical interest has been centered on layered compounds like graphite and transition metal dichalcogenides, because of their unusual anisotropic optical, electrical, mechanical and transport properties (1-4). In addition, the transition metal dichalcogenides have received considerable attention in recent years due to their applicability as cathodes in high energy density batteries (5).

Transition metal dichalcogenides consist of strongly bonded X-M-X sandwiches which are stacked upon each other and held with weak bonds. These interplanar bonds are considered to be of van der Waals type because of their weak nature. Fig. 1.1 shows the general form of these layer structures. The anisotropic properties of layer compounds arise from this highly anisotropic layered structure. For example, the weak bonds between layers permit these crystals to be cleaved parallel to the basal plane easily. The rate of diffusion of intercalants along the Van der Waals gaps is several orders of magnitude higher than that perpendicular to the basal plane (6, 7).

The layered transition metal dichalcogenides (MX_2) are formed by combining the transition metals (M) of group IV, V or VI of the periodic table with the chalcogens (X$,$ S, Se and Te (3). The MX_2 sandwich consists of two hexagonally close-packed chalcogen layers and a transition metal layer where the transition metal ion is found either in a site of octahedral symmetry or of prismatic symmetry (Fig. 1.2). The crystal unit cell consists of either one MX_2 layer or several layers depending on the particular compound. Structurally and chemically, these layer materials form a well defined family of compounds. However, electrically they cover a wide spectrum of properties, from an insulator, a semiconductor and semi-metal to a true metal. A full review of these compounds is found in references 1 - 4.

1.1.2 Intercalation of layered compounds.

Intercalation is the insertion of guest species between the layers of a host structure without greatly altering the structure of the latter. On removal of the guest atoms, the host returns to its original crystal structure. It is possible to control the chemical, electrical and physical properties of the host material by varying the mole fraction (x) of the intercalated guest species (1).

1.2 Staging and models of staging.

Intercalation generally occurs in stages (1). Many studies have been done on intercalated graphite and the

intercalated transition metal dichalcogenides, particularly,
pertaining to the occurrence of staging and stage
transformation (1-4). Staging refers to the phenomenon where
the intercalated species occupies the spaces or galleries
between the host layers in an ordered sequence. In a stage-n
compound, n host layers are found between two consecutive
guest layers. Accordingly, a higher order stage compound is
formed with a lower mole fraction(x) of the guest species.
Stages can transform from one stage to another, and this
phenomenon is known as stage transformation or conversion.

In the classical model for the arrangement of guest
atoms in the host lattice, the van der Waals gaps are
completely full or empty as shown in Fig. 1.3. This model has
difficulty in explaining certain reaction mechanisms such as
stage conversion. The formation of higher stages by
rearrangement of guest atoms in the Van der Waals gaps is
impossible unless the guest atoms penetrate through MX_2
sandwiches. This mechanism is rather unlikely since the
diffusion of guest atoms in the "c" direction is negligible.

To provide a convenient interpretation for stage
conversion and various other reaction mechanisms N. Daumas and
A. Hérold proposed a model (8) which is often referred to as
the domain model, island model or Daumas and Hérold (DH)
model. In the DH model the galleries of the host are only
partially filled and the intercalants are found as collections
of atoms as "islands" in every van der Waals gap. A well-
staged, intercalated compound consists of microscopic domains

such that within each domain the compound is stage ordered in the "c" direction (Fig. 1.4). Each domain resembles a stack of finite, two dimensional islands of intercalants, packed in between the layers of the host. In adjacent domains the intercalant islands reside between different pairs of host layers. Hence the stage conversion can easily occur by moving the islands of atoms from one domain to the other without large movements of intercalants. Thus the DH model avoids the problem associated with the classical model of staging in which it is necessary to empty entire Van der Waals gaps of the intercalated host lattice in order to effect a stage transition.

The DH model gives a reasonable explanation for various experimental results such as stage conversion, reversibility of stage formation, etc. A pressure induced staging transition has been studied in potassium intercalated graphite compounds (9) and the results have shown that the stage 2 to stage 3 transition is reversible. This implies that during the transition the potassium intercalant is not squeezed out of the sample but is redistributed within the graphite host layers as required by the DH domain model. Other studies on stage transitions in potassium/graphite intercalation systems have revealed the need of a domain structure in order to explain the results (10-12). In one study on the $FeCl_3$/graphite system (13), high resolution electron microscope images have shown interpenetration of islands in different stages, supporting the DH model.

Perhaps the most convincing evidence in support of the DH model is the observation of islands in different layered compounds using electron microscopic methods. A wide range of island sizes up to 10,000 A has been reported (14). A study by Levi-Setti et al. (15) using secondary ion mass spectroscopy (SIMS) revealed domains of $SbCl_5$ in the $SbCl_5$/graphite intercalation system. Their SIMS maps of Cl^- on freshly cleaved stage 4 and stage 2 $SbCl_5$/graphite showed domains of typical dimensions of about 2000 A. Electron microscopy has revealed that in the $CoCl_2$/graphite intercalation compound each $CoCl_2$ plane is composed of many island-like clusters of about 100 A in size (16). The intercalation of alkali metals in graphite has been studied for higher stages, and bright field transmission electron micrographs obtained for Rb/graphite samples showed Rb rich regions (or islands) of about 1000 A in diameter (17). In an x-ray investigation, an island size on the order of 100 A has been obtained for stage-2 $NiCl_2$/graphite (18). In addition to the above studies, different island sizes for several other graphite intercalation systems have been reported (19-22). An island size of around 130 A for stage-2 Ag in TiS_2 has been obtained by measuring the profiles of the distribution of Ag intercalants using scanning electron microscopy and x-ray fluorescence spectra (23).

Theoretical models (24-29) of the ordered structures of the intercalation compounds have been developed in the past few years following the initial work by Safran (24). These

models assume that the intercalants distribute continuously over a macroscopic distance in the Van der Waals gaps. Safran suggested that staging occurs due to the electrostatic repulsion between different intercalant layers. Assuming such an interlayer repulsion and an in-plane attraction between intercalant atoms, he showed that the intercalant layers can form periodic structures (24, 25). In Safran's model, the cohesion energy between the adjacent host layers which has to be overcome during intercalation was ignored. A model that explains staging based on elastic energy and interlayer repulsion was introduced by Dahn et al. (26). In their model, the van der Waals bonds between the MX_2 sandwiches and the elastic effects resulting from the intercalated guest atoms were modeled by springs between MX_2 layers. In an attempt to generalize Safran's model, Millman et al. (27-29) pointed out that the cohesive energy which is needed to separate host layers plays an important part in the staging phenomenon and it is thus necessary to consider both cohesive and strongly screened electrostatic repulsive energy in order to explain the occurrence of pure staged compounds.

A basic assumption of the above theoretical models (24-29) of staging is that the galleries between the host layers are intercalated continuously over a large distance. However, there is experimental evidence for the existence of intercalants as microscopic islands of atoms as described in the DH model. The DH model has been used in attempts to explain staging in recent theoretical work (30-34). A

theoretical model of staging based on the DH island model was
presented by G. Kirczenow (33, 34), in which stage order,
stage disorder and phase transitions were considered.
Following Millman and Kirczenow (27), elastic interactions and
strongly screened electrostatic repulsion were taken into
account but the inter-domain interactions were neglected. The
domains were considered to be intercalated to a finite width.
The model predicted that the staging phase transitions in
which the stage index changes proceed via stage-disordered
states and that the stage disorder decreases with large domain
sizes. A kinetic model of stage transformations presented by
Hawrylak and Subbaswamy (35) also predicts that intercalation
and stage transition proceed through the formation and
migration of islands of intermediate stages.

An interesting theoretical model regarding the
dynamics of staging in intercalation was presented by
Kirczenow (36-38). With this model, realistic microscopic
real-space pictures of the staging process have been developed
which are very useful in understanding the questions
associated with intercalation such as the validity of the DH
model, stage transformation and stage disorder. In this work,
the intercalant was considered to be made up of small
identical clusters of islands (elementary islands) which
interact via repulsive electrostatic forces and local elastic
effects. Intercalation was shown to proceed via clustering of
the elementary islands into large islands and their migration
through the crystal until a well defined DH domain structure

is formed. The model parameters were selected to obtain the desired stage. The results have shown that the stage transitions occur via stage-disordered states as mentioned earlier (33, 34, 35).

1.3 Titanium disulphide.

Of all the transition metal dichalcogenides, TiS_2 has received the most attention in studies on intercalation batteries. The ability of TiS_2 to be intercalated with alkali metals, high diffusion rates of alkali metals in the lattice and relatively low specific gravity have made this compound a potential candidate as a cathode material in high energy density intercalation batteries.

TiS_2 is not a naturally occurring compound. Single crystals of TiS_2 can be prepared by standard iodine vapor transport techniques (39, 40) yielding plate-like crystals typically 10 to 100 μm thick and 1 to 5 mm wide. TiS_2 crystals are golden in color and have a metallic luster. TiS_2 is composed of loosely coupled S-Ti-S atom sheet sandwiches as shown in Fig. 1.1 where M = Ti and X = S. Titanium disulphide is commonly designated as 1T-TiS_2 where 1T indicates that there is a one layer stacking sequence and that the primitive unit cell is trigonal. TiS_2 has the cadmium iodide structure (Fig. 1.5) and is found to have semimetallic properties.

Silver (Ag) atoms can be readily intercalated electrochemically into TiS_2 (41). In the system Ag_xTiS_2 (where "x" is the mole fraction of Ag) two phases have been

observed, namely stage 1 and stage 2, where the mole fractions are given as $Ag_{0.42}TiS_2$ and $Ag_{0.20}TiS_2$ respectively (42). In stage 1, Ag is intercalated in every van der Waals gap in the "c" direction while in stage 2 Ag is found in every second gap. Besides well defined stages 1 and 2, mixed stage phases and a dilute stage 1 phase have been observed in Ag/TiS2 (42, 43). Dilute stage 1 refers to a random distribution of intercalated guest atoms in van der Waals layers. In dilute stage 1 phase the intercalated atoms are distributed far apart resulting a low mole fraction of guest atoms. The mole fraction of silver in dilute stage 1 phase in Ag_xTiS_2 has been observed to be $x \leq 1/12$ (42). In the van der Waals gaps of the TiS_2 lattice there are two tetrahedral sites and one octahedral site per Ti atom. In the Ag_xTiS_2 system, Ag occupies octahedral sites (42). The unit cells and the lattice constants for $Ag_{0.20}TiS_2$ and $Ag_{0.42}TiS_2$ are given in Fig. 1.6.

From the point of view of the use of the transition metal dichalcogenides in intercalation batteries, alkali metals such as lithium and sodium are the most interesting guest species for intercalation due to the high cell potential and the high mobility of alkali metals through the host lattice. From an experimental point of view, the high reactivity and the need for water-free electrolytes make it very inconvenient to use the alkali metals in many experiments. To avoid the problems associated with alkali metals, pseudo-alkali metal silver is being widely used in

experiments (44, 45, 46). Ag can be conveniently used as an intercalant to study the problems associated with intercalation such as stage conversion, distribution of intercalant in the host lattice etc., which may not depend on the type of guest species used for intercalation.

1.4 Contributions of this thesis.

The work presented in this thesis is a continuation of research carried out by the author to solve some basic questions associated with the intercalation mechanism. In this previous work the intercalation and motion of stage 1 and stage 2 silver in partially intercalated TiS_2 crystals were studied extensively using the x-ray fluorescence technique in combination with radioactive tracers.

In an attempt to understand intercalation and staging more thoroughly, the 3-dimensional distribution of Ag in Ag_xTiS_2 crystals was studied using the scanning Auger microprobe (SAM) technique and optical measurements. The crystals were intercalated from an edge with Ag for a short period until the initial optical measurements showed stage 2 and empty phases. The surface distribution of Ag across the Ag_xTiS_2 crystal was obtained by AES (Auger electron spectroscopy) line scans. After removing some layers of the crystal by sputtering, repeated line scans were taken to obtain the distribution of silver at different depths. Initial optical measurements, AES line scans and secondary electron images were used in determining the positions of the

intercalation fronts. Finally, the variation of the widths of the intercalated regions with depth from the crystal surface was plotted to obtain a 3-D picture of the Ag distribution in a partially intercalated Ag_xTiS_2 crystal.

In this thesis, chapter 2 presents an introduction to scanning Auger electron microscopy, depth profiling and scanning electron microscopy. The work carried out on Ag/TiS_2 using x-ray fluorescence measurements and tracer experiments is presented in chapter 3. Chapter 4 gives the measurements of the Ag distribution in the partially intercalated Ag_xTiS_2 system obtained from Auger analysis. The determination of the sputtering rate for pure TiS_2 and Ag_xTiS_2 is discussed in chapter 5. The Auger data analysis and the development of a 3-D picture of the Ag distribution in Ag_xTiS_2 are presented in chapter 6. The conclusions drawn from the results of this research are presented in Chapter 7.

Fig. 1.1   Stacking of X-M-X sandwiches in transition metal

dichalcogenides.

X - chalcogen

M - transition metal

C

van der Waals
gap

X
M
X

van der Waals
gap

X
M
X
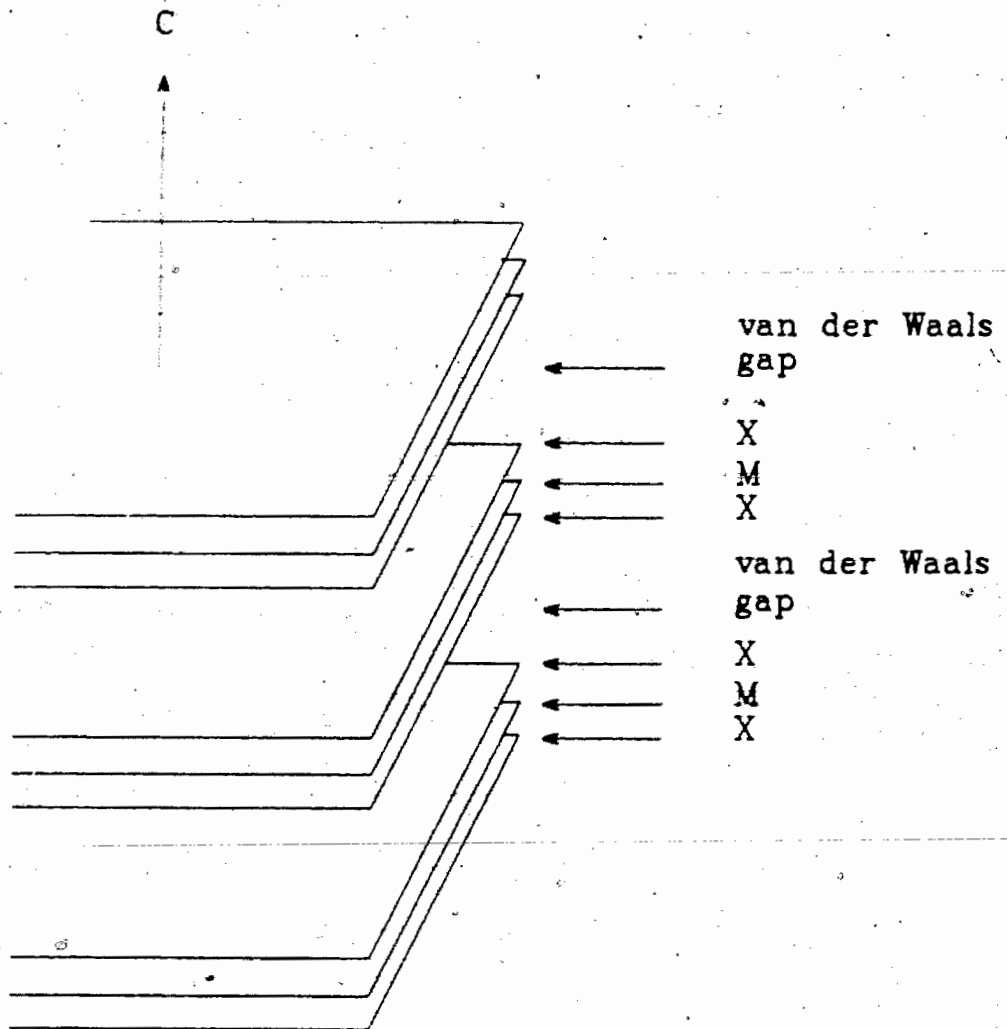
Fig. 1.1

Fig. 1.2 Coordination around transition metal ions.

  (a) Octahedral structure

  (b) Trigonal prismatic structure

    ● – transition metal

    0 – chalcogen
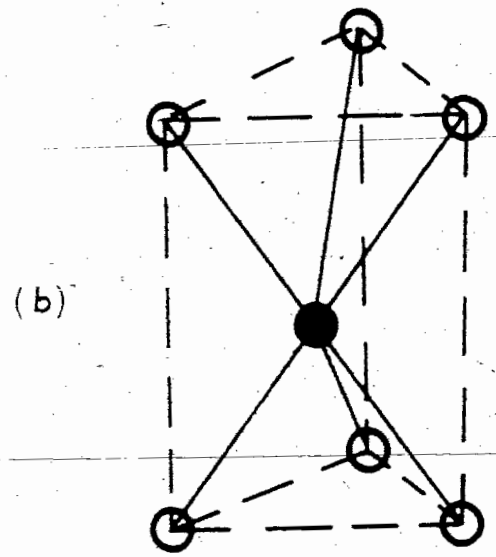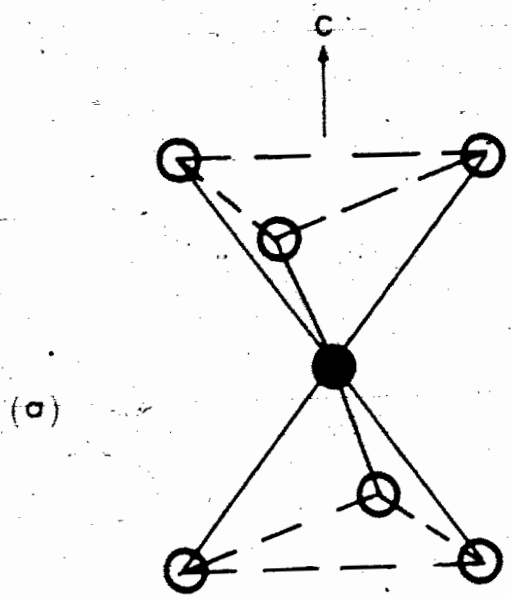
Fig. 1.2

Fig. 1.3 Classical model of staging.

—— MX_2 host layer

●●●● guest atoms

Stage 1

first gap
second gap
third gap
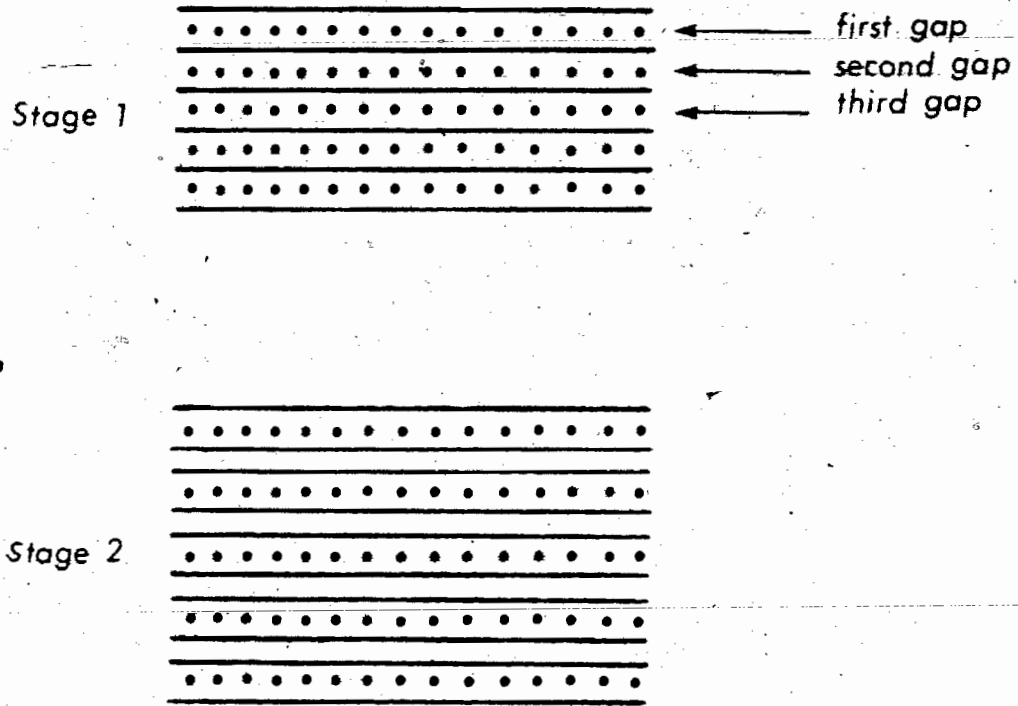
Stage 2

Fig.1.3

Fig. 1.4   Daumas and Hérold's model of staging.

—— MX_2 host layer

●●●●   guest atoms
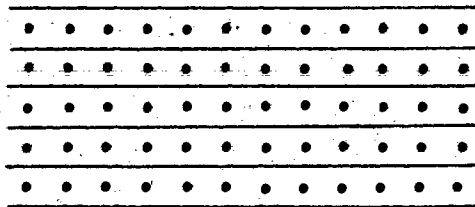
Stage 1

Stage 2
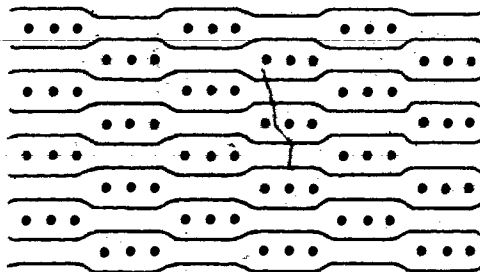
Fig. 1.4

Fig. 1.5 (a) The atomic structure of TiS_2.

(b) The $(11\bar{2}0)$ diagonal cross-section of the TiS_2

unit cell (ref. 42)

$a_o = 3.404 \pm 0.001 \overset{o}{A}$

$c_o = 5.696 \pm 0.003 \overset{o}{A}$

● — Ti

◯ — S
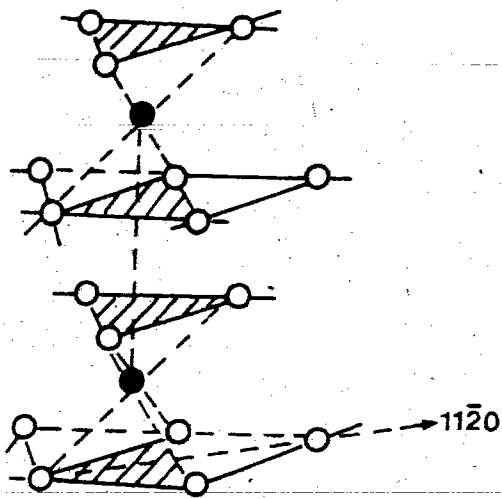
(a) 1 T–TiS$_2$ (b)
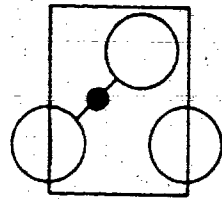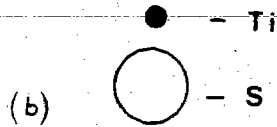
Fig. 1.5

Fig. 1.6   The (11$\bar{2}$0) diagonal cross-section of the unit cells

(ref. 42).

(a) Ag$_{0.42}$TiS$_2$

0.42 of the octahedral sites are occupied with

Ag atoms.

(b) Ag$_{0.20}$TiS$_2$

0.20 of the octahedral sites are occupied with

Ag atoms.

$a_o = 3.437 \pm 0.001 \ \overset{o}{A}$

$c_o = 6.445 \pm 0.003 \ \overset{o}{A}$

● — Ti

◯ — S

☐ — Ag

(a)

$a_o = 3.416 \pm 0.001 \ \overset{o}{A}$
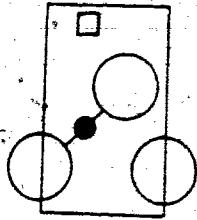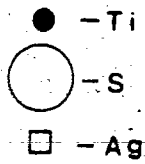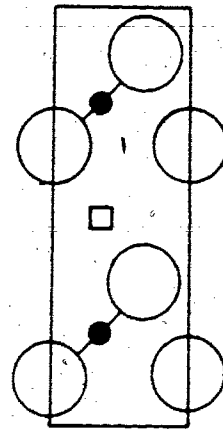
$c_o = 12.145 \pm 0.005 \ \overset{o}{A}$

(b)

Fig. 1.6

CHAPTER 2

INSTRUMENTATION.

2.1 Scanning Auger electron microscopy

During the last decade, the technique of Auger electron spectroscopy (AES) has emerged as one of the most widely used analytical techniques for obtaining chemical composition of solid surfaces (47, 48). In AES, a core level of a surface atom in the sample is ionized by an electron beam followed by relaxation of the atom by filling the hole in the core level with an electron from an outer level. The energy difference between these two levels can be given to another electron either in the same level or in a shallower level, whereupon a second electron (Auger electron) is ejected (Fig. 2.1). Since the energies of the emitted Auger electrons are characteristic of the parent atoms, the analysis of Auger electron energies leads to elemental identification. When Auger transitions occur within a few atomic layers below the sample surface, the Auger electrons can escape from the surface without loss of energy and give rise to peaks in the secondary electron energy distribution.

The quality of a probing technique is characterized by depth resolution, lateral resolution, and sensitivity of the analysis method. The surface sensitivity of the AES technique

is due to the short mean free path of the low energy Auger electrons. The escape depth of the Auger electrons is in the range of 5 to 25 Å for Auger electrons in the energy range of 30 to 2500 eV (49, section 310). The escape depth is independent of the incident beam energy. As shown in Fig. 2.2(a) and (b) the volume excited by the incident electron beam is much larger than the analyzed volume. The lateral resolution is determined by the spot diameter of the probing beam.

The Auger technique can be used to detect all elements except hydrogen and helium. Quantitative analysis using Auger electron spectroscopy can be performed through a comparison of the Auger signal from the sample and the Auger signal from a pure elemental standard. The limit of detectability for the elements are on the order of 0.1% atomic concentration. The sensitivity of the Auger technique is determined by several factors such as transition probability of the Auger transition involved, the incident beam current and energy, and the collection efficiency of the Auger electron analyzer. For a given primary electron beam voltage, different elements can have different relative sensitivity factors (50, p.13).

2.1.1 Instrumentation

The experiments presented in chapter 4 were carried out using a Perkin-Elmer Physical Electronics Model 595 scanning Auger electron microprobe (SAM). The scanning Auger electron spectroscopy system consists of an ultrahigh vacuum

system, a rastering electron gun for specimen excitation, and an energy analyzer for detection of Auger electron peaks (Fig. 2.3). Auger electron spectrometers are operated under ultrahigh vacuum of about 10^{-10} torr to reduce the contamination of the sample surface from the residual gas in the sample chamber. Since the probing depth of AES is only a few atomic layers, the technique is very sensitive to surface contamination. In SAM-595 all electron gun functions are controlled via a microprocessor.

The probing electron beam is produced through thermionic emission by heating a lanthanum hexaboride (LaB_6) filament. The electron beam is accelerated toward the sample using a high voltage (from 3 to 30 kV), and shaping and focusing the electron beam is performed by electromagnetic condenser and objective lenses. Since the beam diameter increases with the beam current one must sacrifice the beam current in order to achieve a small beam size. The SAM-595 provides a minimum beam diameter of about 500 A. While a small beam size is desirable in studying small surface features a high beam current ensures rapid Auger analysis. In the SAM-595 a finely focussed electron beam with conventional deflection and rastering capability is utilized to obtain a two-dimensional compositional analysis of the sample surface. Imaging of a surface is obtained using either secondary electrons emitted from the sample or by measuring the current absorbed by the sample as the electron beam sweeps over various topographical features.

In order to analyze the energies of the Auger electrons emitted from the sample, an energy dispersive cylindrical mirror analyzer (CMA) is used in the SAM-595. The high signal-to-noise ratio of the CMA increases the sensitivity of the instrument. In the CMA two cylinders are positioned coaxially and the outer cylinder is kept at a negative potential relative to the inner cylinder. The Auger electrons emitted from the sample are passed through an aperture in the inner cylinder and those electrons of a particular energy are deflected by the electric field through another aperture to a focus on the axis where a channeltron electron multiplier is located. The energy resolution of the CMA can be varied continuously over the range from 0.3% to 2.0% using a mechanical aperture.

2.1.2. Auger spectrum and line scans

The Auger electrons appear as small peaks in the total secondary electron energy distribution, $N(E)$. Since these Auger peaks are superimposed on a rather large continuous background, small peaks are more easily detected by differentiating the Auger electron energy distribution, $N(E)$ with respect to E. Thus, the conventional Auger spectrum is given as $dN(E)/dE$.

There are several options for analyzing a sample using the SAM-595, such as single or multiple point analysis, Auger line scans, depth profiling and elemental mapping. As the first step of the analysis, an elemental survey (Auger

spectrum) on the sample surface is usually obtained to
identify the elements present. The survey spectrum is also
useful to decide whether the surface is contaminated. The
relative intensities of the Auger peaks are highly degraded
for contaminated surfaces. In order to obtain an Auger survey
spectrum one can choose the single point analysis mode,
multiple point analysis mode or an area-averaged spectrum. In
the single or multiple point analysis mode a stationary
electron beam is used to probe specific points. To obtain an
area-averaged Auger spectrum the beam is rastered across a
selected area on the surface.

An Auger line scan gives a quantitative indication of
the elemental distribution by giving the relative
concentration of a specific element along a line across the
specimen. One can scan several lines simultaneously in order
to obtain the two dimensional distribution on the surface.

2.1.3 Sputtering and depth profiling

In conjunction with inert gas ion sputtering, the SAM
provides compositional variation as a function of sample depth
(47 Ch. 5, 48, 51). High purity argon (or xenon) gas is used
in the sputtering system attached to the SAM-595. Argon atoms
are introduced through a precisely controlled leak valve and
are then ionized by energetic electrons. Positively charged
argon ions are then accelerated through a tube toward the
target (sample). The sputtering ion gun attached to the
SAM-595 provides the smallest ion beam size of about 200 μm.

The sputtering rate is easily controlled by changing either the ion beam current or the raster area. In addition, the sputtering rate depends on many other parameters such as density of target, energy, atomic mass and angle of the incident ion beam, and surface composition of the sample (47 Ch. 5).

Auger analysis of a sample can be done either with continuous or discontinuous sputtering. When in the continuous sputtering mode, the analysis is done simultaneously, while in the discontinuous sputtering mode the analysis is done after sputtering. In the single or multiple point analysis modes, one can obtain the elemental distribution (depth profile) along an axis perpendicular to the sample surface. When operated in the line scan mode with alternating sputtering, the elemental distribution across the layers underneath and parallel to the sample surface can be obtained. Sputter ion etching is also useful in cleaning contaminated sample surfaces prior to Auger analysis. Gentle sputtering is desirable for this purpose since otherwise the surface information may be lost due to erosion.

There are several factors which limit the depth resolution as a result of sputtering (47 chapter 4, 52, 53). Ion bombardment induces changes in the surface topography and inevitably leads to mixing of atomic layers. This induced surface roughness can result in broadening of the depth profiles and hence decrease the depth resolution to several atomic layers. In addition, it has been observed that the

original surface roughness of the sample will also reduce the depth resolution.

A non-uniform ion beam current density over the sputtered area can cause the sample to be eroded to different depths forming a crater. As a consequence AES will in general detect signals from different depths on the crater wall, decreasing the depth resolution. This problem can be avoided by rastering a well focussed ion beam over a large area. In order to avoid the crater wall effects, it is desirable to choose an area on the flat bottom of the crater for Auger analysis.

2.2. Scanning electron microscopy

The basic features of a scanning electron microscope (SEM) are an electron gun, an electromagnetic lens system, an electron detector and a high vacuum system (54, 55). With an x-ray fluorescence (XRF) attachment (i.e. an x-ray detector), the SEM can be used to analyze the bulk of a solid sample, generally within a depth of 1 to 3 μm. The SEM is operated under a vacuum of about 10^{-4} torr. An electron beam is produced from a LaB$_6$ cathode by thermionic emission. The electrons are accelerated toward the sample by a potential of 5 to 40 kV. The condenser and the objective lens system are used to focus the electron beam to a final spot size on the sample. In a manner similar to AES, the area of the sample to be examined is irradiated with a finely focussed electron beam, which is swept in a raster across the surface of the

specimen.

When a sample is bombarded with sufficiently energetic electrons, characteristic x-rays, secondary electrons, Auger electrons and backscattered electrons of various energies are emitted. Incident electrons of sufficiently high energy can remove an inner shell electron of an atom leaving the atom in an excited state. X-ray fluorescence (XRF) spectra are produced as a result of deexcitation of the atom by filling a vacancy in a core level with an electron from an outer shell. The energy of the emitted x-rays, which corresponds to the energy difference between the inner and outer shell of the atom, provides characteristic information of the parent atom (Fig. 2.4). With an XRF attachment, the SEM can provide information such as elemental identification and relative concentration of elements at a given point or along a line across a sample. The energy of the characteristic fluorescent x-rays identifies the x-ray emitting element while the x-ray intensity is proportional to the weight concentration of the element within the analyzed volume. The depth of the analysis volume depends mainly on the primary electron beam energy and the element matrix of the specimen.

In the experiments presented in chapter 3 an ETEC Model Autoscan Scanning Electron Microscope with an energy dispersive x-ray detector (Si/Li detector) was used to obtain the relative amount of intercalated Ag in TiS_2 crystals. Typical XRF spectra for $Ag_{0.4}TiS_2$ (stage 1), $Ag_{0.2}TiS_2$ (stage 2) and pure TiS_2 are shown in Fig. 2.5. The spectra were

obtained at 20 kV and peaks correspond to the S K_α line at 2.308 keV, the Ag L_α line at 2.984 keV and Ti $K\alpha$ line at 4.510 keV. The intensities for the Ag L_α and Ti K_α peaks were measured using an energy window of width 0.30 keV.

As in AES, sample imaging in the SEM is obtained using low energy secondary electrons. The secondary electron images are useful in positioning the sample for analysis and observing it on a microscopic scale. In the experiments described in chap' τ 5, the secondary electron images were used to measure the thicknesses of thin TiS_2 crystals with the aid of an ISI Model DS-130 (International Scientific Instruments, Inc.) electron microscope.

Fig. 2.1 Energy level diagram describing the process

involved in Auger electron spectroscopy.

This figure represents the KMN transition.

Auger electron

E$_f$

N

M

L

Primary electron

K
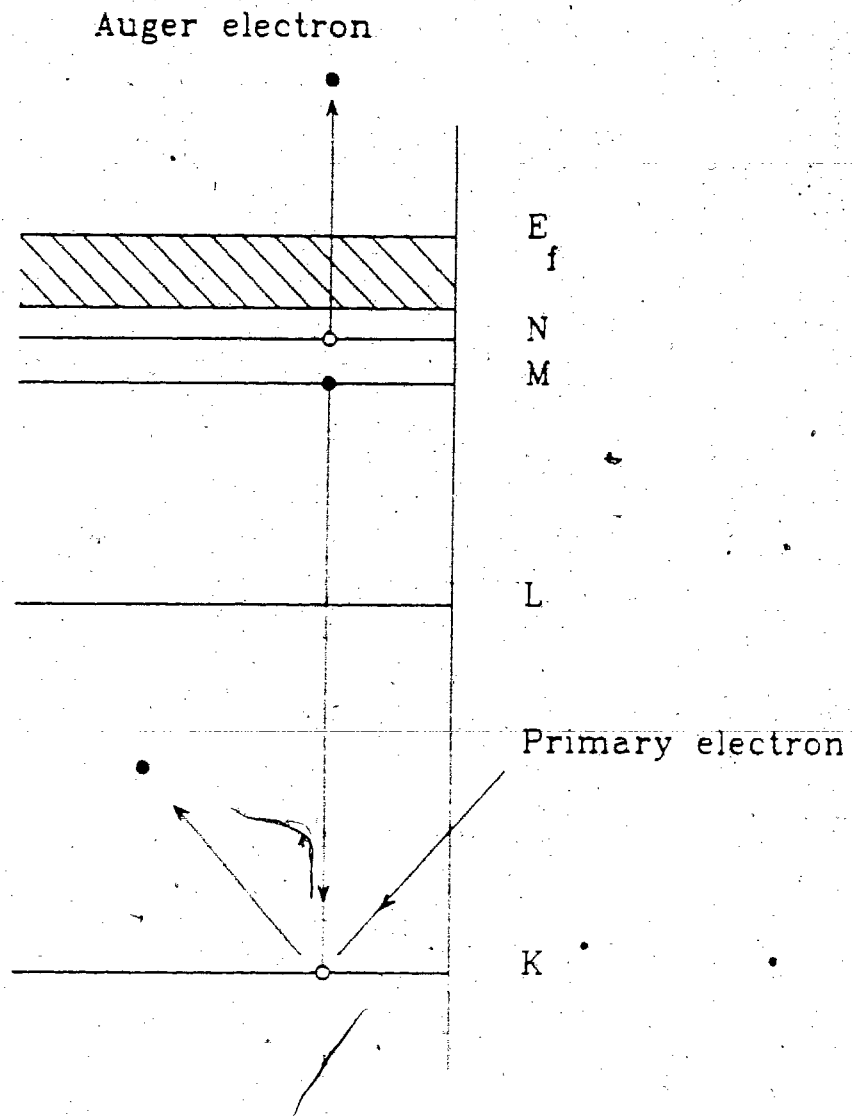
Fig. 2.1

Fig. 2.2 (a) Schematic presentation of electron scattering
             in Auger electron spectroscopy (ref. 47).
          (b) Analysis volume in Auger electron spectroscopy.
             D = diameter of the incident electron beam
             d = depth from which Auger electrons can escape
                without significant energy loss

(a)

Electron beam

Auger electrons

Secondary electrons

Backscattered electrons

Characteristic x-rays

Energetic electrons

1-2 μm

(b)

D

d
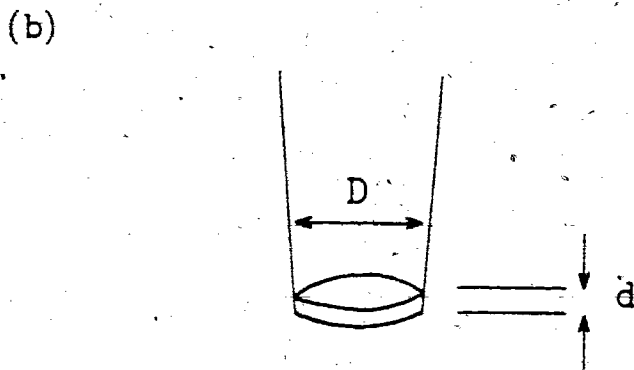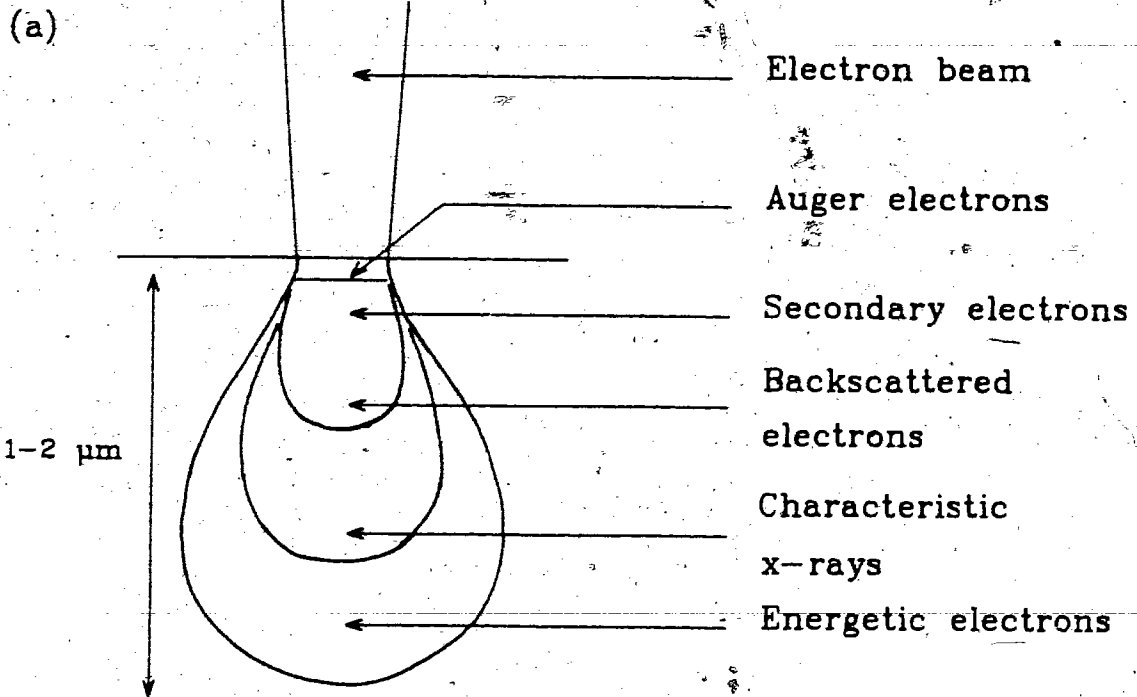
Fig. 2.2

Fig. 2.3 Schematic drawing of the coaxial electron gun

column and the cylindrical mirror analyzer in

SAM (49).

LaB$_6$ cathode

Aperture

Beam blanking

Condenser lenses

Auger electron
collector assembly

Cylindrical mirror
analyzer

Variable objective
aperture

Objective lens

Sputter ion gun

Sample

Secondary electron
detector
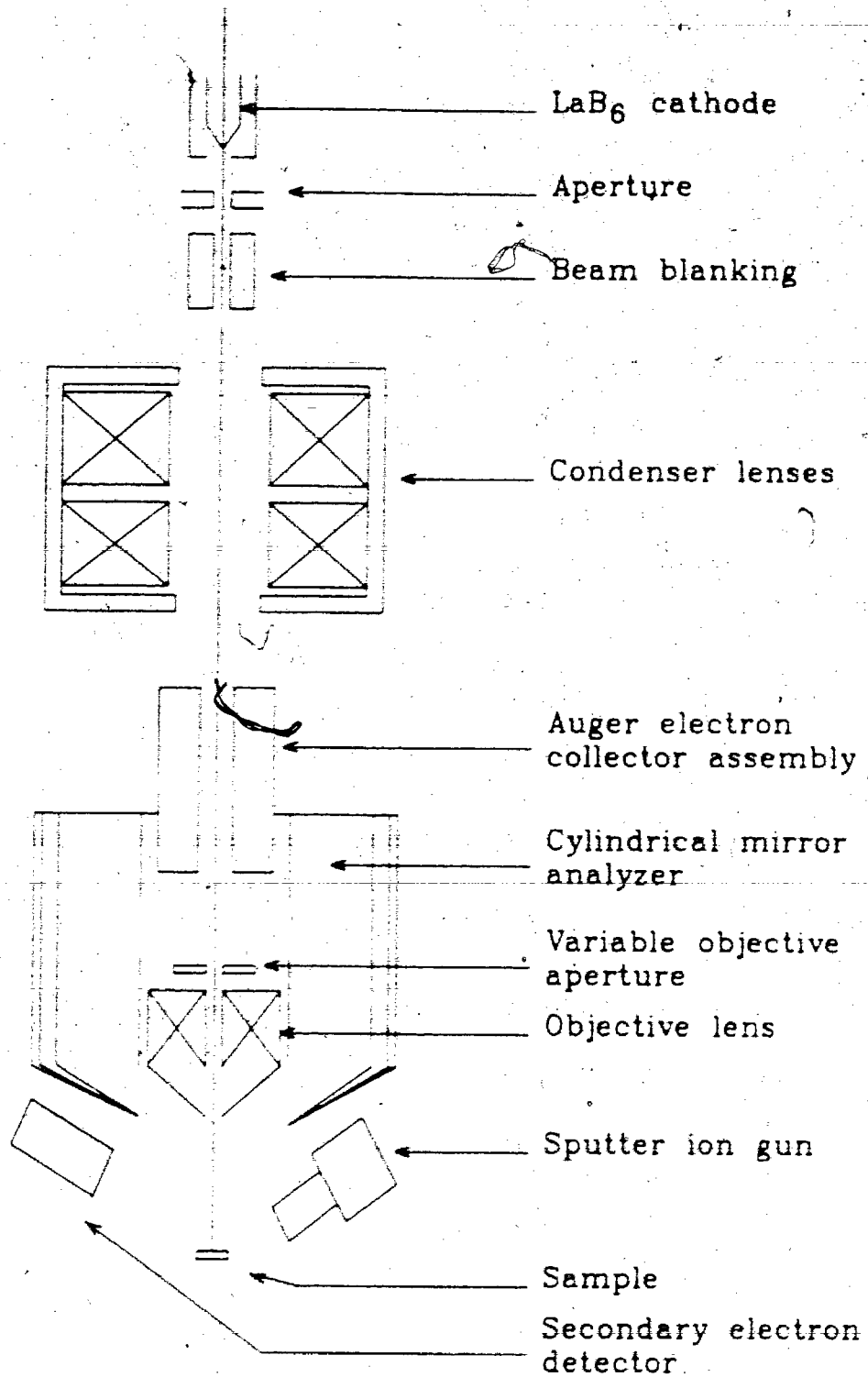
Fig. 2.3

Fig. 2.4 Energy level diagram for an atom showing the
excitation and emission process involved in x-ray
fluorescence (54).
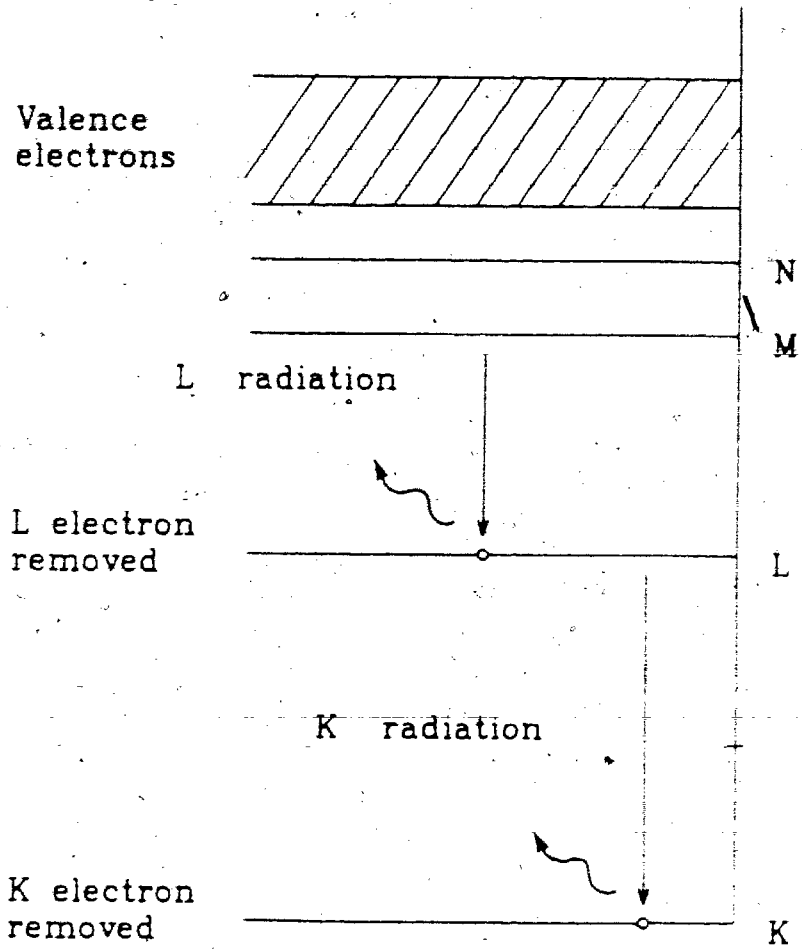
Fig. 2.4

Fig. 2.5   Typical x-ray fluorescence spectra for

(a) $Ag_{0.4}TiS_2$

(b) $Ag_{0.2}TiS_2$ and

(c) TiS_2.

(Courtesy of P. Joensen)
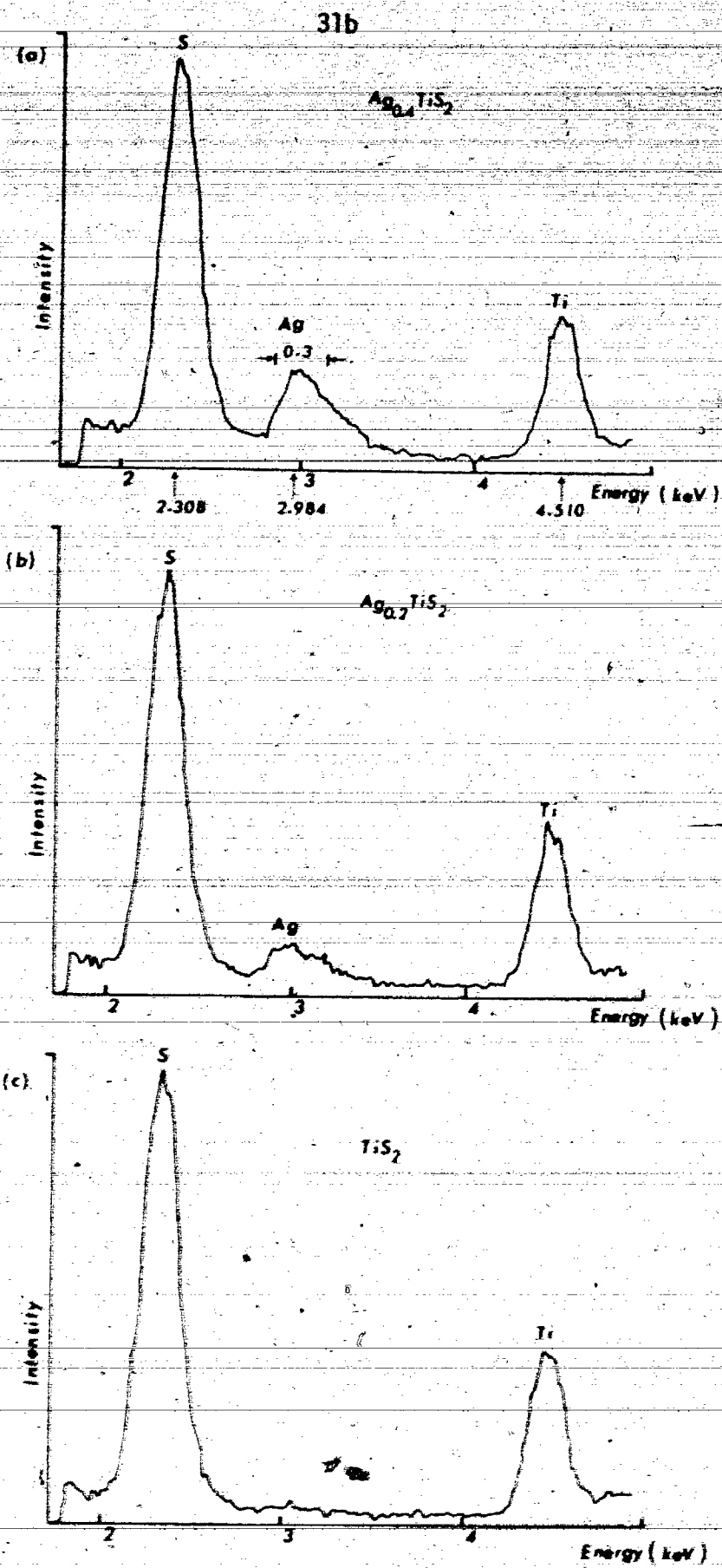
Fig. 2.5

CHAPTER 3

ELECTROINTERCALATION OF SILVER
IN TITANIUM DISULPHIDE

3.1 Introduction

The electrointercalation of TiS_2 with silver is usually carried out using an electrochemical intercalation cell similar to the one shown in Fig. 3.1. A single crystal of TiS_2 is immersed in the electrolyte which is a solution of silver nitrate ($AgNO_3$) in water or glycerol. $AgNO_3$ is chosen since it is one of the few soluble silver compounds available. A piece of pure silver metal acts as the anode while the TiS_2 crystal serves as the cathode. Upon electrically connecting the two electrodes, the Ag^+ ions intercalate into the TiS_2 lattice and electrons pass through the external circuit. The reactions occurring at the two electrodes are:

$$Ag \longrightarrow Ag^+ + e^- \quad \text{at anode}$$
$$TiS_2 + xAg^+ + xe^- \longrightarrow Ag_xTiS_2 \quad \text{at cathode}$$
$$xAg + TiS_2 \longrightarrow Ag_xTiS_2 \quad \text{net reaction}$$
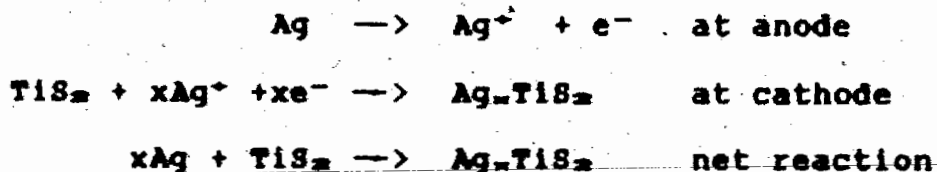
where x = mole fraction of Ag.

The rate of intercalation can be controlled by imposing an external voltage across the cell. The initial

open circuit potential of the Ag/TiS$_2$ cell is approximately

120 mV with respect to the Ag anode (56).

Two stages have been observed when Ag is

electrointercalated into TiS$_2$ crystals using 0.1M AgNO$_3$ in

glycerol or water (6, 41, 42). In a partially intercalated

Ag/TiS$_2$ crystal one can see three regions, namely, stage 1,

stage 2 and empty crystal. Stages 1 and 2 have been observed

optically and detected by x-ray diffraction and x-ray

fluorescence (XRF). When a crystal is optically observed

during intercalation, initially a stage 2 front appears

followed by a stage 1 front. These fronts advance into the

crystal from the crystal edges as the intercalation continues.

The mole fractions of Ag in stage 1 and stage 2 regions are

found to be 0.4 and 0.2 respectively (41, 42). The EMF values

of the Ag$_x$TiS$_2$/0.1M Ag$^+$(glycerol)/Ag cell in stage 1 and stage

2 have been measured to be approximately 40 and 80 mV (56).

After preliminary observation of staging in the

Ag/TiS$_2$ system with XRF, several experiments were carried out

to study the motion of intercalated Ag in the TiS$_2$ lattice

using x-ray fluorescence and radioactive tracer techniques.

3.2 X-ray fluorescence study of stage 1 and stage 2 TiS$_2$

    intercalated with Ag

In this work, partially intercalated Ag/TiS$_2$ crystals

with both stage 1 and stage 2 were studied using optical and

XRF measurements. The aim was to investigate any subsequent

motion of Ag intercalant in stage 1 and/or stage 2 regions

after the intercalation was terminated.

3.2.1 Sample preparation and intercalation

The thickness of the TiS_2 crystals used in this experiment were in the range of 1 to 2 µm. As-grown TiS_2 crystals are usually much thicker (10 to 100 µm) than this thickness range and the procedure for preparing thin TiS_2 samples from as-grown crystals will be described in section 4.2.1. A thin TiS_2 crystal was mounted on a piece of microscope cover glass which was then mounted on a small graphite block fixed onto a SEM sample holder. The graphite block was used to isolate the SEM sample holder from the electrolyte. The crystal was electrically connected to the SEM sample holder with graphite DAG (Fig. 3.2). The crystal was allowed to intercalate only from one edge to avoid merging of intercalation fronts advancing into the crystal from different edges. Except the edge intended to be intercalated, all the other edges were first covered with RTV silicone rubber and then with graphite DAG. The purpose of using graphite DAG was to cover the electrically nonconducting RTV since nonconducting materials tend to charge up when exposed to the electron beam of the SEM. The TiS_2 crystal was intercalated with Ag using a shorted cell (Fig. 3.3.). A 0.1 M solution of $AgNO_3$ in glycerol was used as the electrolyte. Intercalation was carried out observing the crystal through an optical microscope. When the crystal was sufficiently intercalated to exhibit stage 1, stage 2 and an empty region, intercalation

was terminated and optical photographs were taken to measure the widths of intercalated regions (Fig. 3.4). Crystals intercalated through defects such as pinholes or steps were discarded. In this experiment crystals were usually intercalated for 4 to 6 hours. After intercalation, the samples were thoroughly rinsed with acetone to remove the electrolyte and then taken to the SEM for analysis.

3.2.2 SEM analysis: stage 1 and stage 2 motion

The relative amount of intercalated Ag as a function of distance in from the crystal edge was determined by XRF scans along a line perpendicular to the edge of the crystal (Figs. 3.5a and b). The scans were point measurements taken about 5 to 20 μm apart. The primary electron beam used was 20 kV with a scanned area of about 2 μm across. One XRF scan took typically about 2 to 3 hours, depending on the distance intercalated from the crystal edge.

The first XRF scan of the intercalated crystal was made within 30 to 45 minutes after the intercalation stopped. Repeated XRF scans were carried out in 2 to 3 hours time duration and it was observed that the stage 1 region depleted with time while the stage 2 front advanced further into the crystal, increasing the width of the stage 2 region (Fig. 3.6). After sufficient time, only stage 2 Ag was detected in the crystal. No motion of the stage 2 Ag front was observed after the disappearance of the entire stage 1 region. The crystals with only stage 2 and an empty region were then left

at room temperature for periods up to 3 months. Repeated XRF scans performed during this period showed that the stage 2 front was stationary.

Since the stage 2 front was observed to be stationary at room temperature, the samples with stage 2 and an empty region were heated at different temperatures. The temperature was changed by 10°C increments and the sample was scanned after each heating step to observe any change in the stage 2 distribution. A significant motion of Ag in stage 2 was observed only at temperatures above 150°C. Heating the sample at 300°C for 2 hours caused the stage 2 Ag to distribute evenly throughout the TiS_2 crystal. It seemed that the stage 2 was converted to a mixed phase of stage 2 and dilute stage 1 at this temperature.

Although high mobility was observed for stage 1 Ag at room temperature the Ag remained stationary when some Ag/TiS_2 crystals with both stages were cooled down to liquid N_2 temperature (77 K). Some samples with both stage 1 and stage 2 were left in liquid N_2 for about a day and the fronts which were observed optically before and after cooling revealed the same front positions.

3.2.3 Discussion - XRF analysis: stage 1 and stage 2 motion

It is evident from Figs. 3.5b and 3.6 that stage 1 Ag in a partially intercalated TiS_2 crystal rapidly converts into stage 2 Ag at room temperature. It is also clear from the results presented above that the motion of Ag in TiS_2 can be

observed at room temperature only when stage 1 is present in the crystal. These observations indicate that the stage conversion is probably driven by strong repulsive Coulomb forces between charged Ag^+ ions in the van der Waals gaps in the stage 1 region. Since the interlayer Ag atoms in stage 2 are twice as separated as those in stage 1, a higher Coulomb repulsion can be expected between the interlayer Ag atoms in stage 1. The rate of stage 1 to stage 2 conversion was found to be 7 μm/hr. The fact that the stage 1 front remains stationary at 77 K indicates that some thermal activation of the Ag atoms is also required for Ag motion along with the repulsive driving forces. Using this fact, the thermal energy associated with stage 2 island formation during the stage conversion is estimated to be about 25 meV. The observation that the motion of stage 2 Ag occurs only at elevated temperatures also implies that some thermal energy is required to overcome the energy barrier associated with stage 2 Ag motion. This thermal energy is estimated to be about 40 meV considering the fact that the motion of Ag was observed to start around 150°C.

3.3 Study of migration of Ag in stage 1 and stage 2 using radioactive silver

The stationary behavior of stage 2 Ag observed at room temperature has brought up some questions. (a) Where do Ag atoms reside after they enter a partially intercalated crystal with only stage 2? Is stage 2 Ag mobile during intercalation?

(b) How does the Ag in the stage 1 region redistribute to become stage 2 Ag during the stage 1 to stage 2 conversion? Is stage 2 Ag mobile during the stage conversion or does stage 2 Ag remain stationary while stage 1 Ag is being redistributed?

To find the answers to these questions, some experiments were carried out using radioactive silver (Ag^{110}). In order to study the stage conversion, Ag^{110} was used to label the Ag in the stage 1 region. For studying the stage 2 intercalation, Ag^{110} was used to monitor the new guest atoms entering a partially intercalated stage 2 crystal. The location of the active Ag was monitored by detecting the radioactivity in different regions of the intercalated crystal.

3.3.1 Sample preparation and intercalation: motion of stage 2 Ag

Since the amount of silver intercalated and hence the radioactivity increases with thickness it is advantageous to use the thickest crystals available in counting experiments. However, the induced elastic strains during intercalation cause thick crystals to crack from the intercalated edge, and the cracks will then propagate into the interior of the crystal (Fig. 3.7). It was found by trial and error that the crystals in the thickness range of 3 to 6 µm did not crack severely and gave reasonable counting statistics.

The same procedure that will be described in section 4.2.1 was used to prepare the TiS_2 crystals of the above thickness range from the as-grown TiS_2 crystals. It was very important to use crystals without any defects since the active

silver can intercalate through defects giving undesirable
counts. In order to avoid this possibility, a thin layer of
RTV silicon rubber was spread on the bottom surface of the
crystals and all the visible defects of the top surface were
carefully covered with tiny dots of RTV. The crystals were
first mounted on pieces of cover glass which were then fixed
onto SEM sample holders. (A SEM sample holder was used only
for convenience.) For safety reasons, it is desirable to use
the smallest amount of the radioactive electrolyte. A small
intercalation cell was made as shown in Fig. 3.8a. A tiny
piece of silver was attached to the crystal to serve as the
anode. An electrolyte container was made using a rubber
O-ring. The crystal was intercalated from all edges to
increase the number of intercalated silver atoms and hence the
activity of the crystal.

Two electrolytes were used, one with radioactive Ag^{110}
and the other with nonactive Ag^{109}. The active electrolyte was
a solution of 0.001 M Ag^{110} in 0.05 M HNO_3 in water. (This was
prepared from a solution of 0.1 M Ag^{110} in 0.5 M HNO_3 in
water, purchased from New England Nuclear of Canada.) The
nonactive electrolyte was prepared with the identical molarity
and solvent as that of the active one. Since the amount of
the electrolyte used in a cell was very small (about 55 μl),
the cell was covered with a microscope cover glass to prevent
evaporation of the solvent (Fig. 3.8b).

In order to study stage 2 silver motion, a crystal was
first intercalated with nonactive Ag^{109} until the stage 2

front moved a distance x, and then the crystal was further intercalated with active Ag^{110} to a total stage 2 width of y (Fig. 3.9a). The crystal was photographed after each intercalation to measure x and y. The typical values of x and y are about 60 to 100 μm and 90 to 140 μm respectively. The width z of the stage 2 region intercalated with the active Ag^{110} was calculated from x and y, where $z = y - x$. After intercalation, the crystal was removed from the sample holder and thoroughly rinsed with acetone to wash off the excess active electrolyte. Handling of the crystal was done under an optical microscope using fine tools.

The procedure used to monitor the location of active silver in a crystal was as follows. The total crystal activity was first measured and then narrow sections of the crystal edges were cut with a razor blade as shown in Fig. 3.9c. The crystals were always intercalated such that the final stage 2 width, $y > 2z$. Hence, it was possible to cut the edges of the crystal so that the widths of the cut sections and the remaining stage 2 region in the middle part were greater than z. The idea was to check whether the Ag^{110} atoms which have entered later into the stage 2 region, (a) remained near the edge, or (b) moved to the interior of the crystal passing the preintercalated nonactive Ag^{109} atoms, or (c) mixed together with the preintercalated Ag^{109} atoms. Using an optical microscope it was possible to cut strips from the crystal edges with an accuracy of about ± 10 μm. After cutting, the activities of all cut sections and the remaining middle part

of the crystal were measured separately. Ag^{110} emits a wide spectrum of gamma radiation, 95% of which is 657 keV gamma rays. To measure the crystal activity the gamma spectrum was detected with a NaI well-type scintillation spectrometer.

3.3.2 Sample preparation and intercalation: study of stage 1 to stage 2 conversion

The sample preparation for the study of stage conversion was essentially the same as that described in section 3.3.1. The nonactive electrolyte used was a solution of 0.01 M $AgNO_3$ in 0.05 M HNO_3 acid. The active electrolyte was a mixture of Ag^{110} and Ag^{108} with a concentration of 0.01 M in 0.05 M HNO_3. Some nonactive Ag^{108} solution was mixed with the active solution to reduce the high activity for safety reasons.

A crystal was first intercalated with nonactive Ag^{108} until a region of stage 2 of width q (typically, q = 100 to 130 μm) was obtained. Then the crystal was further intercalated with active Ag^{110} until a stage 1 region of width p (typically, p = 30 to 50 μm) was formed at the crystal edges. To ensure that Ag^{110} atoms intercalate only as stage 1 Ag^{110}, the switching of the electrolyte was done just after observing a narrow region of stage 1 Ag^{108} at the crystal edges. After intercalation the crystal was removed from the sample holder, washed with acetone and left for about a day in order to give sufficient time to convert stage 1 Ag^{110} into stage 2 Ag^{110}. Since the width of the stage 2 Ag^{110} becomes

2p after the stage conversion, the crystals were always
intercalated such that q > 2p. In order to determine the
location of Ag^{110} after the stage conversion, three
possibilities were considered: (a) Ag^{110} atoms from stage 1
remain near the crystal edges while stage 2 Ag^{108} atoms move
further into the crystal from the edges, (b) Ag^{110} atoms move
to the interior of the crystal by passing the stage 2 Ag^{108}
atoms and (c) most of the Ag^{110} atoms from stage 1 reside near
the edge, but some of them can be mixed with stage 2 Ag^{108} at
the stage 2 Ag^{110} - stage 2 Ag^{108} interface.

After the stage 1 Ag^{110} converted into the stage 2
Ag^{110}, the total crystal activity was counted and then
crystal sections were cut with a razor blade at a distance
slightly greater than 2p from the crystal edges. The
activities in the cut sections and the remaining middle part
of the crystal were measured separately.

3.3.3 Results and discussion: Tracer experiments

The results from section 3.3.1 showed that when guest
atoms enter a partially intercalated stage 2 crystal, newly
intercalated atoms reside mainly near the crystal edge. The
results obtained for two samples are shown in Table 3.1. It
is clear from the results that most of the active Ag^{110}
remained in the cut sections of the crystal. A low but not
negligible activity was found in the middle part, showing
there is no sharp boundary between the active and the
nonactive regions. This may be partly due to atomic mixing

between silver in the neighboring sites. The fact that the
Ag^{110} atoms were detected near the crystal edge shows that the
preintercalated stage 2 Ag^{ion} atoms have moved into the
crystal, thereby clearing the sites near the edge for newly
intercalated atoms. This observation leads to the important
conclusion that the silver in stage 2 region is mobile during
intercalation.

The study of the stage 1 to 2 conversion also showed
that most of the Ag^{110} from the stage 1 region had been located
near the crystal edge during the stage conversion. The results
of one sample are given in Table 3.2. Even though most of the
activity was detected in a region 2p from the crystal edges,
some activity was also measured in the remaining middle part
of the crystal. In order to find how far this Ag^{110} has
distributed, a second cut was made around the edges of the
remaining middle part and the activities in the cut sections
and the remaining crystal parts were measured separately. As
given in Table 3.2, a very low activity was measured in the
remaining middle part of the crystal after the second cut.
The results showed that, during the stage conversion, the
silver in the stage 1 region pushes stage 2 silver into the
crystal while remaining near the crystal edge. The activity
found beyond the expected region, 2p, implies that the silver
from both stages tend to mix at the interface. From the
results in this section, it is clear that the silver in the
stage 2 region is mobile during stage 1 to stage 2 conversion.

As explained in section 3.2.3 the driving force for

stage 2 silver motion in the presence of stage 1 can be the
strong repulsive Coulomb forces between charged Ag^+ ions in
the van der Waals gaps in the stage 1 region. Even though it
has not been proven yet, it is believed that there may exist a
very narrow region of stage 1 at the edge of an intercalating
crystal. The driving force for the stage 2 silver motion
during the intercalation may have derived from a narrow stage
1 region present at the crystal edge.

The stage 1 to stage 2 conversion will be further
discussed in section 3.4.2.

3.4 Study of the migration of silver perpendicular to the layers of TiS_2

The diffusion of intercalated atoms in layered
structures is highly anisotropic. A higher diffusivity in the
van der Waals layers than that along the c axis has been
observed (7, 57). A study carried out to check the possible
motion of silver perpendicular to the layers of TiS_2 lattice
is presented in this section. In this experiment, TiS_2
crystals with thin steps were used, and only the base part of
the crystal steps were intercalated with silver. The idea was
to supply a good source of silver to the step from the base
crystal. The distribution of silver in the crystal step was
determined in the same way as discussed in section 3.2.2 using
the SEM with the XRF attachment.

3.4.1 Sample preparation, intercalation and XRF measurements

As-grown TiS_2 crystals with thin steps were selected so that in a crystal the height of the step was much smaller than the height of the base crystal. The thicknesses of the steps and the base crystals ranged from 2.5 to 10 μm and 25 to 50 μm respectively. A crystal was first mounted on a piece of microscope cover glass which was then mounted on a SEM sample holder as shown in Fig. 3.2. All the edges of the step were then covered with a thin layer of RTV to prevent any possible intercalation of silver into the step through its edges. The electrolyte used for intercalation was 0.1 M $AgNO_3$ in glycerol. The SEM sample holder was kept upright and an edge (or two) of the base crystal was wetted with a few drops of the electrolyte such that no part of the step was in contact with the electrolyte. A small strip of silver immersed in the electrolyte was connected to the crystal. The base crystals were intercalated for 4 to 8 days, depending on the thickness of the crystal. The stage 2 front had moved underneath the step within 2 to 5 days and the intercalation was stopped when the stage 1 front approached the edges of the step since some cracks developed in the base crystal with the progress of the stage 1 front. After observing the motion of the intercalation fronts we assumed that the base crystal provided a good source of silver for the step.

After intercalation the crystal was analyzed using the SEM. As described in section 3.2.2, the crystals were scanned along a line perpendicular to a crystal edge used for

intercalation (Fig. 3.10). Both the step and the base crystal were scanned. A low accelerating voltage (10 kV) for the primary electron beam was used to reduce the maximum penetration depth of the electron beam. When scanning the steps, a high energy electron beam can penetrate through thin steps down to the base crystal producing x-rays from the silver in the base crystal.

3.4.2 Results and discussion: Ag motion along the "c" axis

All samples (8 altogether) were scanned after intercalation was stopped and no silver was found in the steps. This shows that the silver had not moved along the c axis during intercalation. The samples were checked intermittently during the next two months and no motion of silver perpendicular to the layers was observed.

After obtaining this result, it was clear that the results of the tracer experiment for stage 1 to stage 2 conversion (section 3.3.3) support Daumas and Hérold's model (Fig. 1.4) for intercalation. The type of motion of stage 1 Ag into stage 2 Ag required by the tracer results can only be reasonably explained with islands of atoms within the host layers. The conversion from stage 1 to stage 2 in the classical model for staging is only possible if migration of Ag atoms perpendicular to the layers of the TiS_2 lattice occurs. Since we showed that the motion of Ag atoms perpendicular to the layers is negligible, the classical model

fails to explain the tracer results. In the tracer experiment which was done to study the migration of Ag in the stage 1 to stage 2 conversion, some activity was found beyond a distance from the edge greater than twice the width of the stage 1 region (Table 3.2). This agrees with the electron microprobe results where it was observed that the intercalation fronts are not sharp and that the stage 2 front becomes wider after the conversion of stage 1 into stage 2.

To interpret the results obtained by both XRF analysis and the tracer experiments, an island model based on Daumas and Hérold's model was proposed as shown in Fig. 3.11. Fig. 3.11a shows the upper half of a partially intercalated crystal with stage 1 and stage 2. The lowest layer in Fig. 3.11a represents the layer at the center of the crystal. The silver distribution in the whole crystal is expected to be symmetrical around the center of the crystal. The islands are arranged in the crystal in such a way that the fronts are V - shaped giving broad intercalation fronts. Fig. 3.11b shows how Ag atoms in stage 1 can remain near the crystal edge in the stage 1 to stage 2 conversion, as required by the tracer results. In this model the stage 1 Ag acts as a source of moving stage 2 islands.

The stationary behavior of silver found in stage 2 TIS$_2$ crystals at room temperature was an advantage for studying the intercalation reaction at room temperature. Because of this convenience stage 2 Ag/TIS$_2$ crystals were used in the experiments described in the following chapters.

Fig. 3.1 Schematic diagram of silver/titanium disulphide cell
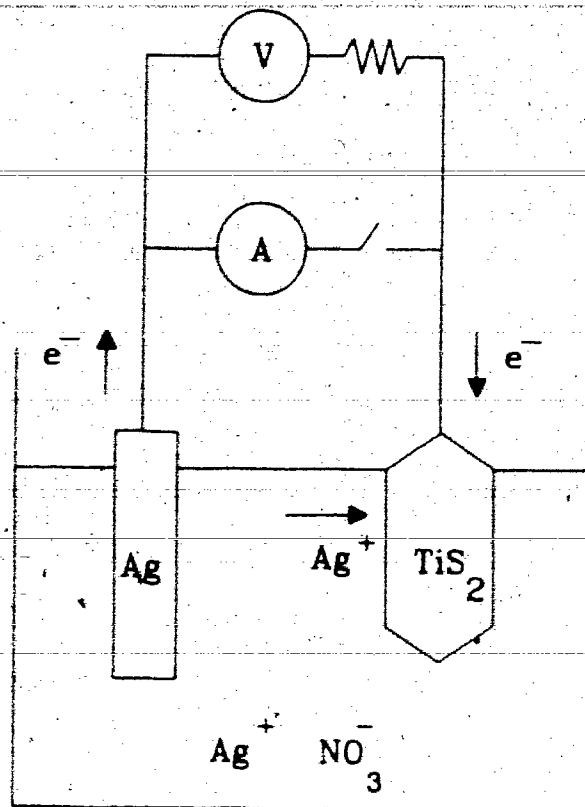
Fig. 3.1

Fig. 3.2 A TiS$_2$ crystal prepared for intercalation.

Crystal

Cover glass

SEM sample
holder

Graphite
DAG

Graphite
block
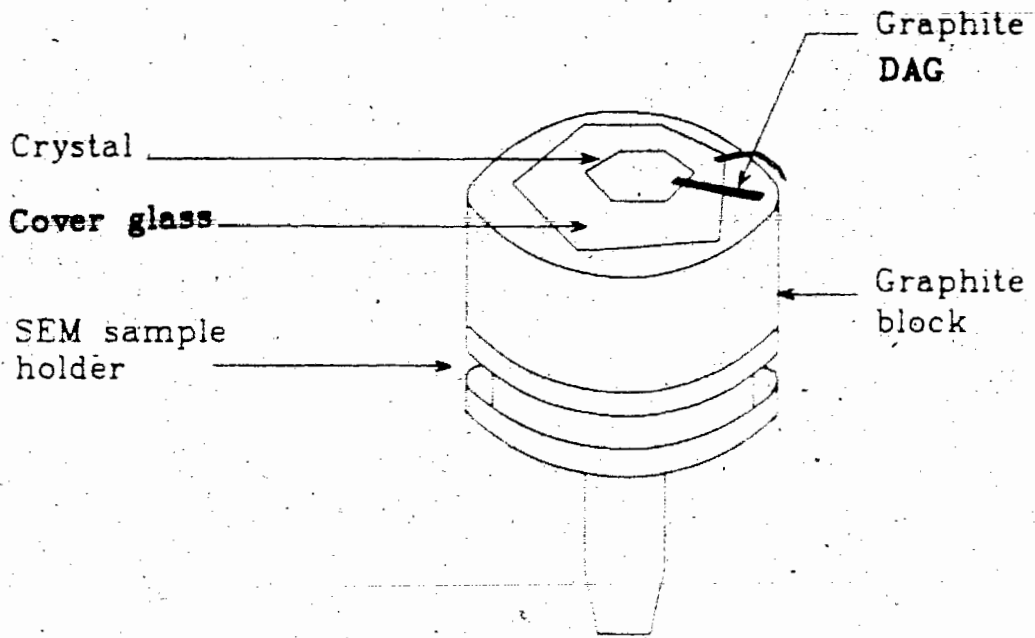
Fig. 3.2

Fig. 3.3 The setup used for electrointercalation of TiS$_2$

crystals.

SEM sample holder

Electrolyte

TiS$_2$ crystal

Ag electrode

Optical microscope
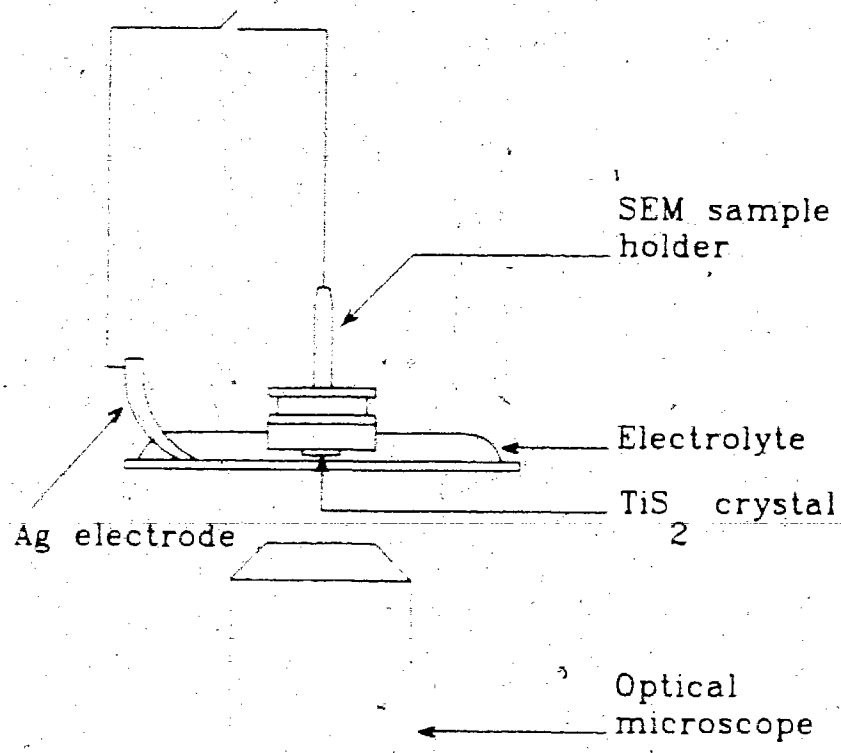
Fig. 3.3
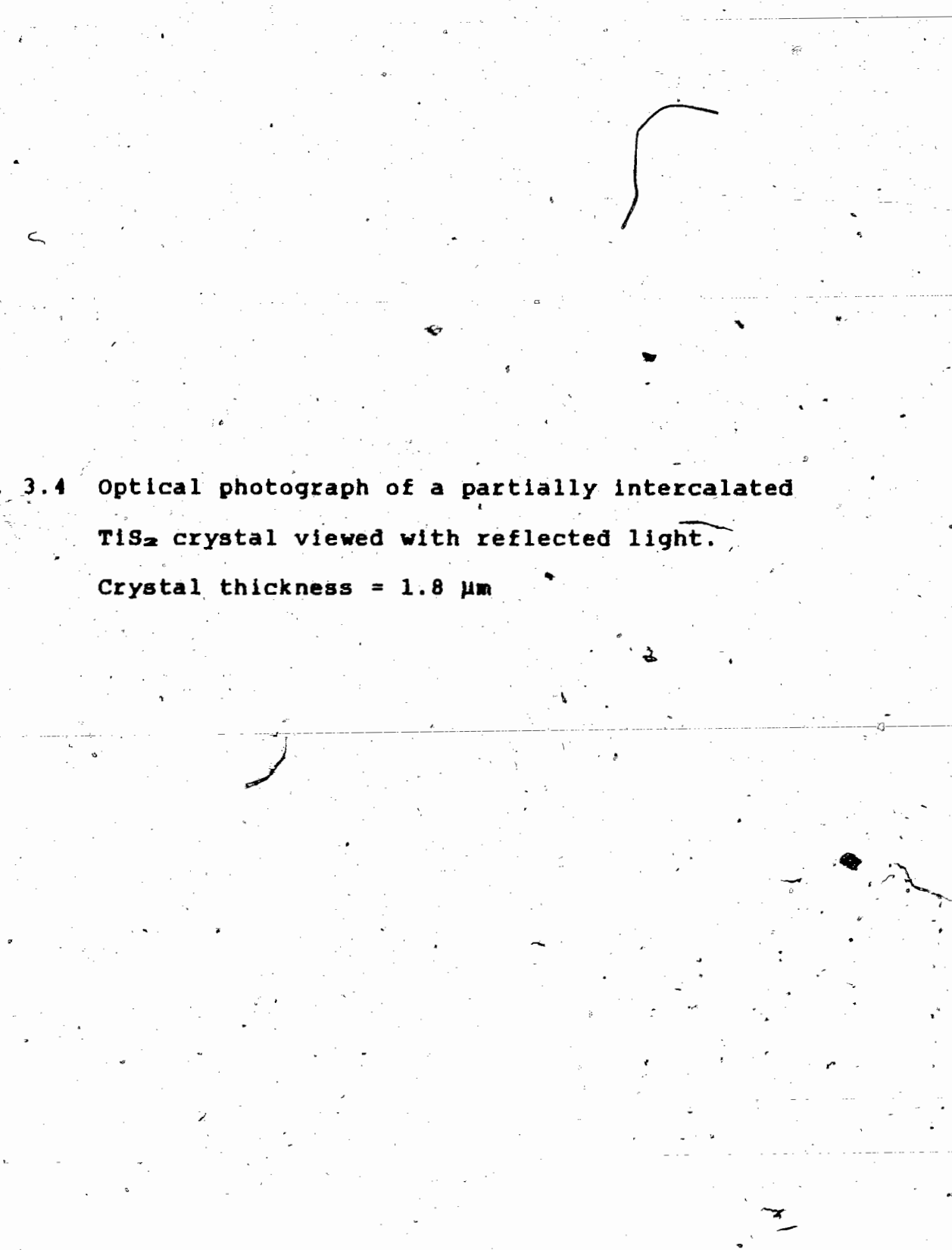
Fig. 3.4 Optical photograph of a partially intercalated

TiS_2 crystal viewed with reflected light.

Crystal thickness = 1.8 μm

100 μm

empty
crystal

stage 2

stage 1

edge of crystal
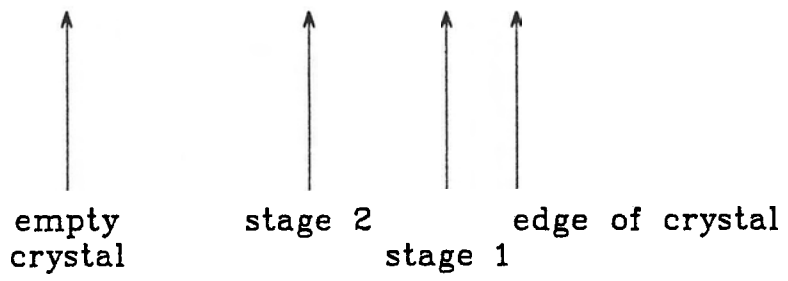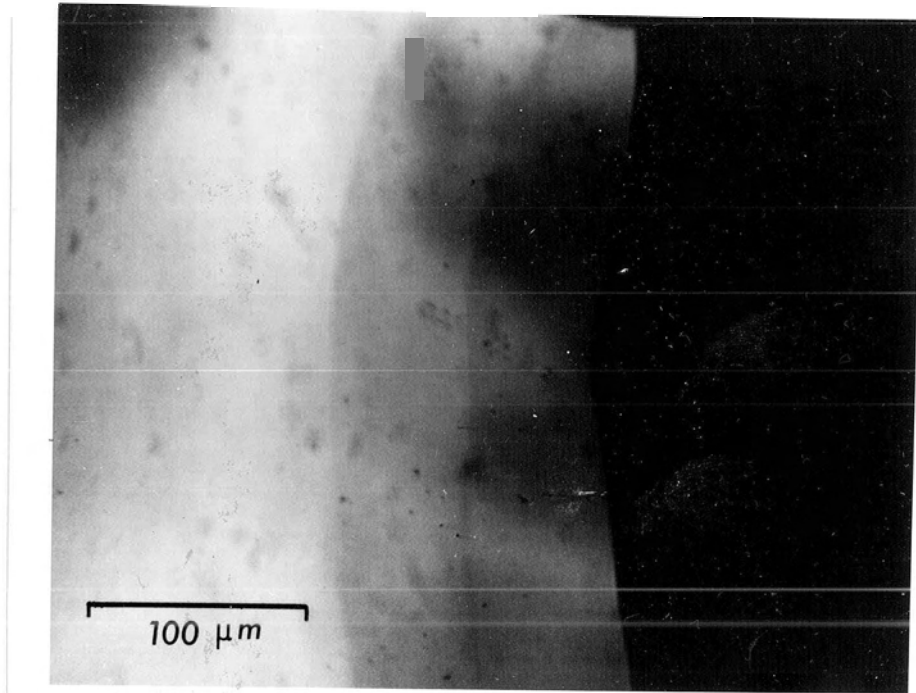
Fig. 3.4

Fig. 3.5 (a) Sketch of a partially intercalated TiS_2 crystal.

XRF scans were made along a line perpendicular to the intercalated crystal edge.

(b) XRF scan of the distribution of Ag content in a partially intercalated TiS_2 crystal.
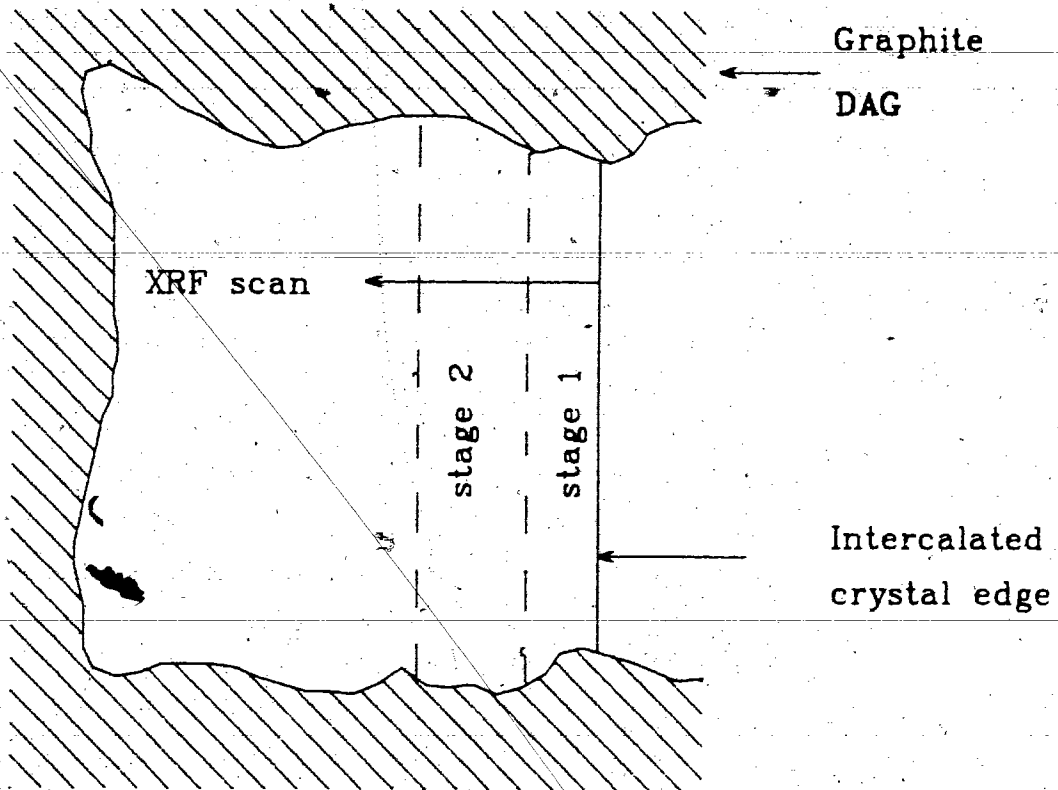
Fig. 3.5a
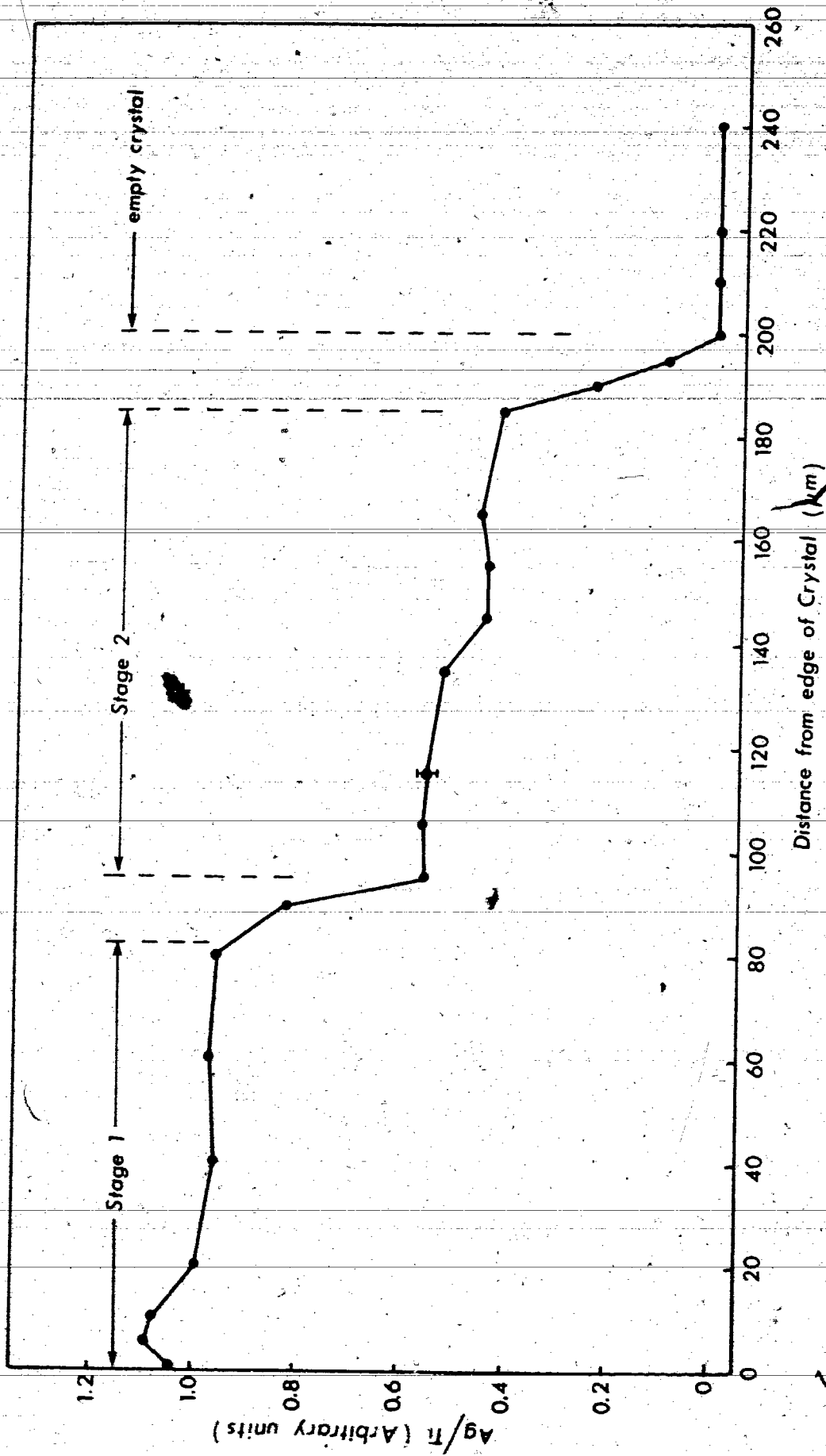
Fig. 3.5b

Fig. 3.6 XRF scans showing stage 1 to stage 2 conversion
at room temperature.

Time after intercalation:

(a) 0 - 45 min.

(b) ● - 2 3/4 hrs.

(c) △ - 4 1/4 hrs.

(d) + - 6 1/2 hrs.

(e) □ - all stage 1 Ag has moved (Data taken after
two days).
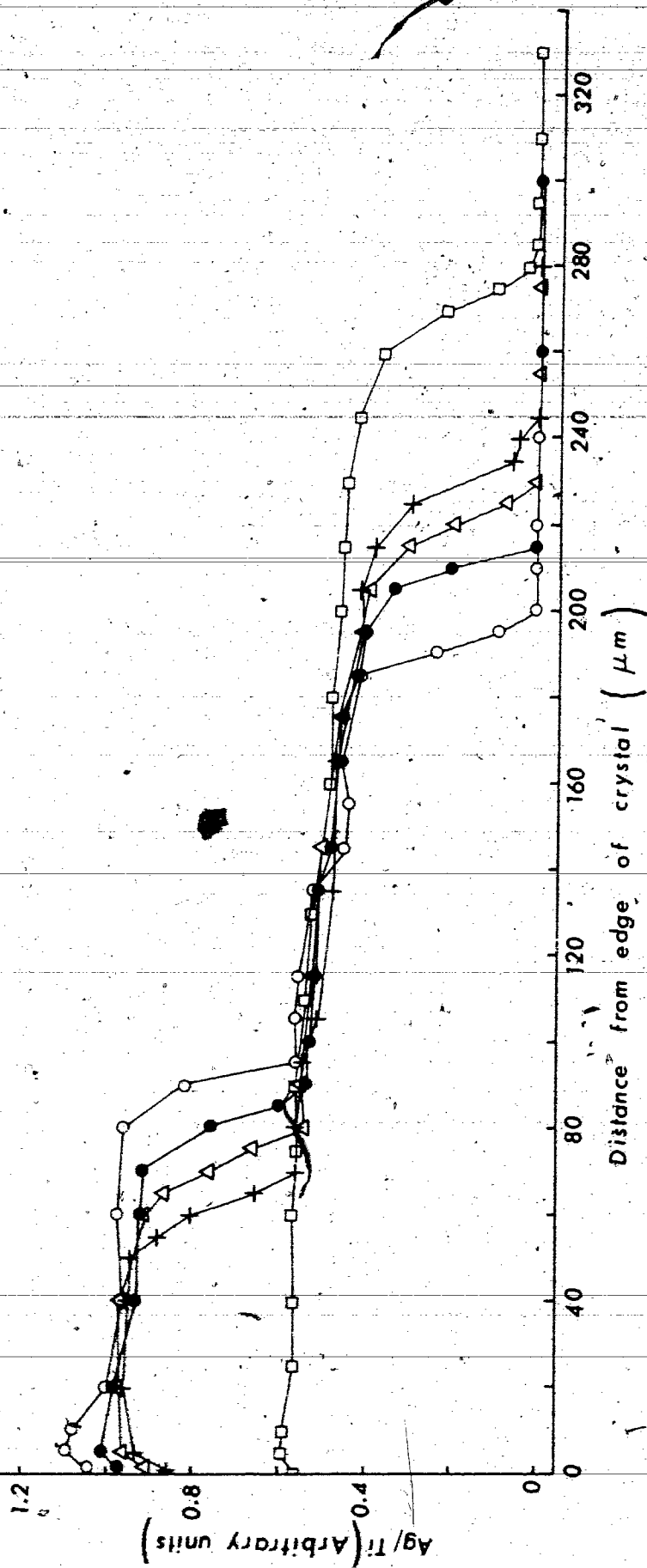
Fig. 3.6
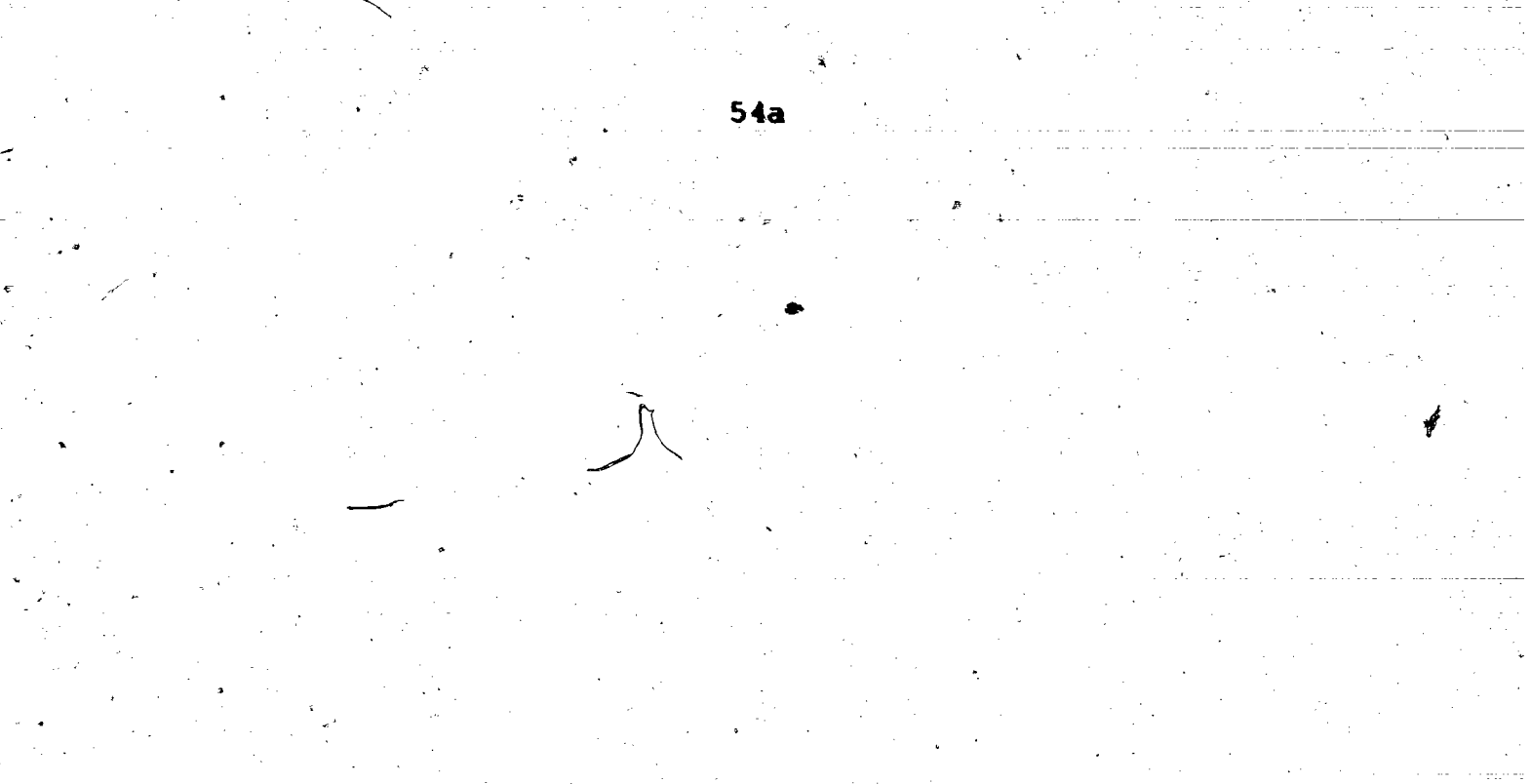
53b

Fig. 3.7 Optical photograph of an intercalated TiS_2

crystal showing cracks formed at edges.

Crystal thickness ~ 50 μm.

(Courtesy of P. Joensen)
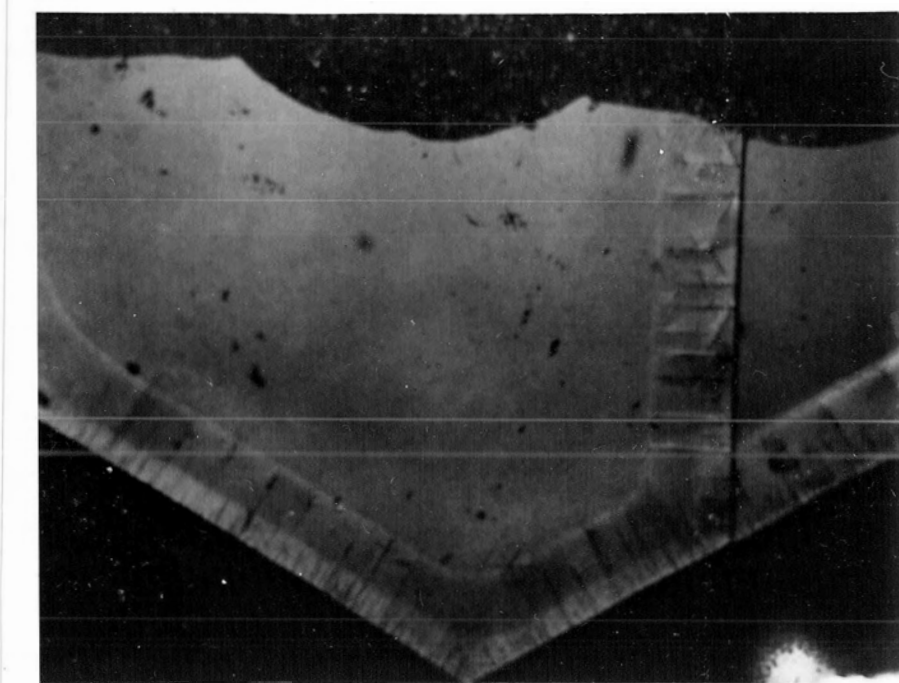
Fig. 3.7

Fig. 3.8 (a) TiS_2 sample prepared for the radioactive

tracer experiment (top view).

(b) Setup used for intercalation in tracer

experiments (side view).

(Drawn to scale.)

(a)

SEM sample
holder

Small strip
of Ag

TiS_2 crystal
mounted on a
cover glass

Rubber
"O" ring

5 mm

(b)

Top cover
glass

Rubber
"O" ring

SEM sample
holder
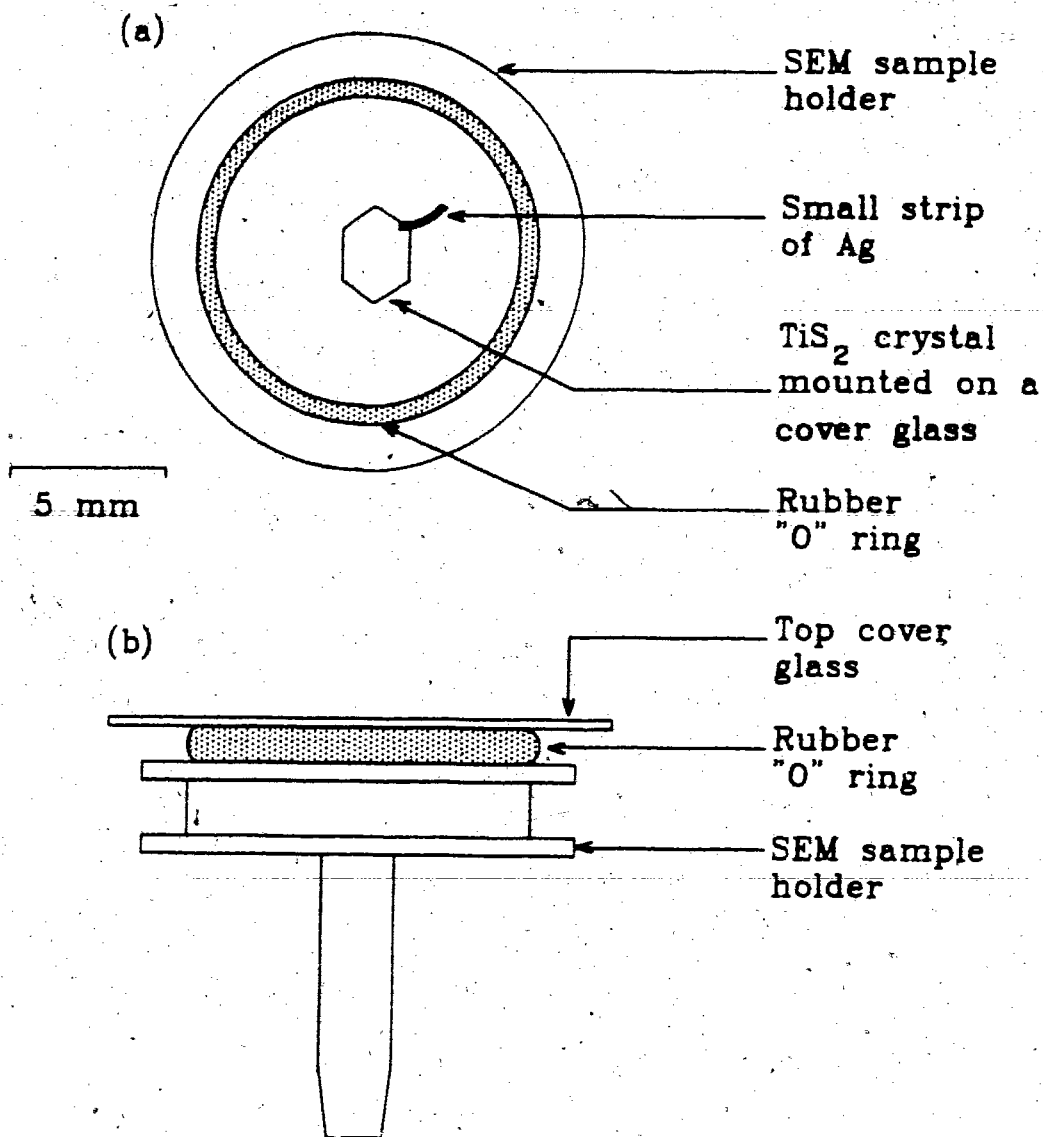
Fig. 3.8

Fig. 3.9 The sequence of intercalation of a crystal and

cutting the edges for tracer experiments.

Dashed line depicts Ag intercalation front.

(a) X is the width of the stage 2 Ag^{108}

(b) Y is the width of the stage 2 made up of

both Ag^{108} and Ag^{110}

(c) The width of the cutoff sections and the

width of the stage 2 region in the remaining

part of the crystal are slightly greater than

the width of the active region Z, where

$Z = Y - X.$

(a)

(b)

Intercalation
Ag^{108}

Intercalation
Ag^{110}

X

Y

Cut off

(c)
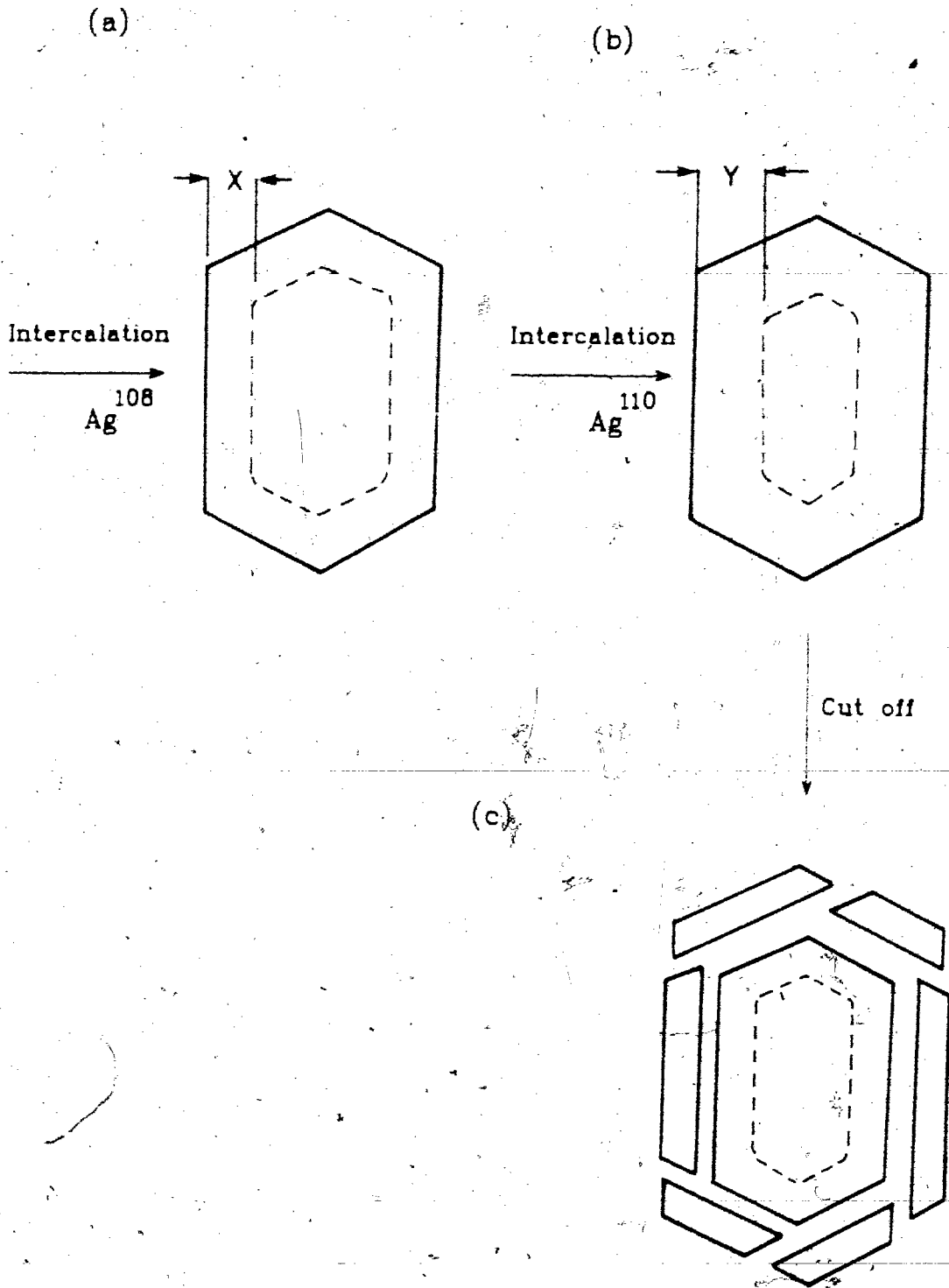
Fig. 3.9

Table 3.1 Results of the tracer experiment: study of stage 2

region during intercalation of a crystal.

Table 3.1

Sample #	Thickness ± 0.1 µm	x ± 5 µm	z ± 5 µm	Width of cut sections ± 10 µm	Counts per second		
					Whole crystal	Cut sections	Remaining crystal
1	6.0	60	30	40	9.62 ± 0.23	8.14 ± 0.22	1.38 ± 0.18
2	5.8	80	30	40	9.13 ± 0.23	7.92 ± 0.22	1.23 ± 0.18

Table 3.2 Results of the tracer experiment: study of stage 1
to stage 2 conversion after intercalation.

Table 3.2

			Counts per second				
p ± 5 μm Ag^{110}	q ± 5 μm Ag^{108}	2p ± 10 μm	Whole crystal	First cut width = 100 ± 10 μm		Second cut width = 35 ± 10 μm	
				Cut off sections	Remaining crystal	Cut off sections	Remaining crystal
50	110	100	15.26 ±0.23	12.72 ± 0.22	2.64 ± 0.19	2.30 ± 0.19	0.31 ± 0.18

58b

Fig. 3.10 Schematic diagram of a sample prepared for the study of motion of Ag along the "c" axis of the TiS_2 lattice.

Graphite dag

scan

scan

Step

RTV
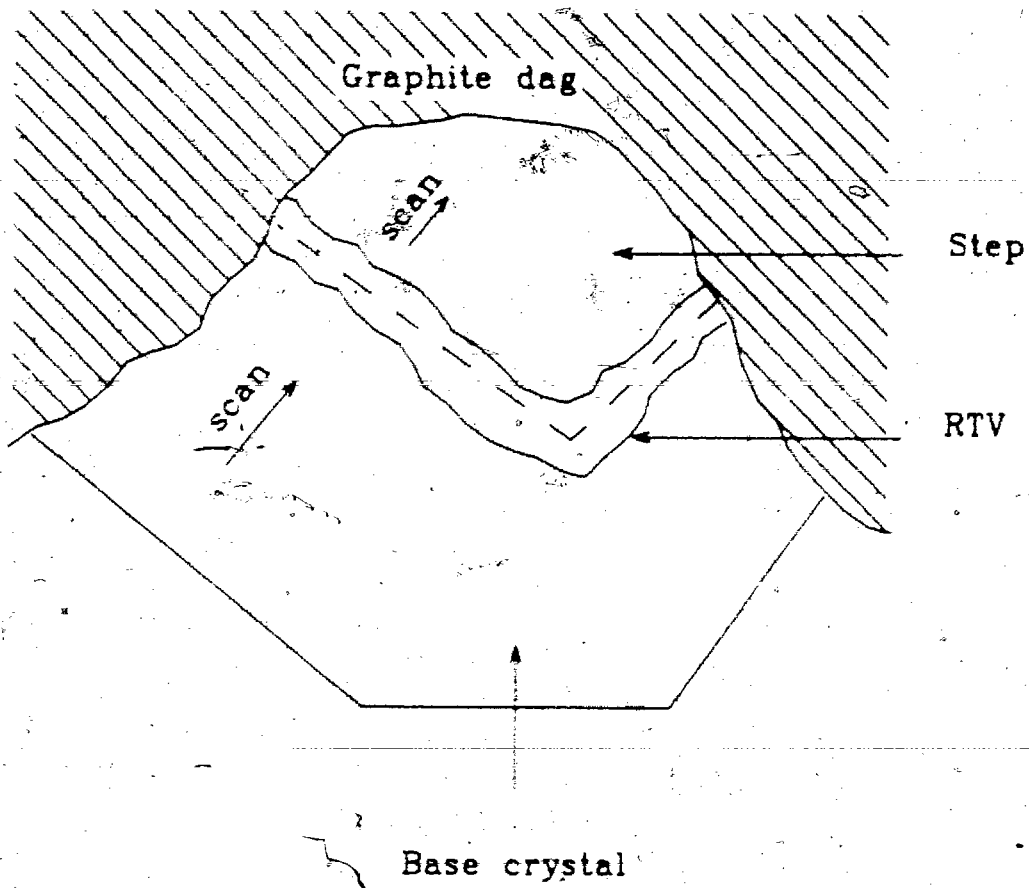
Base crystal

Fig. 3.10

Fig. 3.11 (a) The island model proposed for a partially
intercalated TiS_2 crystal with stage 1,
stage 2 and empty regions (based on the DH model
of intercalation).

(b) The distribution of intercalants after the stage 1
to stage 2 conversion is completed.

This is a schematic diagram of the cross-section of an
intercalated crystal where the host layers are depicted
by lines and the circles depicts regions of intercalated
Ag. Dark circles are the originally stage 1 Ag. Light
circles depict Ag in stage 2 islands.

60b

empty crystal

stage 2

stage 1

(a)

(b)

Crystal edge
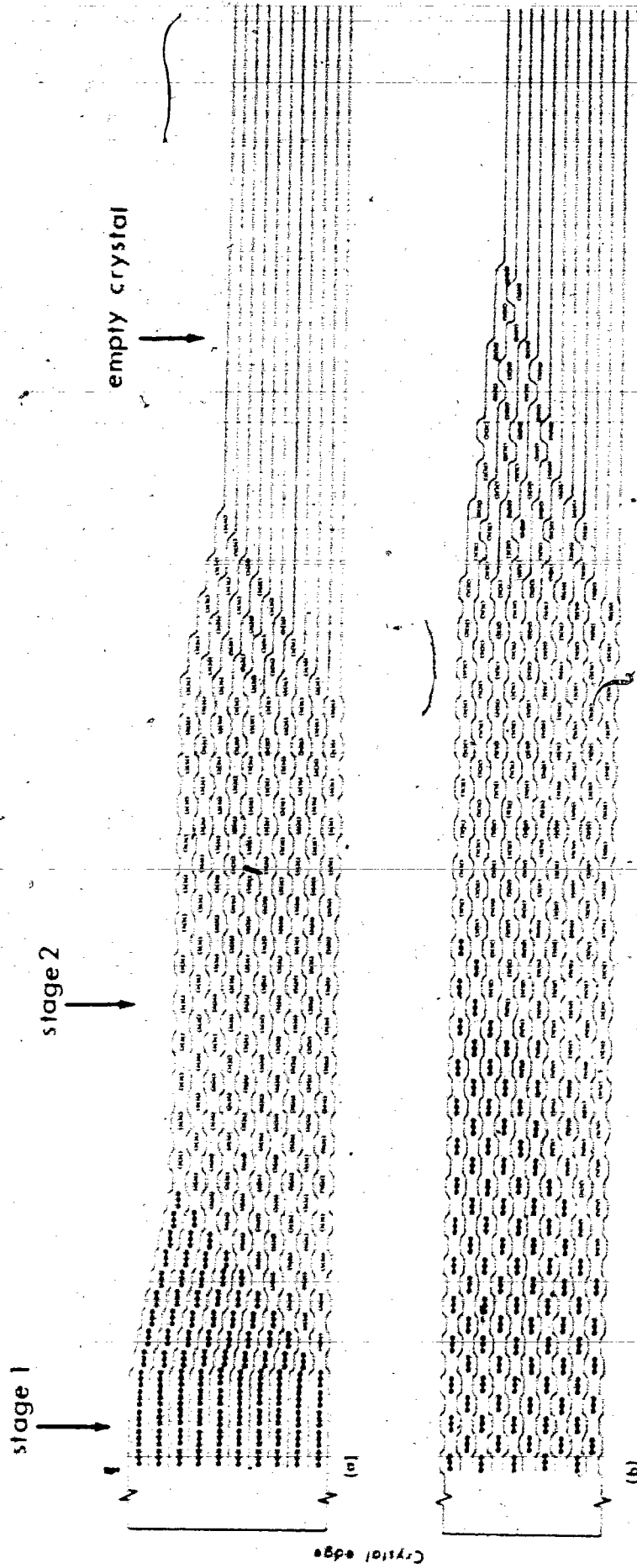
Fig., 3.11

CHAPTER 4

MEASUREMENT OF SILVER DISTRIBUTION IN PARTIALLY
INTERCALATED *Ag/TiS$_2$ - AUGER ANALYSIS

4.1 Introduction

In the study carried out to understand intercalation
and the resulting distribution of Ag in TiS$_2$ crystals
described in chapter 3, the variation (if there is any) of Ag
distribution along the c axis was not considered. The
distribution of intercalated Ag found in that study with XRF
measurements and tracer experiment was considered to be a
constant throughout the total crystal thickness. In fact, it
has been assumed over the years that the distribution of
intercalants in a host lattice along the c axis is continuous
and a variation of intercalant concentration is only observed
parallel to the basal planes of the host.

The elastic strain induced by the intercalated atoms
due to the separation of the host layers during intercalation
was known to play an important role in staging and
intercalation (26-29). It was observed that the intercalation
rate is strongly thickness dependent and thick crystals are
intercalated more slowly than thin crystals. Since an elastic
energy is required to bend a host layer upon intercalation, an
increasing elastic energy must be overcome with every new

intercalating layer. Considering these facts, it is reasonable to assume that a crystal will intercalate more easily at the basal surfaces. Also, it is of interest to know the possible variation of the distribution of intercalants as a function of depth from the basal planes.

This investigation can be carried out with the aid of the SAM/AES surface analytical technique in conjunction with inert gas ion sputtering for microsectioning the sample parallel to the basal planes. The analyzed depth in Auger electron spectroscopy is less than 30 A and the distribution of intercalant given in an Auger line scan is an average over that depth. With the help of ion sputtering one can obtain the distributions of the intercalants at different depths from the crystal surface. With this information, a 3-D distribution of the intercalant in the host crystal can be developed.

This study was carried out for the Ag_xTiS_2 system as presented below.

4.2 Sample preparation and intercalation

4.2.1 Sample preparation

The thicknesses of the TiS_2 crystals used in these experiments were in the range of 2 to 4 µm and the lateral dimensions were (2 to 3 mm) x (1 to 2 mm). It was preferable to use crystals with thicknesses in the above-specified range since those with large thicknesses (> 10 µm) take longer times to intercalate the entire thickness.

Single crystals of TiS$_2$ were prepared by the iodine vapor transport technique (39, 40). The crystals obtained by this method were typically 10 to 100 μm thick. The following procedure was used to prepare thin crystals from as-grown crystals. Some large and reasonably flat crystals were selected and placed on half-set five-minute epoxy on a glass slide. The crystals were gently pressed down until the bases of the crystals were settled in the epoxy. After the epoxy was cured the crystals were peeled off using sticky tape (DRG Sellotape). By this method, it was possible to obtain many thin crystals from one as-grown crystal. The peeled thin crystals attached to the sticky tape were viewed under an optical microscope (Reichert) at low magnification to select good crystals with large areas and no visible defects such as steps, scratches or cracks. Even though only one side of the crystals was checked at this stage (with the other side being stuck to the tape) it was advantageous to select only the best available samples, considering the tedious and difficult procedure for sample preparation. The selected samples were soaked in trichloroethylene for about half an hour to remove the crystals from the adhesive on the sticky tape. It is very important to select a suitable sticky tape and a solvent for dissolving the adhesive because some tapes will leave traces of the adhesive on the crystal surfaces, and this contamination can be extremely difficult to remove. After soaking, the crystals were carefully picked up with an eye-dropper and washed several times in fresh

trichloroethylene. The crystals were then placed on pieces of cover glass. Cover glass was used since it provides a flat, smooth surface. After placing the crystals on the pieces of cover glass, the samples were again thoroughly rinsed in trichloroethylene. Since the crystals were mounted on transparent glass, it was possible to check both surfaces of the crystals at this stage and only the crystals without any visible defects were chosen for further sample preparation. The thicknesses of the crystals were measured to an accuracy of $\pm$ 0.06 μm using a Wild M 20 optical microscope with an interference attachment.

4.2.2 Intercalation

The intercalation of Ag in TiS_2 was carried out only from one edge. When the experiment was first started, the crystals were intercalated such that all edges except the edge to be intercalated were covered to prevent the intercalation through them, and the whole crystal was immersed in the electrolyte. Since the analyzing depth in Auger analysis is only several monolayers, the question arose later whether one would inadvertently detect any silver possibly intercalated into the crystal through any micro-defects such as steps or scratches which may be present on the crystal surfaces. If so, this silver will also contribute to the true distribution of Ag which is intercalated through the crystal edge of interest. To avoid this possibility it was then decided to make contact with the electrolyte only at the edge to be intercalated. The

procedure was as follows.

After measuring the crystal thickness, the sample was soaked in methanol to remove the crystal from the cover glass substrate. The crystal was carefully picked up with a pair of fine forceps (#5, DUMOXEL) and a small force, just enough to hold the crystal, was applied to the forceps by wrapping adhesive tape around it. The crystal was held in such a way that the edge to be intercalated was horizontal below the forceps. The set up for intercalation is shown in Fig. 4.1. The forceps were attached to a stand which was movable in the x, y and z directions using three micrometers with fine adjustments. The electrolyte used was 0.1 M AgNO$_3$ in glycerol. Below the crystal, the electrolyte was placed on a horizontal glass slide which could be moved vertically using a fine micrometer. A small piece of clean Ag metal which served as the anode was partially immersed in the electrolyte. A wire was attached to the metal forceps to make electrical contact to the crystal. Using a horizontal optical microscope (Olympus Model FH) with a white-light lamp, the crystal was viewed with light reflected from its surface. Observing through the microscope, the crystal was carefully lowered until the edge to be intercalated just touched the electrolyte. (This was a very delicate task since a small vibration may move the crystal too far into the electrolyte, wetting the surfaces of the crystal near the edge. Also, if the crystal edge is not parallel to the surface of the electrolyte only one side of the crystal will touch the

electrolyte while the other will remain in the air.)

After the crystal edge was in contact with the electrolyte, an electrical connection between the crystal and the Ag anode was made and the intercalation was started. The intercalation was carried out until the stage 2 front had moved in from the edge about 10 to 20 μm as observed through the optical microscope. (This distance was chosen to be appropriate after several samples were analyzed.) In most samples only stage 2 was observed while in a few of them, depending on the thickness, a narrow strip of stage 1 was visible near the edge. This narrow stage 1 region disappeared (by conversion to stage 2) soon after the intercalation was stopped and the crystals with only an apparent stage 2 region were used in AES analysis. After the crystal was intercalated to a sufficient distance, the circuit was disconnected and the crystal was carefully removed from the electrolyte. An optical photograph of the intercalated edge region was then taken, and was used to measure the front width seen optically and also to position the sample in Auger analysis. The crystal was then removed from the forceps into a clean petri dish and rinsed with acetone to wash off the electrolyte remaining on the crystal, followed by a final rinse with methanol.

4.2.3.   Sample mounting for Auger analysis

Samples to be used in Auger analysis were mechanically clamped onto sample holders specially provided for the SAM.

Since the TiS$_2$ crystals are too small to be clamped directly, they were first mounted on a clean, flat copper substrate (1 cm x 1 cm). Sample mounting was done under an optical microscope. To mount the TiS$_2$ crystal on the copper substrate, a tiny amount of graphite DAG was first placed on copper and then the crystal was gently pressed down on it until the graphite DAG was evenly spread underneath the crystal. When mounting the crystal, it was important to adjust the crystal orientation such that the intercalated edge was perpendicular to the x-direction (see Fig. 4.2) along which the line scans were to be carried out. The SAM-595 does not have the facility for adjusting the crystal orientation. The SAM sample holder with the Ag/TiS$_2$ crystal was then mounted on the specimen stage (carousel) in the main chamber of the SAM.

When mounting samples, great care had to be taken not to contaminate the sample, the copper substrate or the SAM sample holder. The forceps, petri dishes and glass slides used in the sample preparation were cleaned from time to time in order to remove dust particles deposited on them. The sample preparation in the experiments given here was extremely delicate from beginning to end, and many samples had to be discarded at various stages of the sample preparation procedure.

4.3 Auger analysis and sputtering

4.3.1 Auger analysis

The specimen stage of the SAM-595 provides stability and precise specimen movement via micrometers in the x, y and z directions. The accelerating potential of the electron beam used in Auger analysis was 3 kV and the beam size was about 0.4 μm.

The principal Auger peak energies obtained from standard spectra (50) are, 387 eV and 418 eV for Ti (LMM) from the elemental Ti spectrum, 152 eV for S (KLL) from the spectrum for CdS and 351 eV and 356 eV for Ag (MNN) from the elemental Ag spectrum. A deviation of several eV in peak energy from those obtained from a standard spectrum can be expected due to different chemical bonding if the element in question is in a different chemical environment.

After mounting the Ag/TiS_2 crystal on the specimen stage, the area to be analyzed was positioned on a TV monitor displaying the secondary electron image. Prior to the first line scan an Auger survey spectrum was obtained to identify the surface constituents using the area-averaged spectrum mode. A typical survey Auger spectrum $N(E)$ obtained for a Ag/TiS_2 sample is given in Fig. 4.3. The differentiated Auger spectrum $dN(E)/dE$, of Fig. 4.3 is shown in Fig. 4.4. Contamination of the sample surface with C and O was often found in Ag/TiS_2. This C and/or O layer must be removed by

brief sputtering before the analysis.

The locations of line scans on the sample were selected using secondary electron images displayed on a storage-type oscilloscope. The parameters specified for line scans are given in Appendix 1. For comparison, usually two or three line scans were performed at different locations on the sample surface. For every line selected the elemental distributions of Ag, S and Ti were obtained. Since the Ag signal was much weaker than S and Ti, a longer (10 times higher) data acquisition time was used for Ag to improve the signal to noise ratio. Another problem associated with the Ag signal was overlapping of the main Auger peaks for Ag (351 eV, 356 eV) with a minor Auger peak for Ti (354 eV). Since this was unavoidable, both signals were measured together and the Ti signal increased the background level of the Ag signal. The results of the line scans are given in Section 4.4.

Secondary electron images of the sample were useful for observing the intercalated regions directly where the intercalation fronts appeared as boundaries between regions with different contrast. During the analysis, polaroid photographs of the secondary electron images (SED photographs; SED stands for "secondary electron detection") of the sample were obtained at different depths.

4.3.2 Sputtering

After every line scan, the Ag/TiS$_2$ samples were sputtered using high purity argon ions to expose the underlying layers for analysis. The sputtering was done over a 2 mm x 2 mm raster area and the ion beam voltage used was 3 kV. The sputtering angle was about 40° to the sample surface. Since the depth to be sputtered is initially specified as the time to be sputtered, one has to know the sputtering rate for the sample material in order to find out the depths where the line scans are performed. The sputtering rate for Ag/TiS$_2$ samples was found to be 120 A/min (chapter 5) for the settings used. In the results presented in section 4.4, the sputtered depths were calibrated using this sputtering rate.

4.4 Results - Line scans

The Auger line scans obtained at depths near the crystal surface revealed that Ag had intercalated not only near the edge as shown on the optical photographs, but all the way across the crystal as far as the line scans were carried out, typically up to about 300 to 400 μm. As the sputtering depth was increased, some intercalated regions were detected which were much wider than the initial intercalated region seen on the optical photographs. In some line scans more than one intercalated region with different Ag concentrations were detected at a given depth. As the sputtering depth was

increased much deeper into the middle of the crystal, the widths of the intercalated regions decreased gradually. The line scans and the SED photographs obtained at a given depth were correlated to determine the locations of the intercalation fronts at that depth.

To present these results more clearly, the data obtained from one sample are given here as an example. Fig. 4.5 shows an optical photo of an intercalated TiS_2 crystal with an intercalated region of ~ 15 µm measured from the crystal edge. The initial line scan for this sample was obtained at a depth (d) of 50 Å below the surface and the Ag distribution is presented in Fig. 4.6 (Line 1 or L1). The high noise level seen in the Ag line scans was unavoidable as discussed in section 4.3.1. (For this sample, the data acquisition time was doubled after the second line scan to improve the signal to noise ratio.) To find the relative amount of Ag in each line scan and to compare the values with other line scans obtained at different depths, the ratio of Ag to S average counts will be considered later (chapter 6). The Ag line scan given in Fig. 4.6 shows more or less a constant distribution of Ag up to a distance of 320 µm from the crystal edge. The area beyond this distance was checked on a SED image displayed on the storage monitor, but no intercalation fronts were observed. Following the Line 1, a series of line scans were performed at different depths, the results of which are presented below.

<u>d = 170 A</u>: After the Line 1 the sample was sputtered for another minute (120 A) and a Ag line scan obtained at this depth (d = 170 A) is given in Fig. 4.7 (Line 2 or L2). It seems that there is a slight decrease of Ag after 230 µm.

<u>d = 410 A</u>: Next, the sample was sputtered for another 240 A (i.e., d = 410 A) and a silver line scan obtained at this depth is given in Fig. 4.8. This line scan (L3) shows a significant decrease in the Ag signal near 25 µm. A fairly sharp intercalation front near 25 µm and another faint front near 35 µm were observed on the SED image displayed on the storage monitor. Unfortunately, these fronts are not seen very clearly on the SED photograph given in Fig. 4.9. In L3, the region 0 - 25 µm seems to have been intercalated with the same silver concentration. The intercalated region seen on the SED photograph from 25 to 35 µm appears to be a transition region between the two intercalated regions seen on the line scan with different silver concentration. (A similar effect can be seen in the line scan given in Fig. 4.11.)

The line scan L3 shown in Fig. 4.8 was performed near the edge area up to 100 µm, in order to study the area of interest more carefully. An SED image of the crystal at low magnification did not show any fronts other than the ones given here. Line 3 shows that the crystal has been intercalated beyond the distance shown in the original optical photograph (15 µm) in Fig. 4.5.

<u>d = 530 A</u>: An SED image obtained after sputtering the sample
for another minute (d = 530 A) showed a clear front near 35 μm
and another less sharp front near 47 μm (Fig. 4.10). The Ag
line scan (L4) obtained at this depth is given in Fig. 4.11.
In L4, a drop of the Ag amount is seen near 38 μm. The front
seen near 35 μm on the SED photograph seems to correspond to
the front seen near 38 μm in L4. The low contrast region seen
on the SED photograph between 35 and 47 μm seems to be a
transition region which separates the two intercalated regions
seen in Fig. 4.11 from 0 to 38 μm and beyond 38 μm.

The SED photograph in Fig. 4.10 shows a front near 15
μm even though the line 4 indicates that the region from 0 to
38 μm has intercalated with the same concentration of Ag. It
is possible that the bright region seen on the SED photograph
from 0 to 15 μm is due to the detection of Ag which is
distributed at a greater depth as in Line 6. A high
concentrated Ag region was found in L6 from 0 to 15 μm (see
Fig. 4.16 later). Although the secondary electron detector in
the SAM-595 is more sensitive to the low-energy secondary
electrons (~ 50 eV), the high energy backscattered electrons
travelling towards the detector may also be detected. The
high energy backscattered electrons coming from greater depths
in the sample may carry information from underlying layers.
Since the Auger analysis is surface sensitive, the results
obtained from line scans are considered to be more accurate
for surface analysis.

<u>d = 650 A</u>: An SED photograph and a Ag line scan (Line 5) obtained at d = 650 A are shown in Figs. 4.12 and 4.13, respectively. The front seen on the SED photograph near 43 μm corresponds to the front seen in L4 near 40 μm. Again it seems that there exists a transition region between 40 and 50 μm.

<u>d = 890 A</u>: The sample was then sputtered for another two minutes (d = 890 A). Two SED photographs taken at high and low magnification are presented in Figs. 4.14a and b. Fig. 4.14a shows that the intercalated regions have advanced slightly farther into the crystal. No line scan was obtained at d = 890 A.

<u>d = 1130 A</u>: An SED photograph and a Ag line scan (Line 6) obtained at this depth are presented in Figs. 4.15 and 4.16, respectively. This is the first line scan which shows a sharp decrease in the Ag distribution near 15 μm. This indicates that the stage 2 region is present in the crystal at this depth.

<u>d = 1370 A and 1600 A</u>: The SED images were checked at these depths but no line scans were obtained. No major changes were observed on the SED images. However, the intercalation front which was at 56 μm in Line 6 had advanced by few μm.

<u>d = 1850 A</u>: Figs. 4.17 and 4.18 show an SED photograph and a

Ag line scan (Line 7) obtained at d = 1850 A. The second
intercalated region from the edge has advanced farther into
the crystal. After the first intercalated region ($\sim$ 13 μm),
the line scan shows a slight slope indicating that the Ag
concentration is not exactly constant but slightly decreasing.
After this line scan (i.e. at greater depths) the width of the
second intercalated region started to decrease. The front
near 13 μm is not clearly shown on the SED photograph but was
observed on the image on the storage monitor.

d = 2090 A and 2570 A: The SED photographs obtained at these
depths are shown in Figs. 4.19 and 4.20, respectively. The
first front near the edge ($\sim$ 13 μm) is not seen in these SED
photographs, most probably due to poor contrast between the
two regions. However, this front was slightly visible on the
SED image display. The front seen at 60 μm in Fig. 4.17 has
advanced to 63 μm in Fig. 4.19 and then to 65 μm in Fig. 4.20.
No line scans were performed at these depths.

d = 3050 A: Figs. 4.21 and 4.22 show an SED photograph and
a Ag line scan obtained at this depth, respectively.

d = 3770 A: A decrease of the width of the second intercalated
region was observed in the SED photograph (Fig. 4.23) and in
the Ag line scan (Line 9, Fig. 4.24) obtained at this depth.
Both figures show a front near 65 μm. The front which is seen
near 52 μm on the SED photograph does not appear clearly on

the line scan. The higher contrast in the region from 13 to 52 μm in Fig. 4.23 may have arisen from a Ag region at a depth higher than d = 3770 Å (see page 73).

d = 4730 Å: An SED photograph and a Ag line scan obtained at this depth are presented in Figs. 4.25 and 4.26. As one can see in the line scan, the width of the broader intercalated region is decreasing. The front observed at 42 μm on the SED photograph in Fig. 4.26 does not appear clearly in the line scan (L10) in Fig. 4.26. Since the width of the intercalated region is decreasing it is possible that a front was present near 42 μm at a depth greater than d = 4730 Å.

d = 5930 Å: The sample image was checked on the storage monitor and three fronts were seen at 35, 30 and near 13 μm. No line scan was performed at this depth.

d = 6890 Å: Data obtained at this depth is given in Figs. 4.27 and 4.28. From the line scan (L11), it is clear that the width of the intercalated region beyond 11 μm has reduced. Also the concentration of Ag in this region seems to be gradually decreasing. (The uneven widths of the intercalated regions seen in this sample (Fig. 4.27) may possibly be due to a defect at the crystal edge.)

d = 8330 Å: A line scan obtained at this depth, presented in Fig. 4.29, shows only one intercalation front near 12 μm. It

seems that the intercalated region beyond 12 μm has disappeared totally. An SED photograph is not included here since the front was only barely visible. However, the position of the front on the photograph was consistent with that found in the line scan.

d = 9290 Å: An Auger Ag line scan obtained at this depth is shown in Fig. 4.30 (Line 13). Only one intercalated region near the crystal edge is evident as observed in L12.

d = 10,730 Å: Fig. 4.31 shows a Ag line scan (Line 14) obtained at this depth. This line scan is similar to L12 and L13.

After L14, another line scan was done at d = 13,600 Å and a distribution of Ag similar to that of L14 was found. Since the surface irregularities due to sputtering became prominent beyond around 10,000 Å, the analysis was not carried out further. The original thickness of the TiS₂ crystal described here was 3 μm, thus, about half of the crystal thickness has been analyzed. Figs. 4.32a and b represent the typical Auger line scans for sulfur and titanium in a Ag/TiS₂ crystal.

The line scans obtained for this sample at different depths are compiled in chapter 6 for comparison. Consistent results were obtained from all samples (about 10) used in Auger analysis.

The data presented in this chapter is discussed in

chapter 6. Additionally, more data is presented to clarify some observations of the motion of Ag atoms.

Fig. 4.1 Schematic diagram of the setup used for
electrointercalation of TiS_2 crystals.
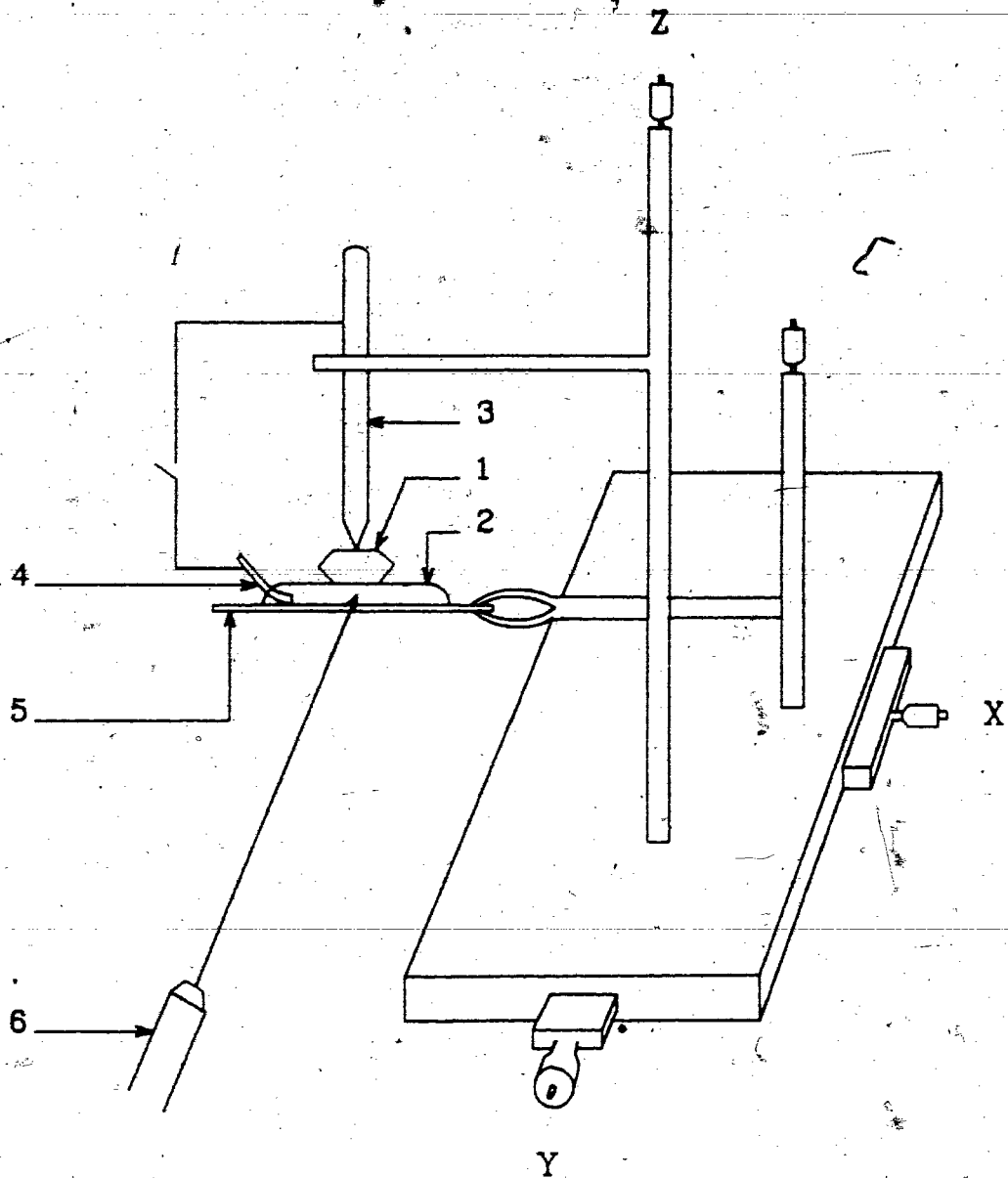
1	TiS$_2$ crystal	4	Piece of Ag (anode)
2	Electrolyte	5	Glass slide
3	Forceps	6	Optical microscope

Fig. 4.1

Fig. 4.2 (a) Ag/TiS$_2$ sample mounted on a SAM sample holder.

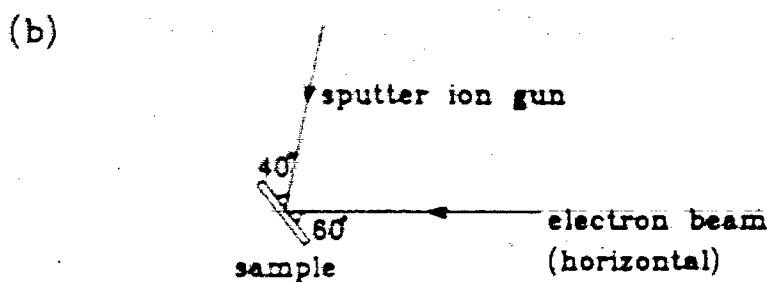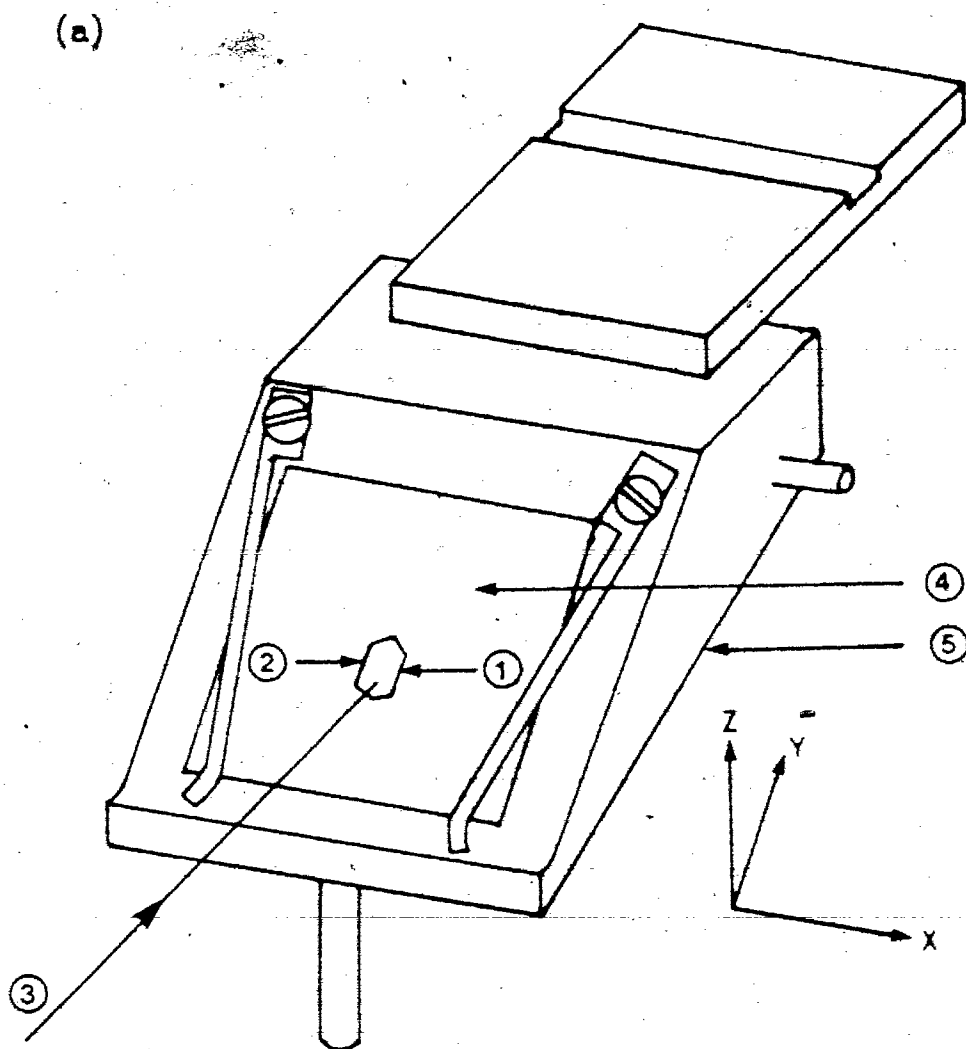(b) Sketch showing the direction of the electron

beam and the sputter ion beam.

(a)

① Ag/TiS₂ crystal   ④ Cu substrate
② Intercalated crystal edge ⑤ SAM sample
③ Electron beam   holder

(b)

Fig. 4.2

Fig. 4.3 Typical Auger survey spectrum for a Ag/TiS$_2$ crystal.

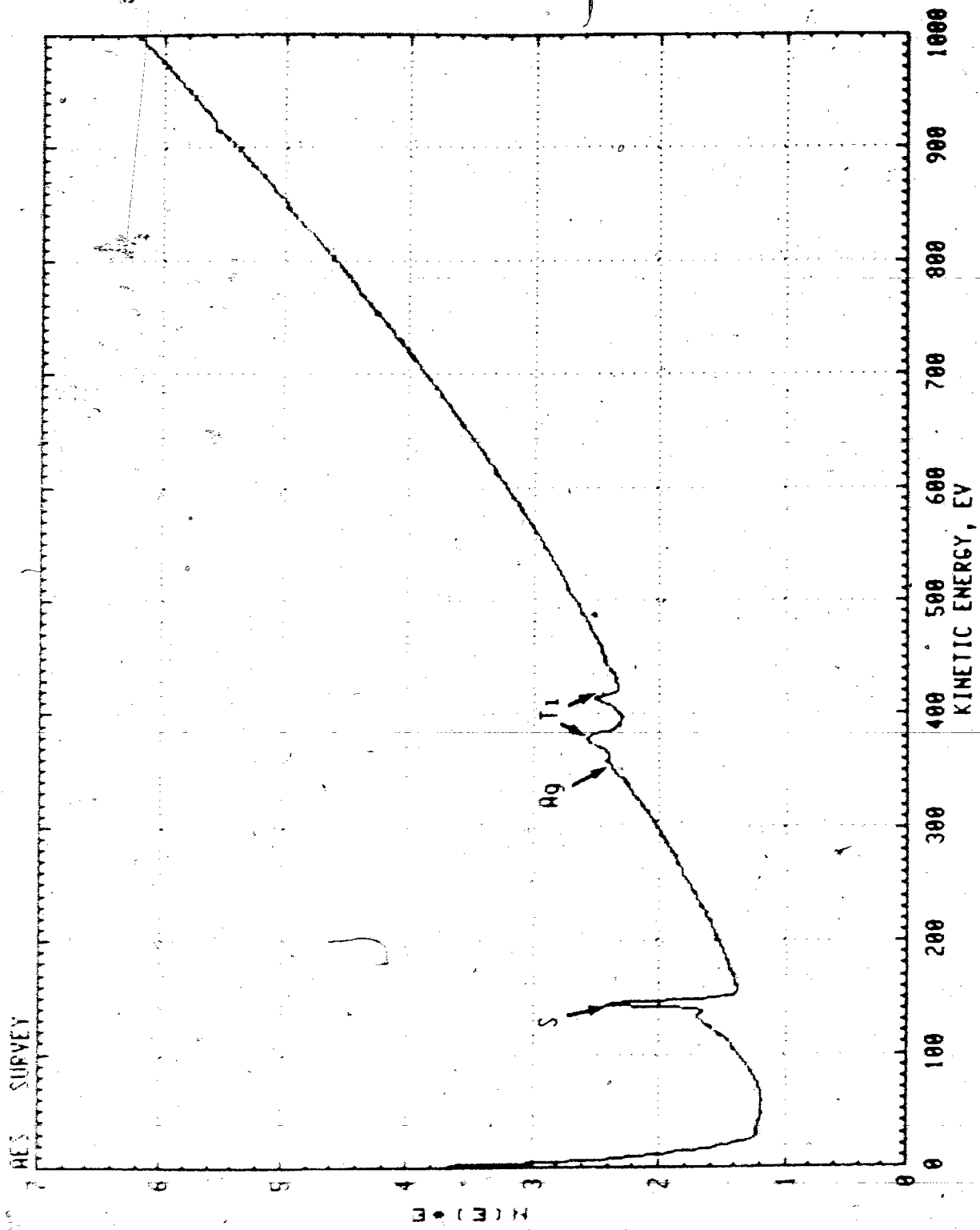AES SURVEY

Fig. 4.3

KINETIC ENERGY, EV

$H(E)*E$

Fig. 4.4   dN(E)/dE spectrum of the Auger survey given in
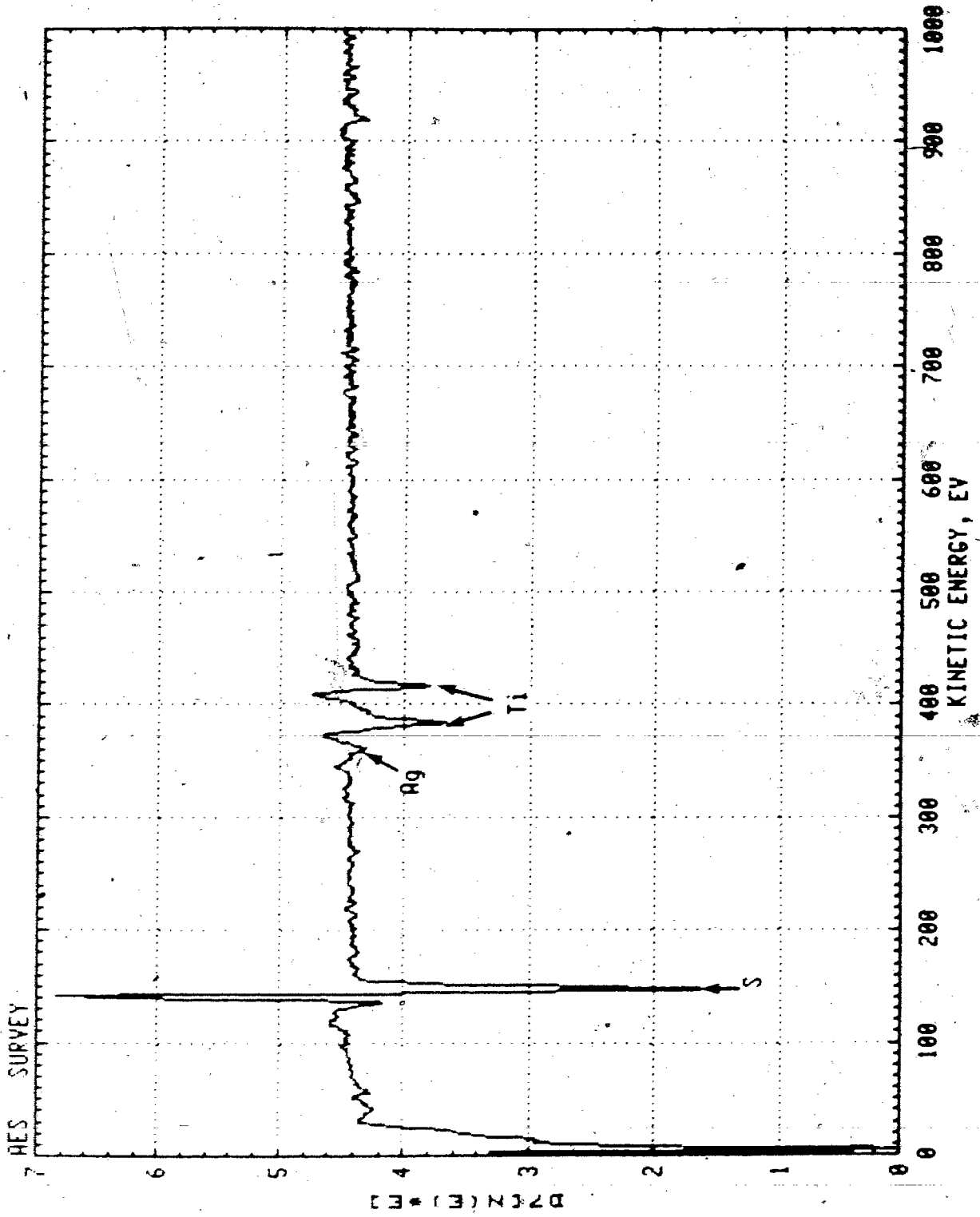
Fig. 4.3.

AES SURVEY

Fig. 4.4

Fig. 4.5 Optical photograph of the intercalated Ag/TiS$_2$

crystal used for line scans presented in

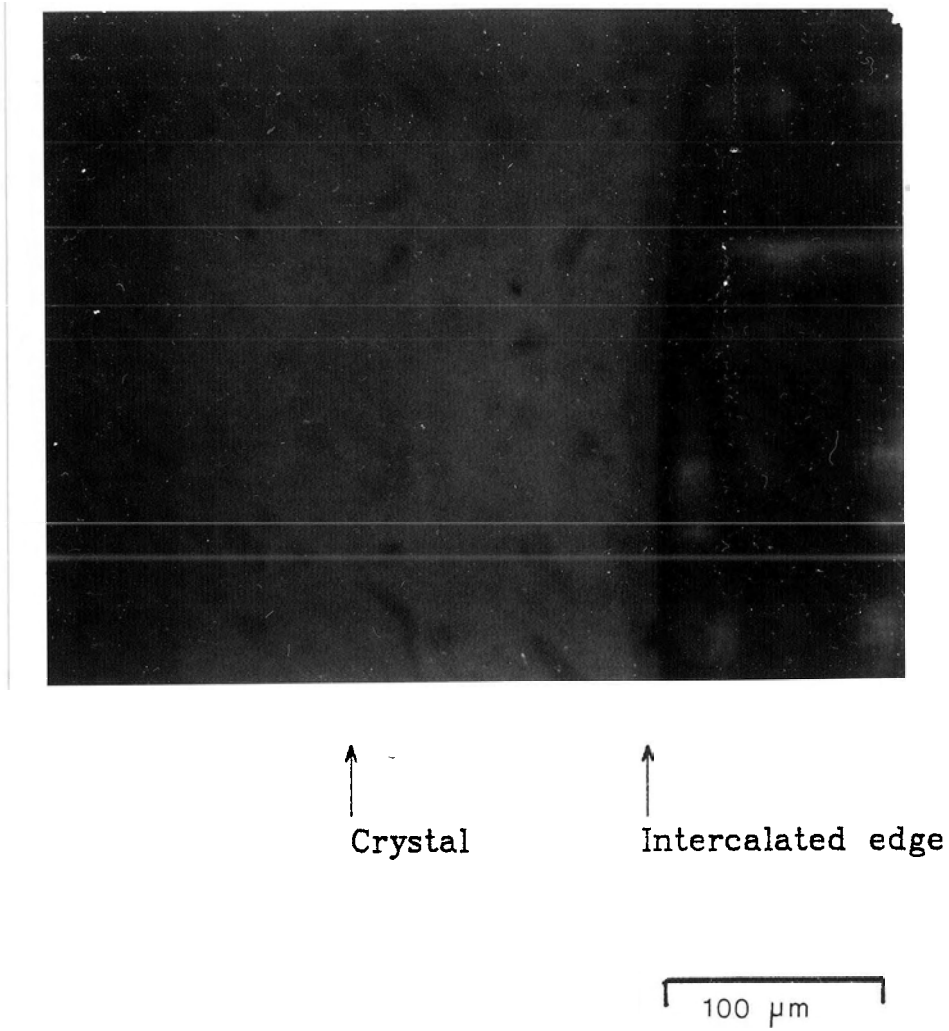section 4.4.

Width of the intercalated region = 15 µm.

Crystal   Intercalated edge

100 μm

Fig. 4.5

Fig. 4.6 Auger line scan for Ag at d = 50 A.
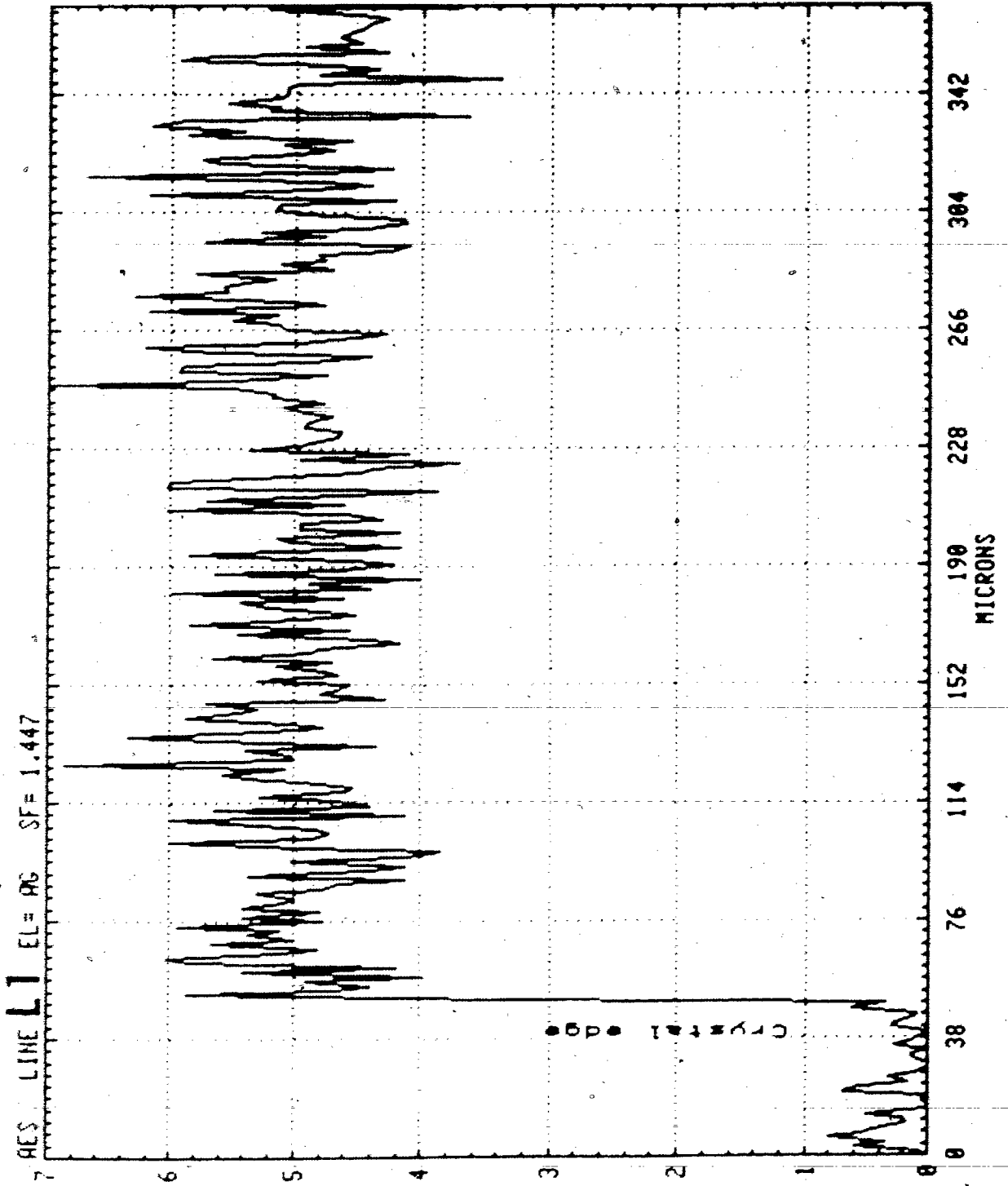
Fig. 4.6

Fig. 4.7 Auger line scan for Ag at d = 170 A.
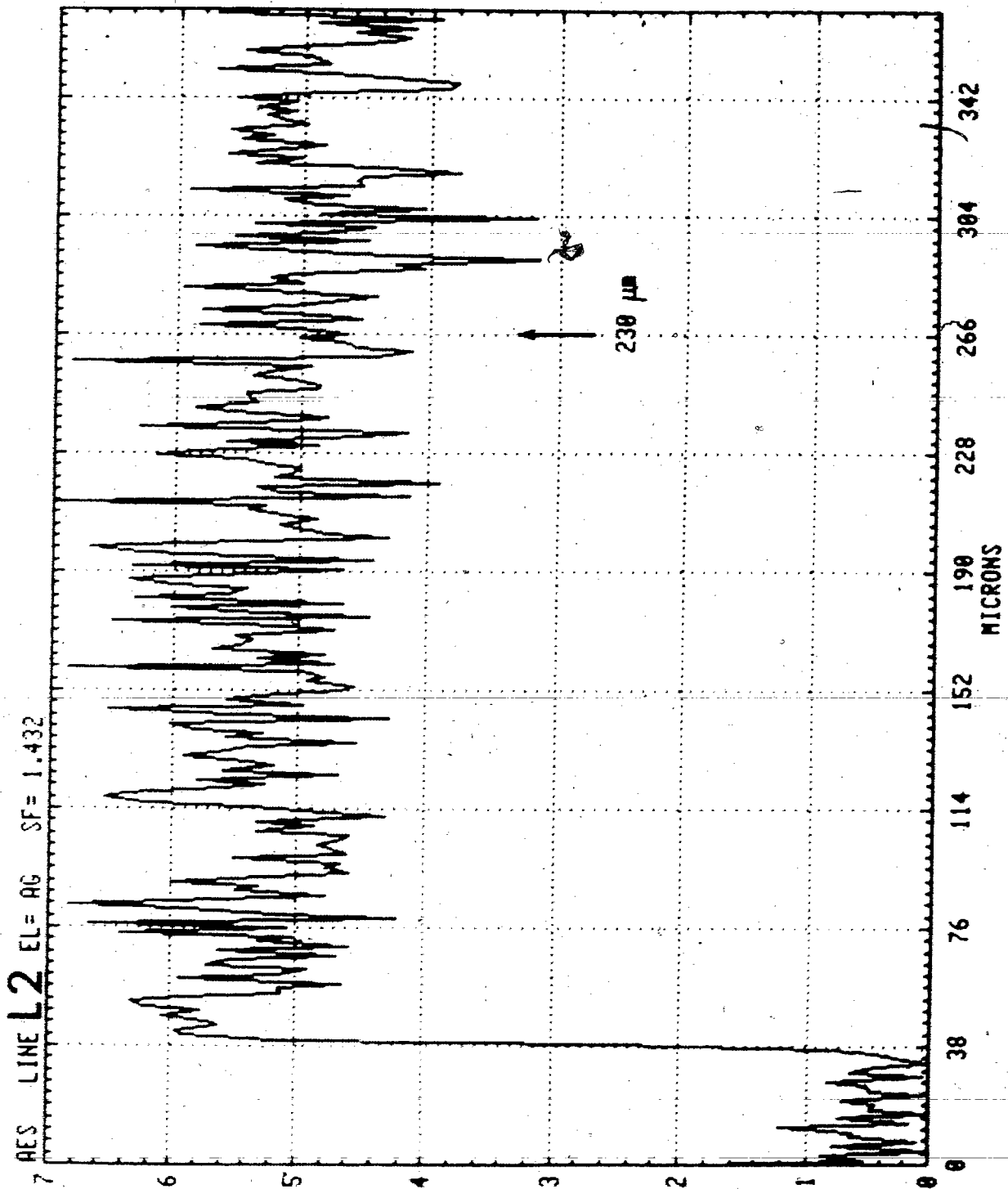
Fig. 4.7

Fig. 4.8 Auger line scan for Ag at d = 410 A.

A decrease of the Ag amount is seen near 25 μm.
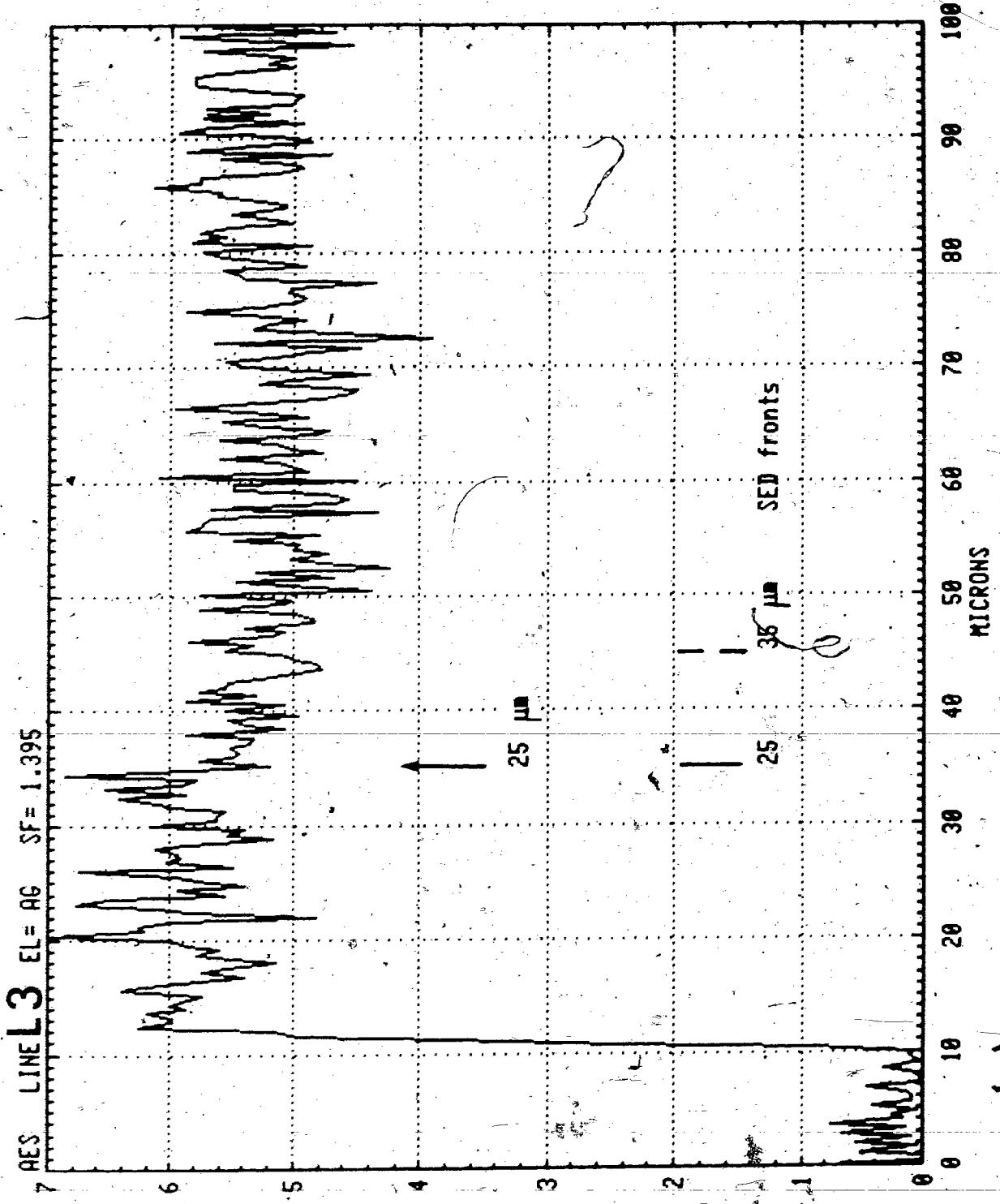
Fig. 4.8

Fig. 4.9 SED photograph of the crystal at d = 410 A.

The photograph does not show the fronts very clearly.

As seen on the SED image the fronts were found at

25 μm and 35 μm.
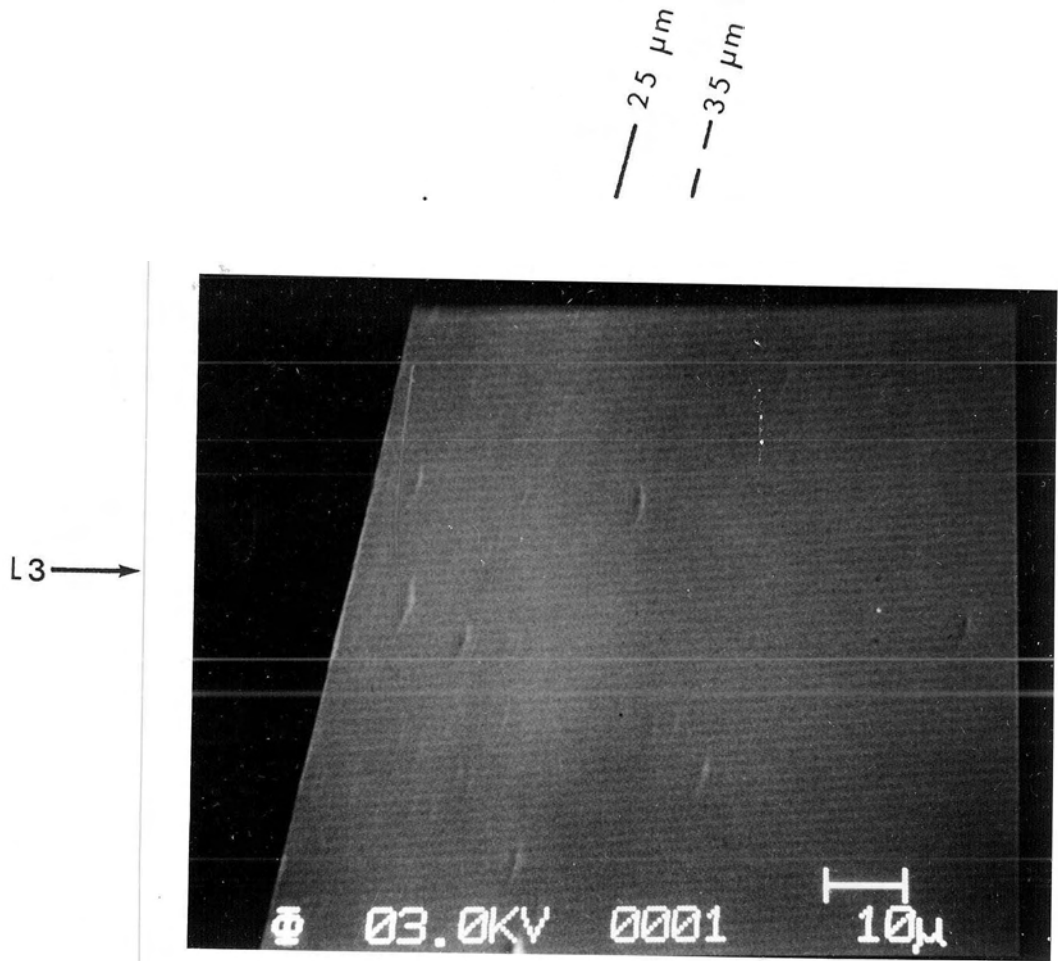
Fig. 4.9

Fig. 4.10 SED photograph of the crystal at d = 530 Å.

Two fronts were seen at

35 μm - sharp
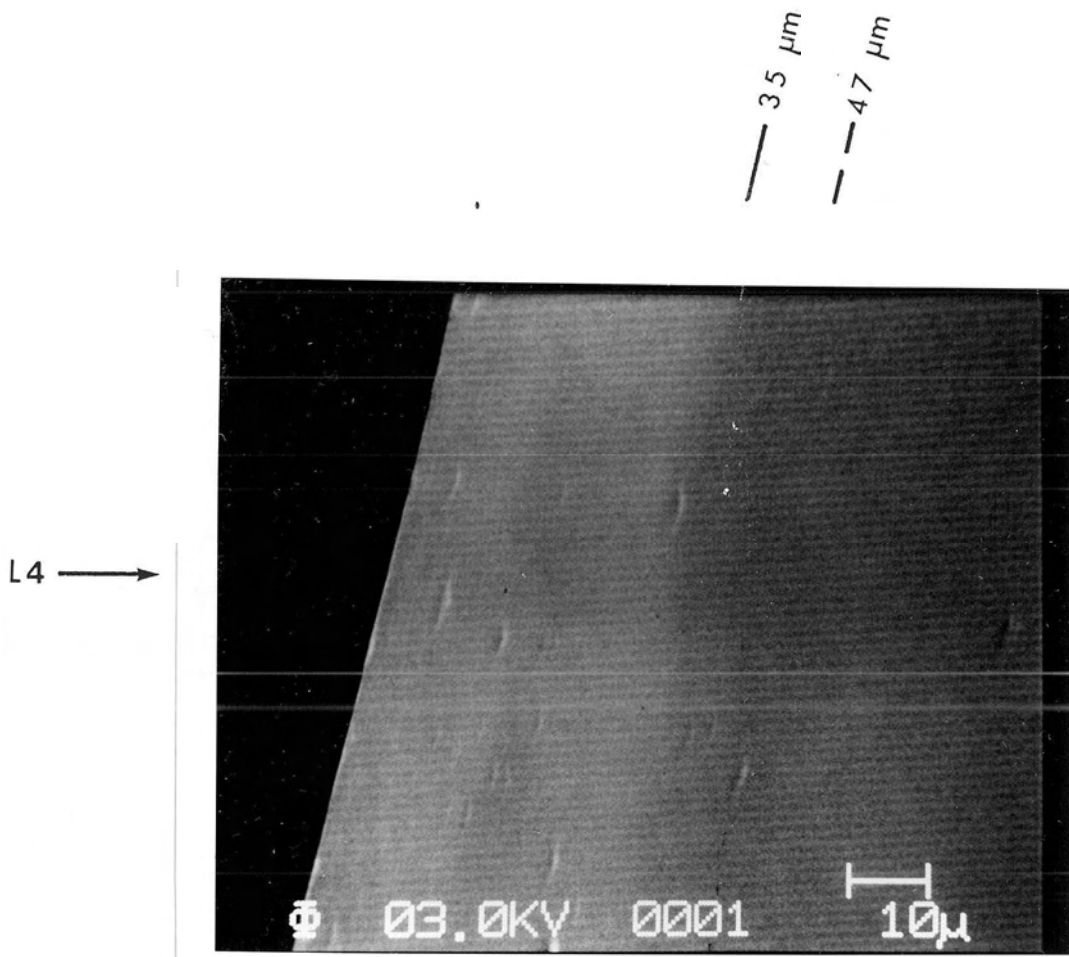
47 μm - not sharp.

Fig. 4.10

Fig. 4.11 Auger line scan for Ag at d = 530 A.
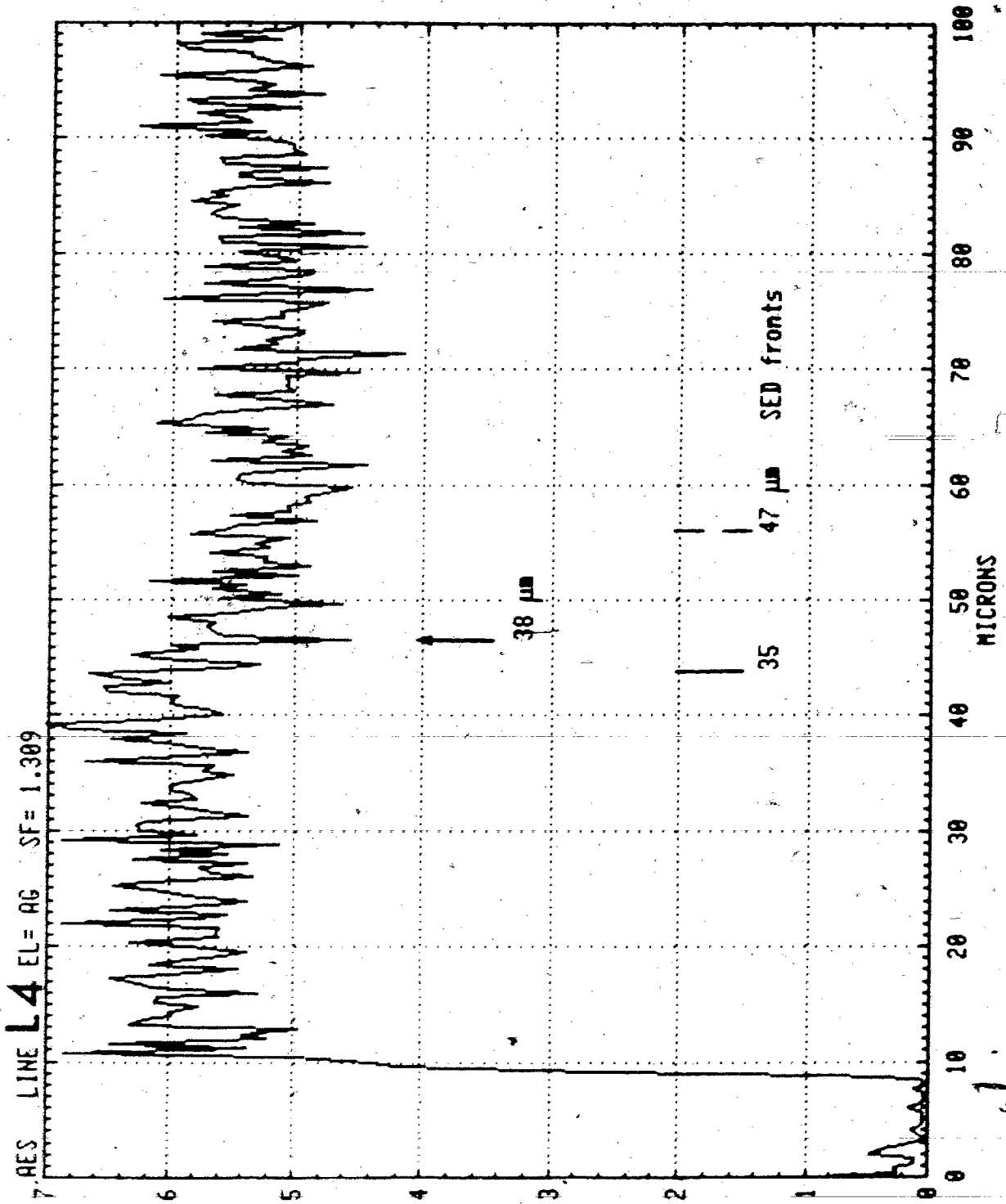
Fig. 4.11

Fig. 4.12   SED photograph of the crystal at d = 650 Å.

Fronts were seen at

43 µm   - sharp

50 µm   - not sharp.

43 μm
50 μm

L5 →

03.0KV 0001 10μ
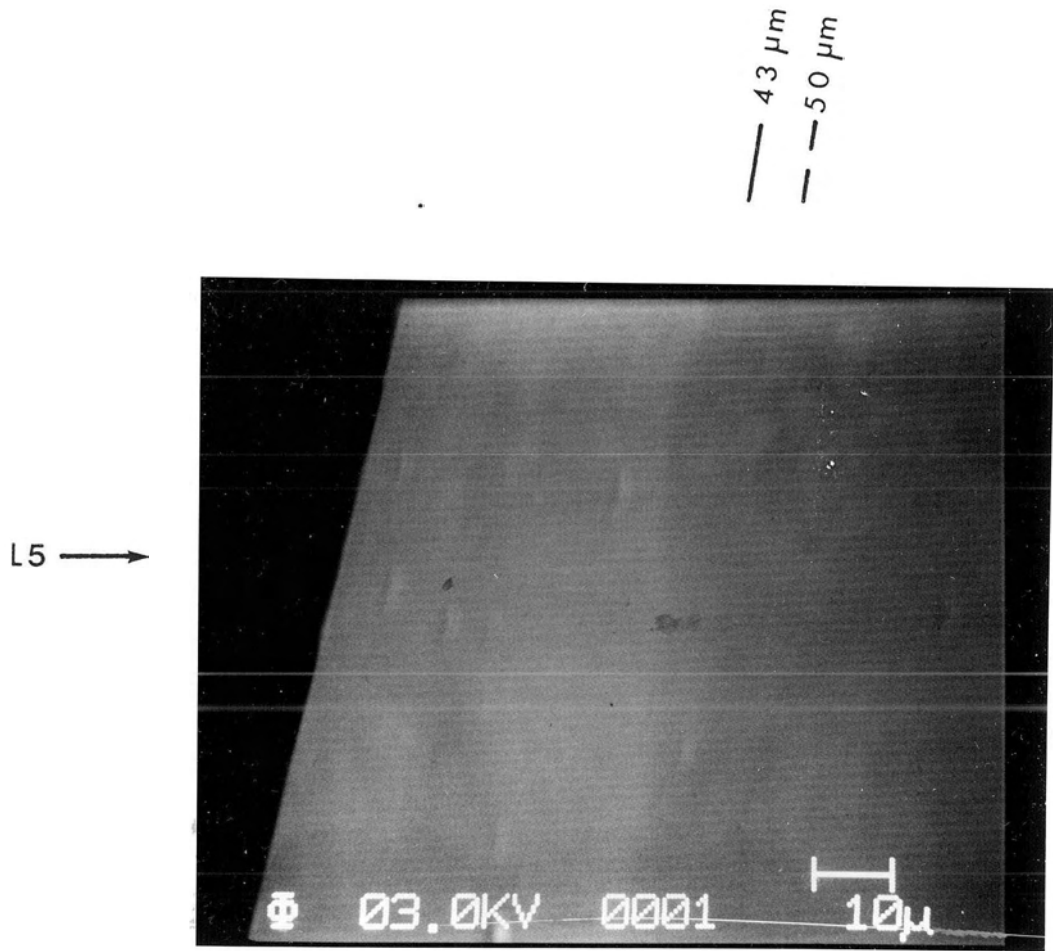
Fig. 4.12

Fig. 4.13 Auger line scan for Ag at d = 650 A.
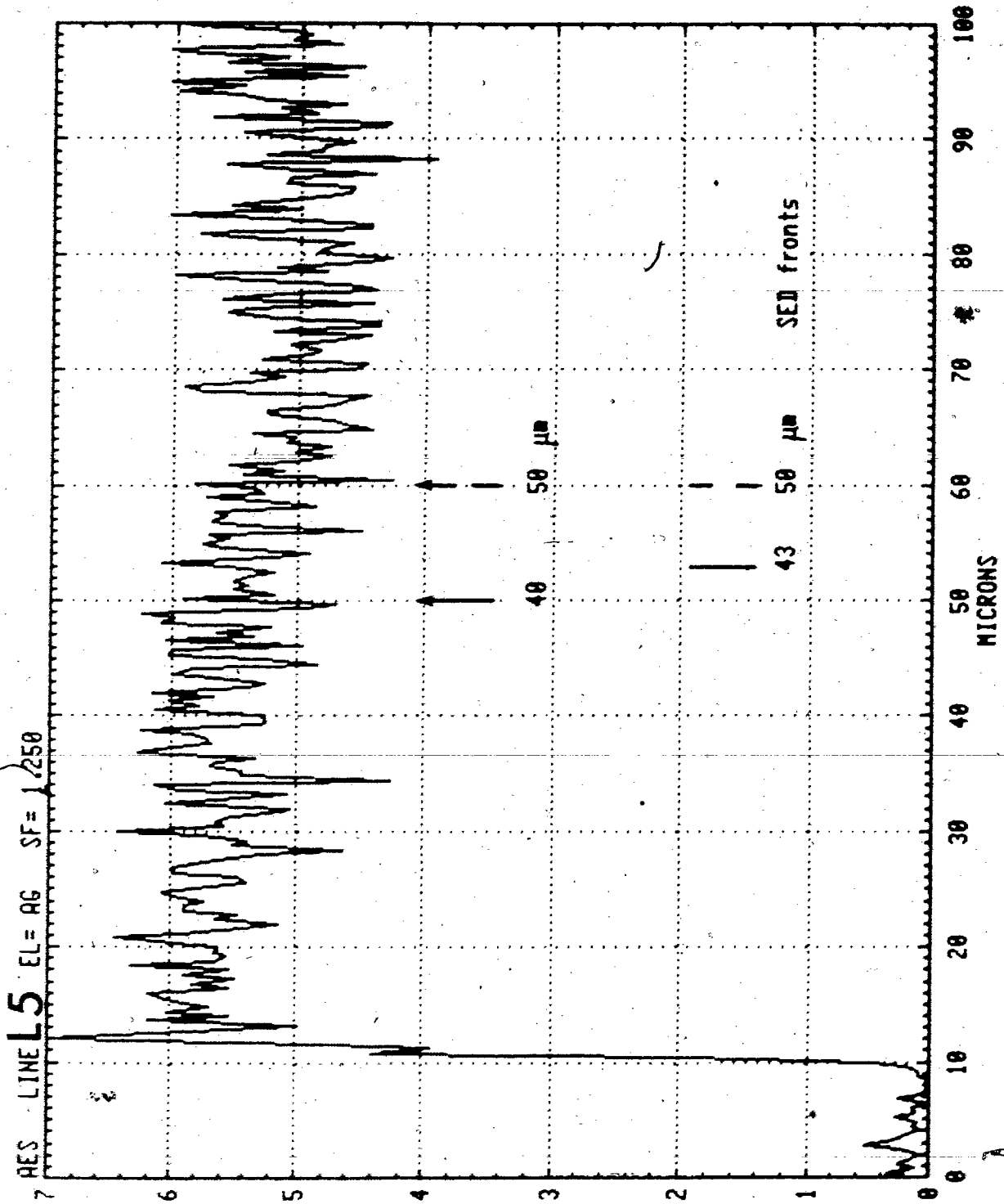
Fig. 4.13

Fig. 4.14   SED photograph of the crystal at d = 890 A.

    (a) at magnification x 1000 fronts were seen at

       50 μm - sharp

       .57 μm - not sharp.

    (b) at magnification x 124

(a)

50 μm
57 μm

Φ 03.0KV 0001 10μ

(b)

ᴃ 03.0KV 0001 100μ
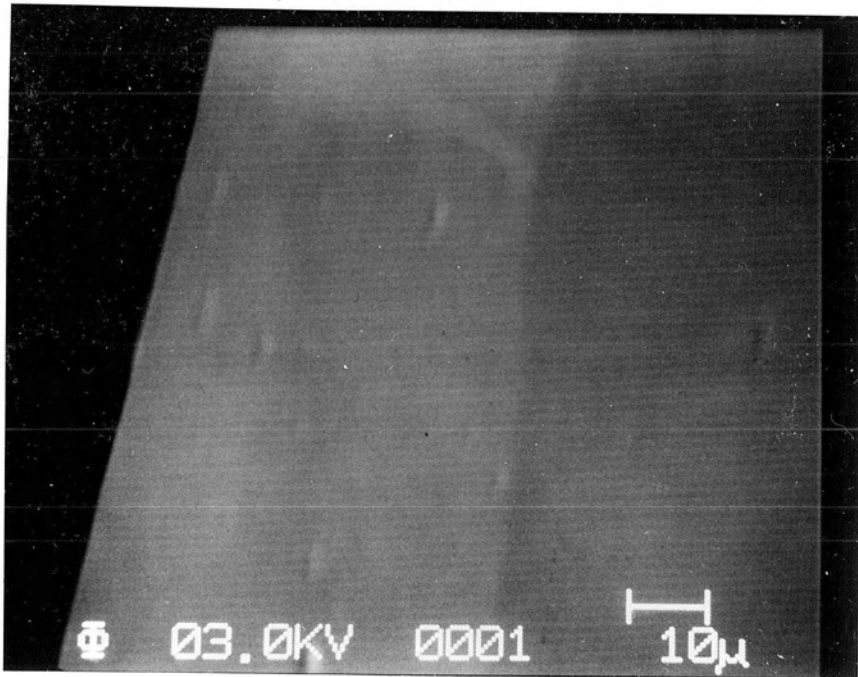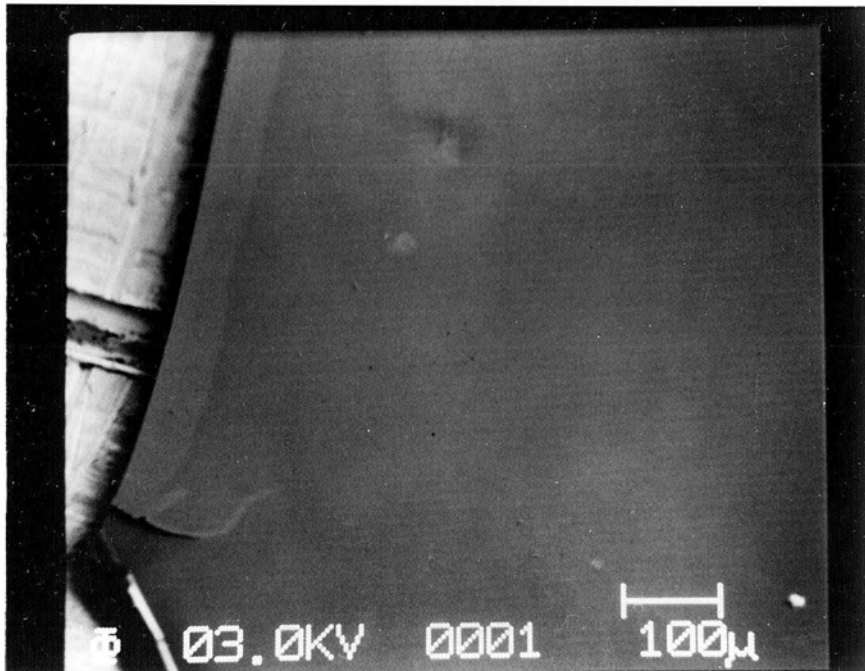
Fig. 4.14

Fig. 4.15 SED photograph of the crystal at d = 1130 A.

~ 15 μm

5 4 μm

L6 ⟶

Φ 03.0KV 0001 10μ
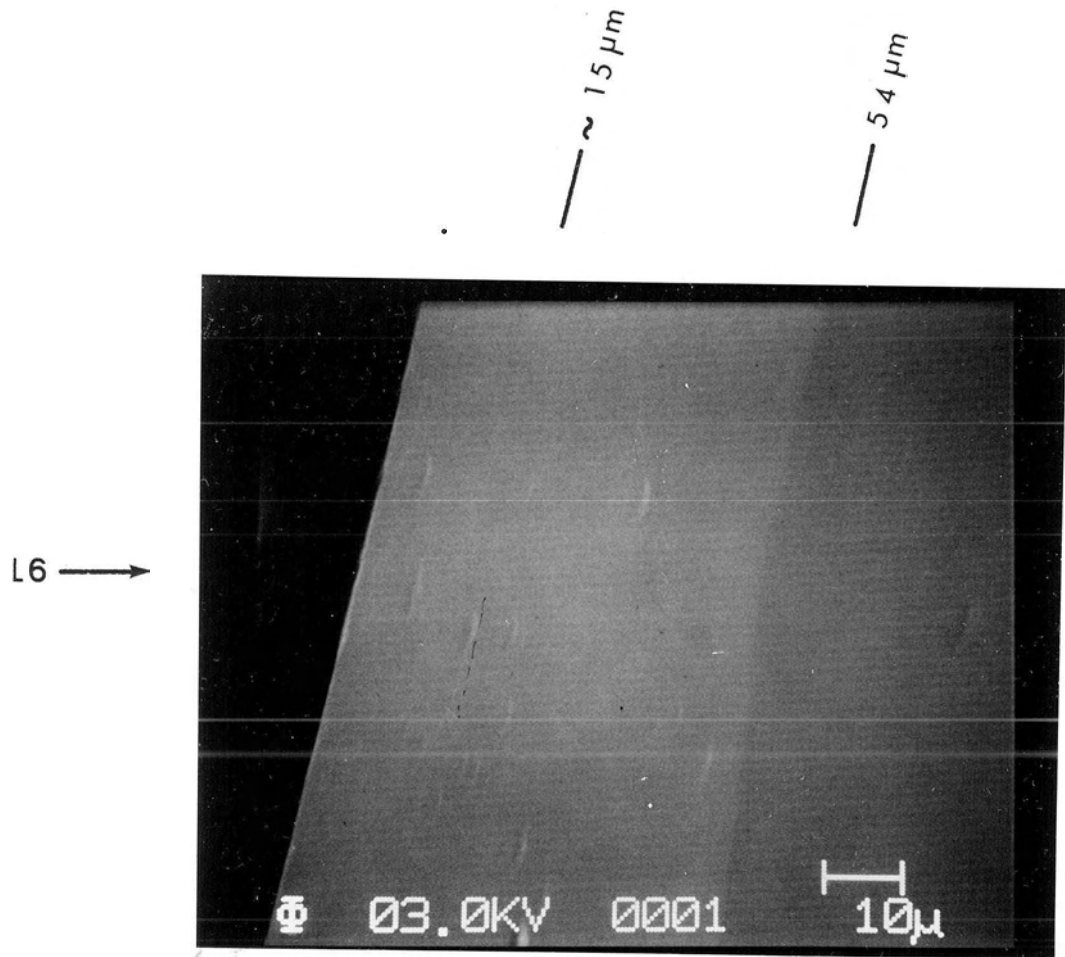
Fig. 4.15

Fig. 4.16 Auger line scan for Ag at d = 1130 A.
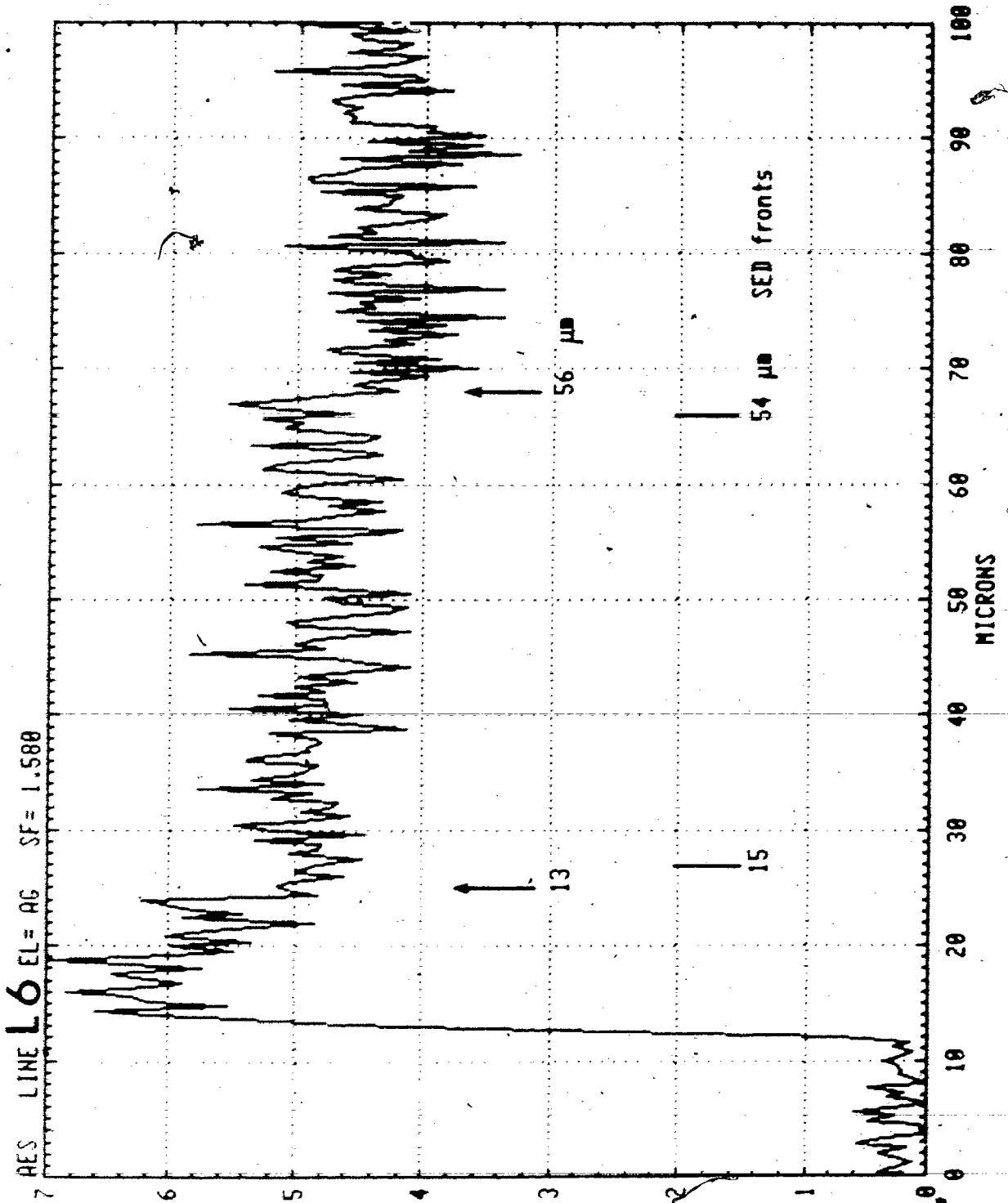
Fig. 4.16

Fig. 4.17   SED photograph of the crystal at d = 1850 A.

Fronts were seen at

62 μm - sharp

73 μm - not sharp.

13 µm

62 µm

73 µm

L7 →

Φ 03.0KV 0001 10µ
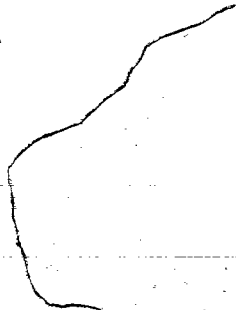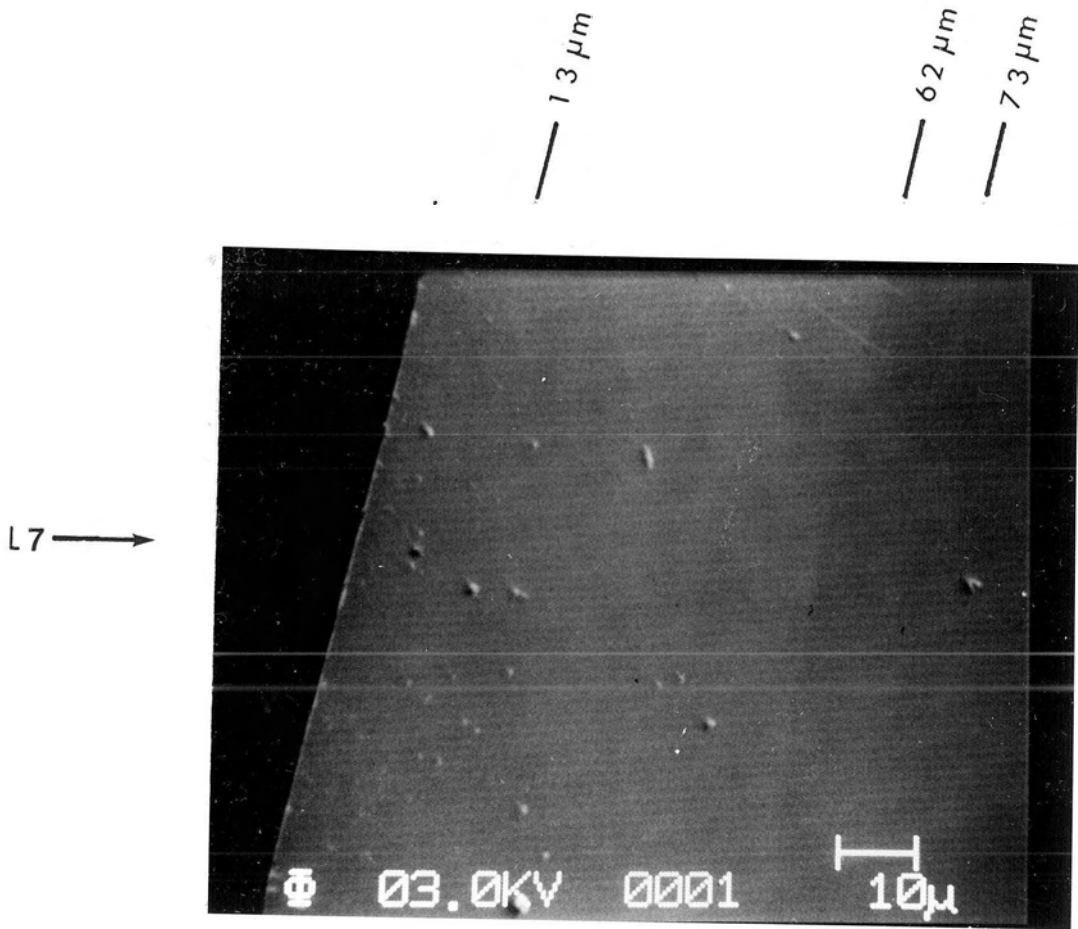
Fig. 4.17

Fig. 4.18   Auger line scan for Ag at d = 1850 A.
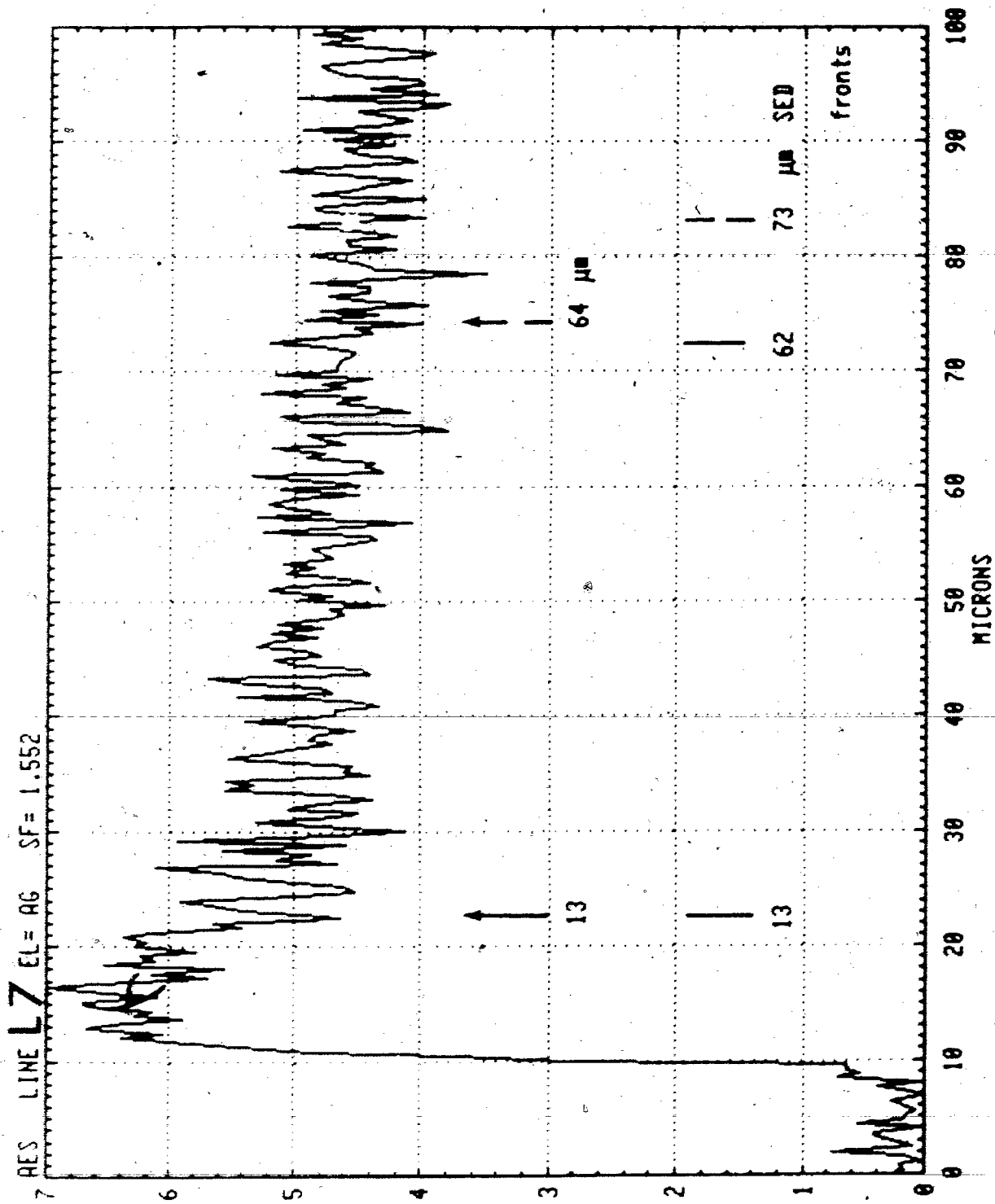
Fig. 4.18

Fig. 4.19 SED photograph of the crystal at d = 2090 A.

13 μm

63 μm

Φ 03.0KV 0001 100μ
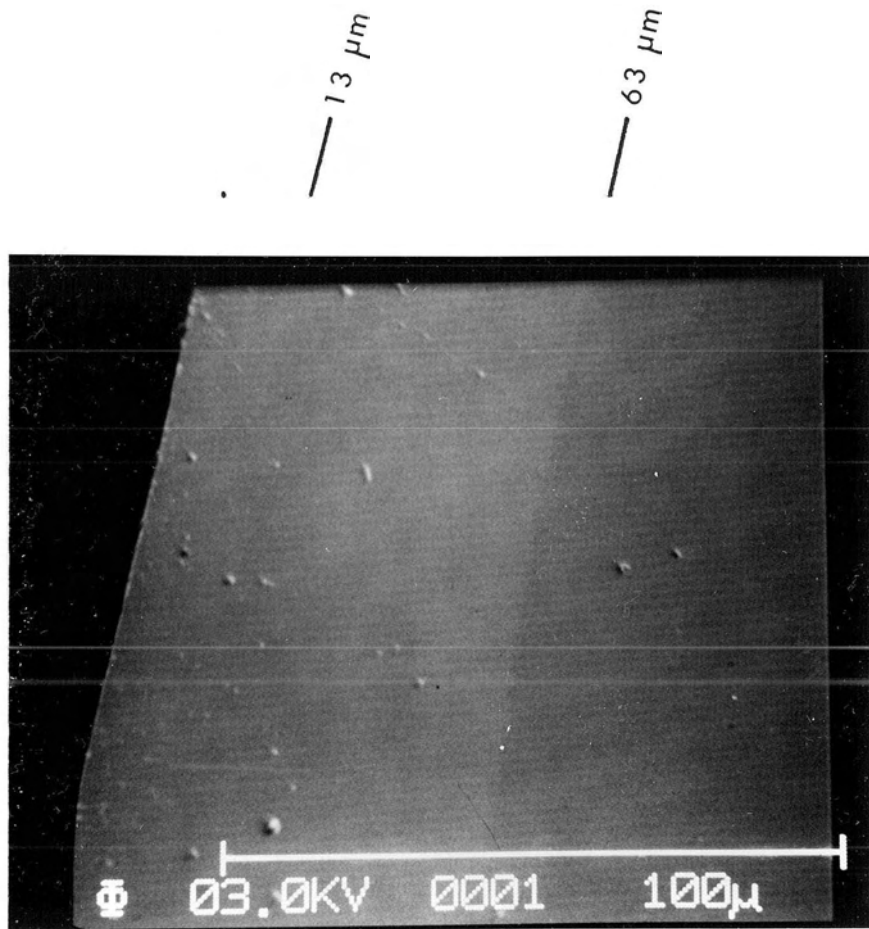
Fig. 4.19

Fig. 4.20   SED photograph of the crystal at d = 2570 A.

13 μm

65 μm

Φ 03.0KV   0001   100μ
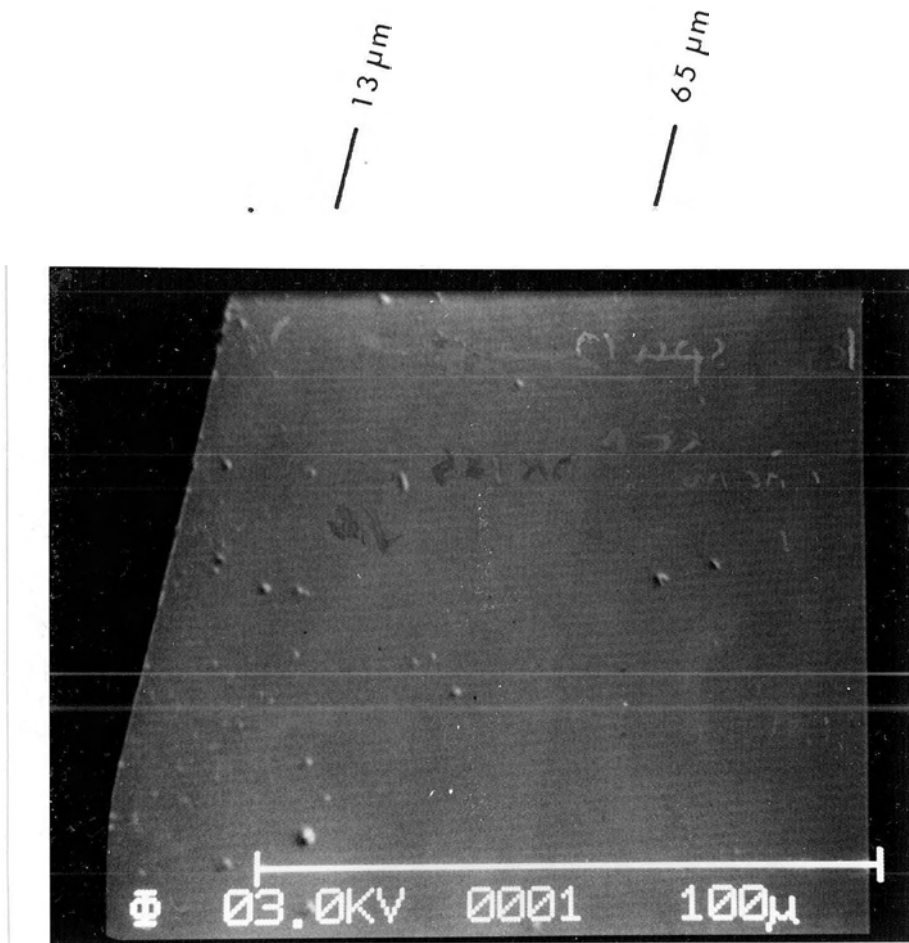
Fig. 4.20

Fig. 4.21 SED photograph of the crystal at d ≠ 3050 A.

Three fronts were seen

near 13 μm (clearly seen on the SED display)

at 61 μm

at 66 μm.

13 μm

61 μm
66 μm

L8 →

Φ 03.0KV   0001   100μ
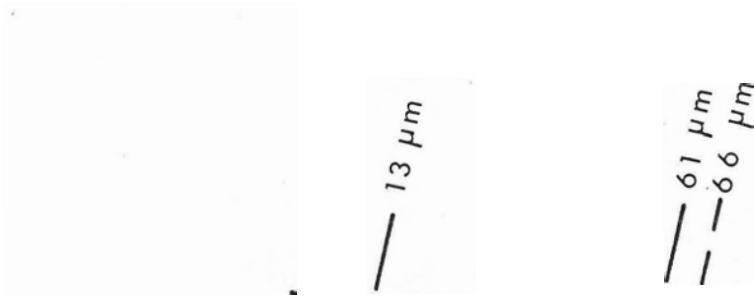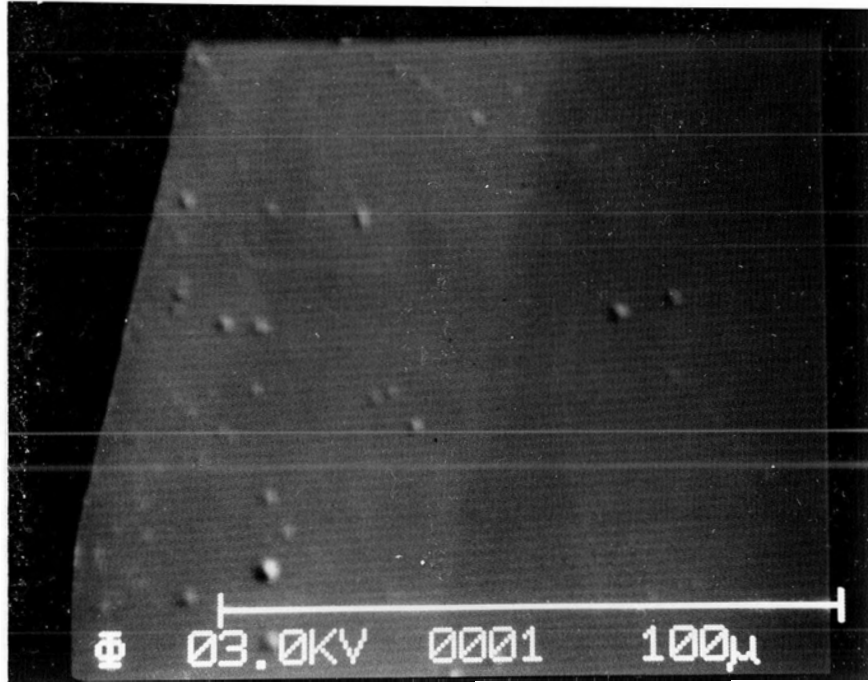
Fig. 4.21

Fig. 4.22   Auger line scan for Ag at d = 3050 A.
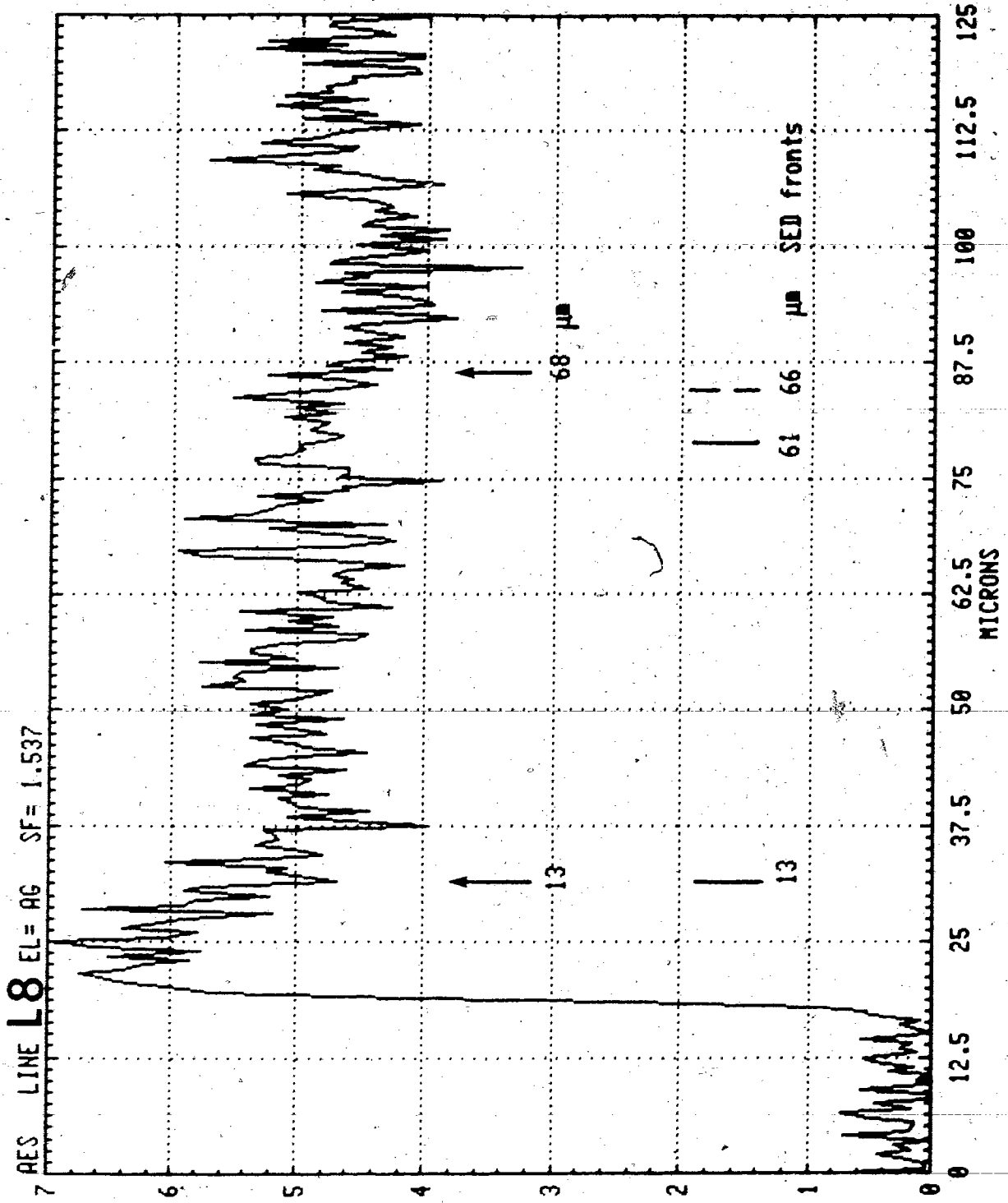
Fig. 4.22

Fig. 4.23   SED photograph of the crystal at d = 3770 A.

Fronts were seen at

13 μm

52 μm

65 μm.
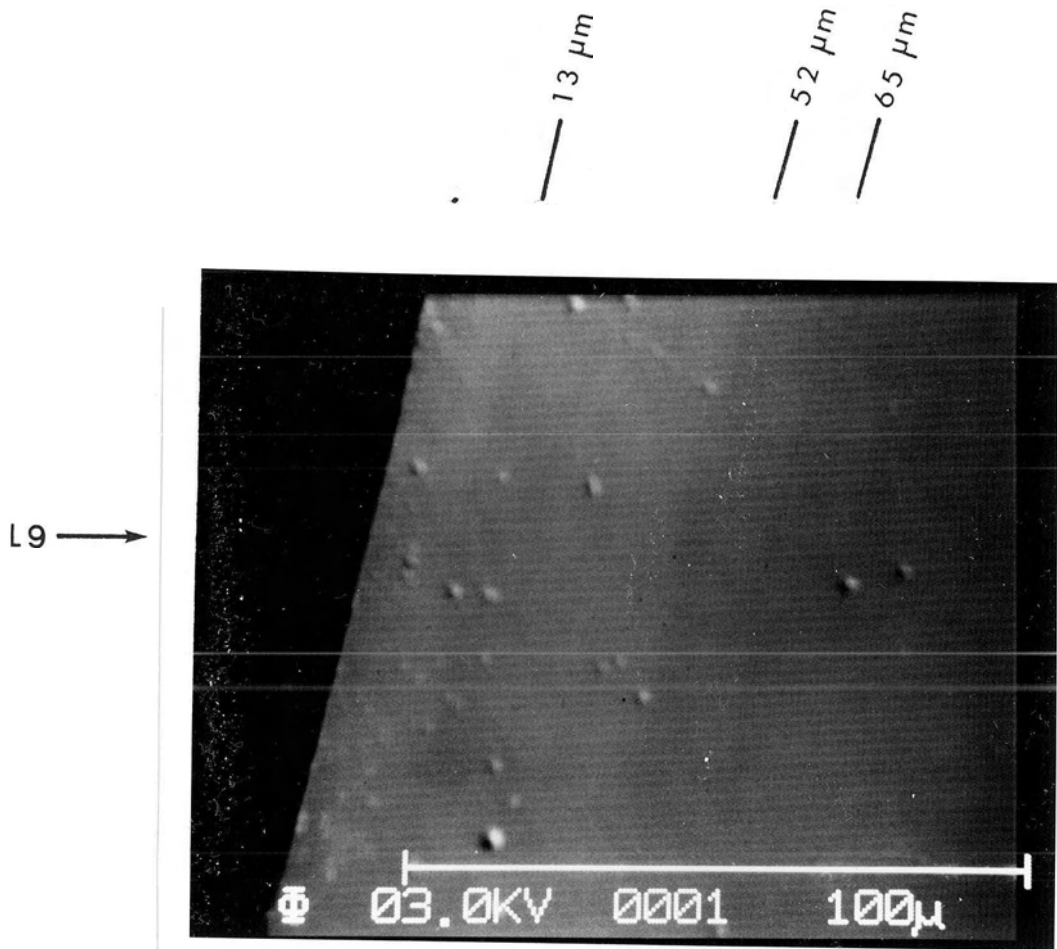
Fig. 4.23

Fig. 4.24   Auger line scan for Ag at d = 3770 A.
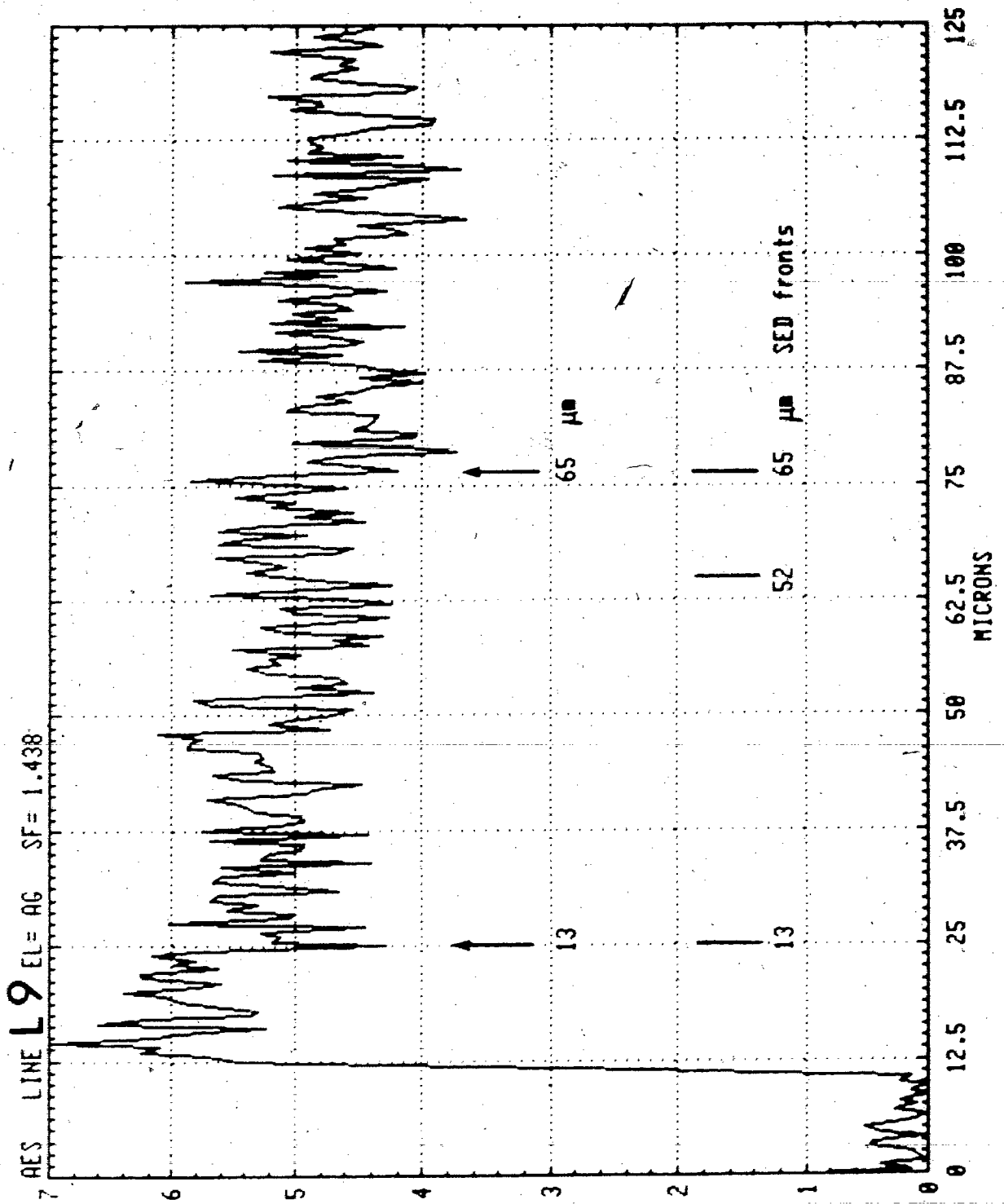
Fig. 4.24

Fig. 4.25   SED photograph of the crystal at d = 4730 A.

Fronts were seen at

13 μm

42 μm

58 μm.

13 μm

42 μm

58 μm

L10 →

Φ 03.0KV 0001 100μ
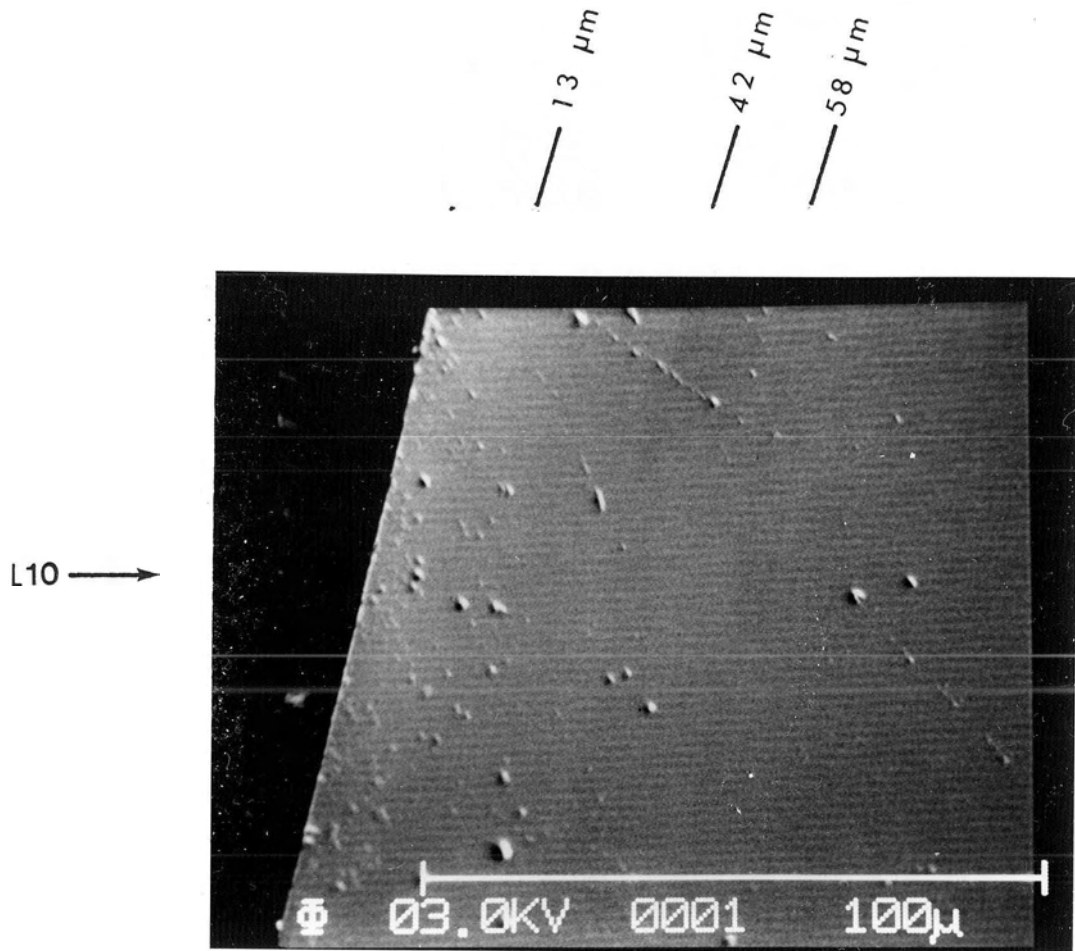
Fig. 4.25

Fig. 4.26. Auger line scan for Ag at d = 4730 A.
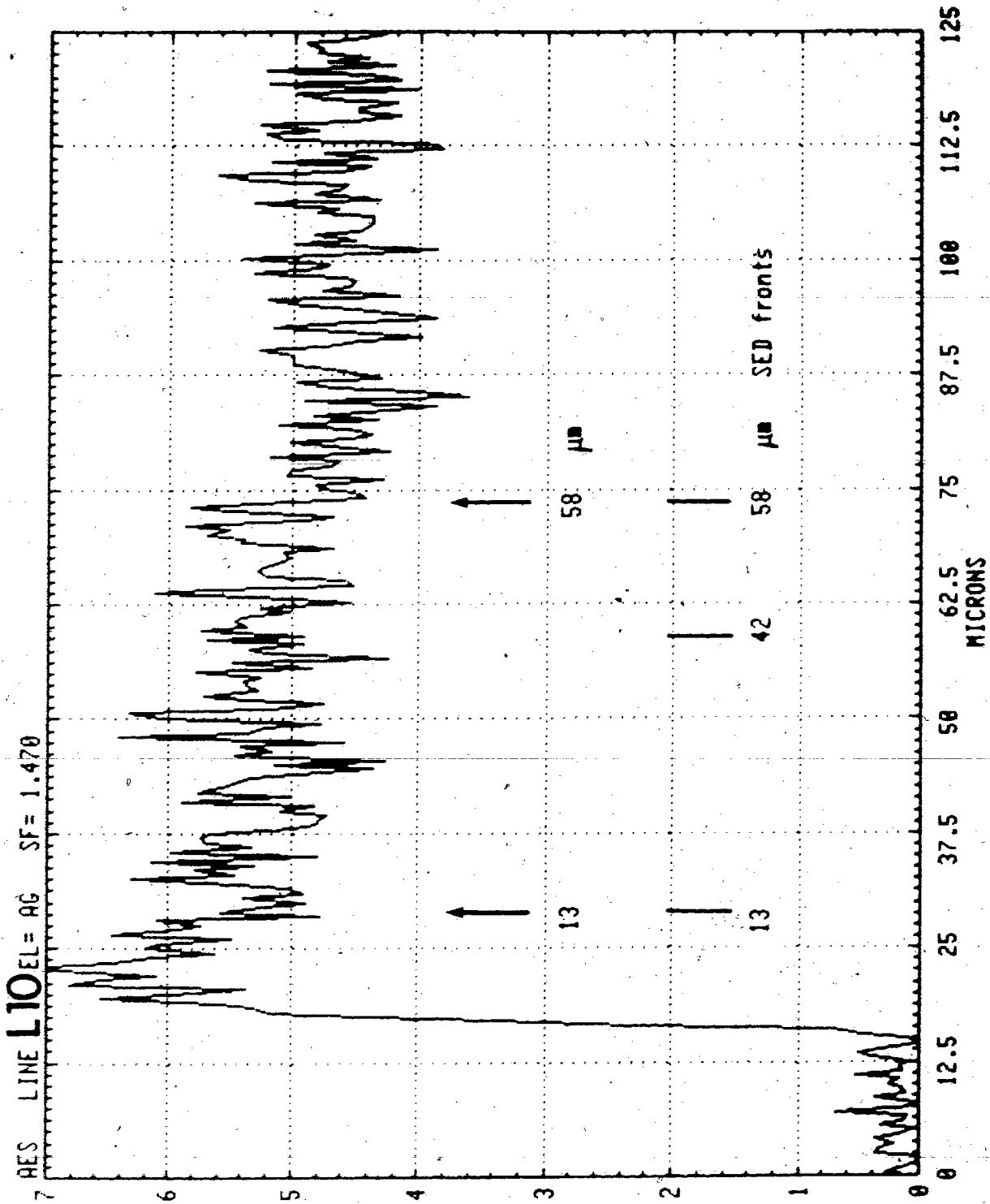
Fig. 4.26

Fig. 4.27 SED photograph of the crystal at d = 6890 A.

Fronts were seen at

20 µm

34 µm.
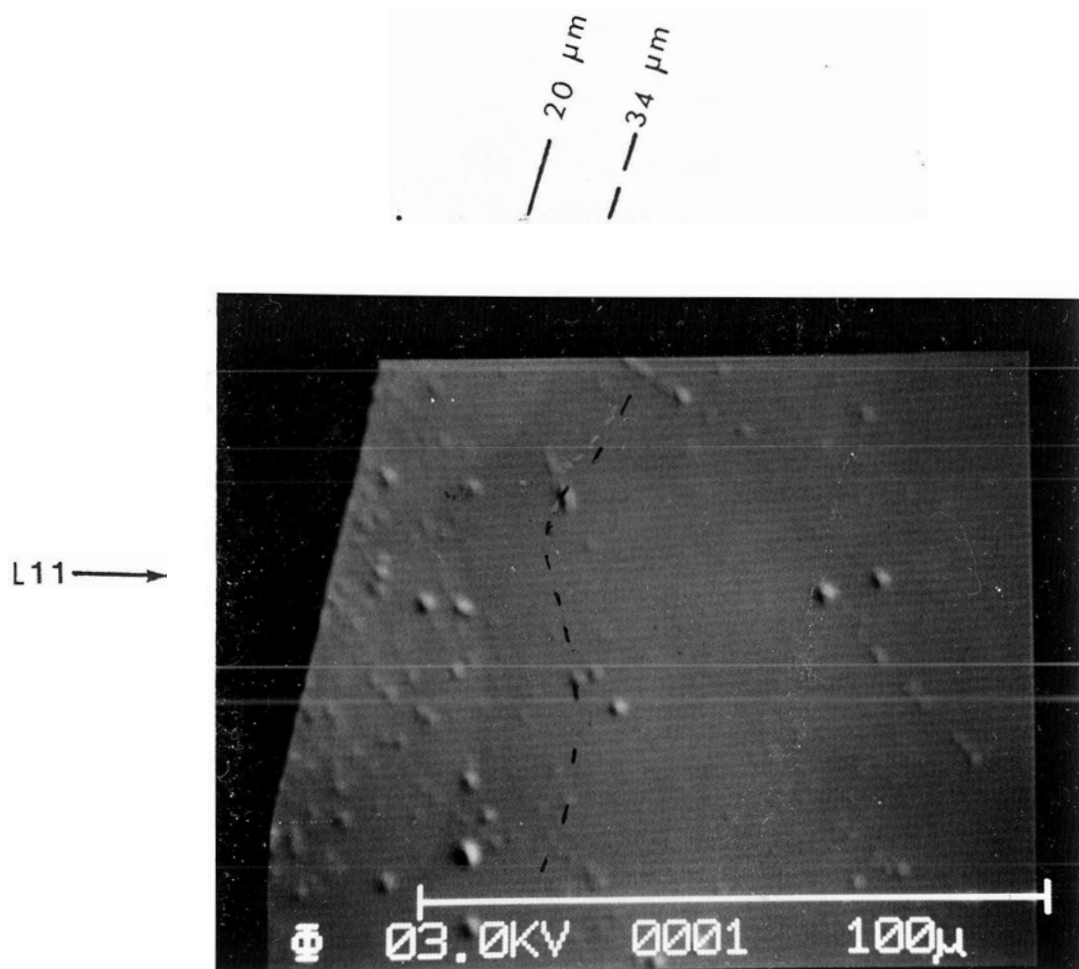
Fig. 4.27

Fig. 4.28   Auger line scan for Ag at d = 6890 Å.
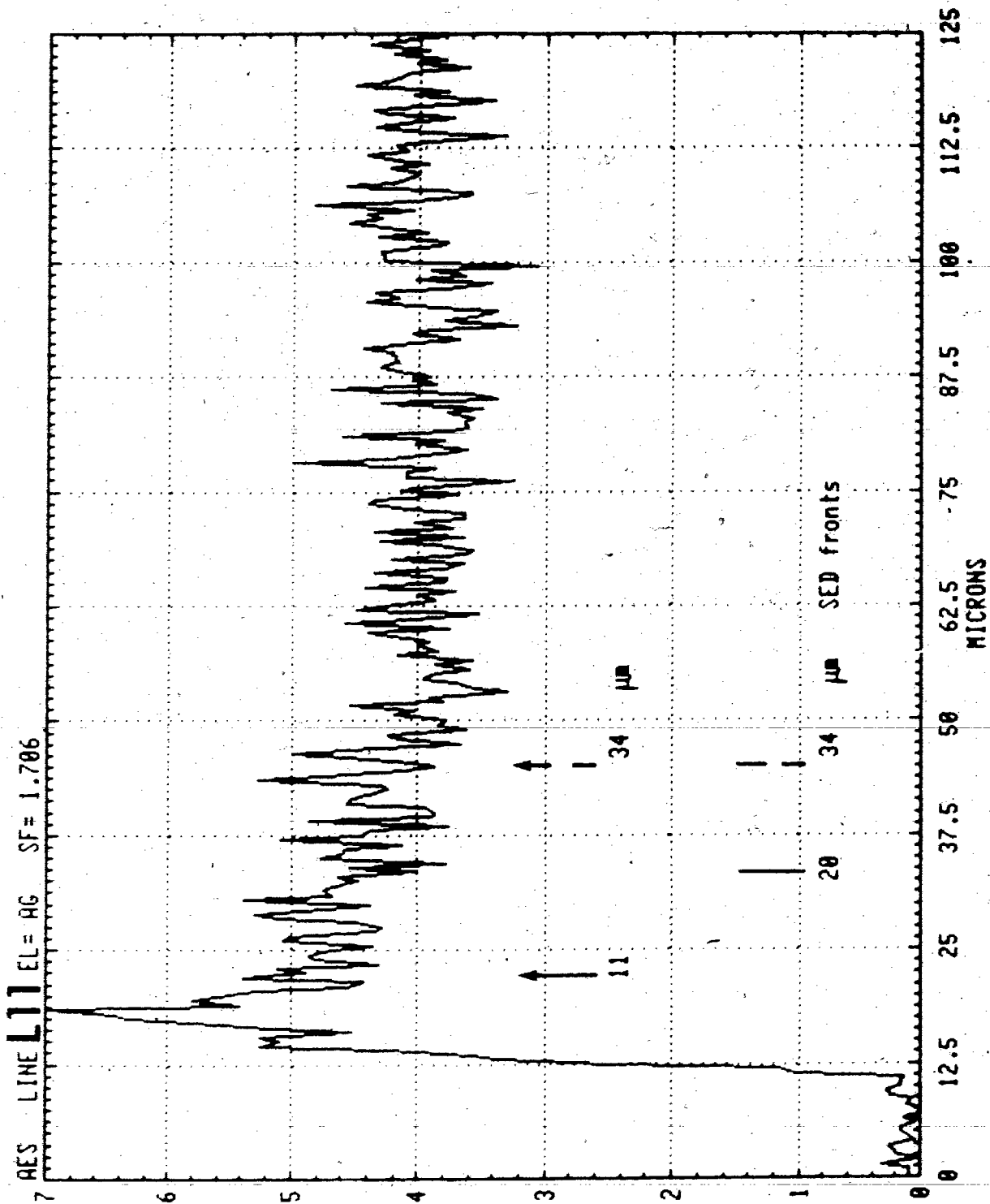
Fig. 4.28

Fig. 4.29   Auger line scan for Ag at d = 8330 A.
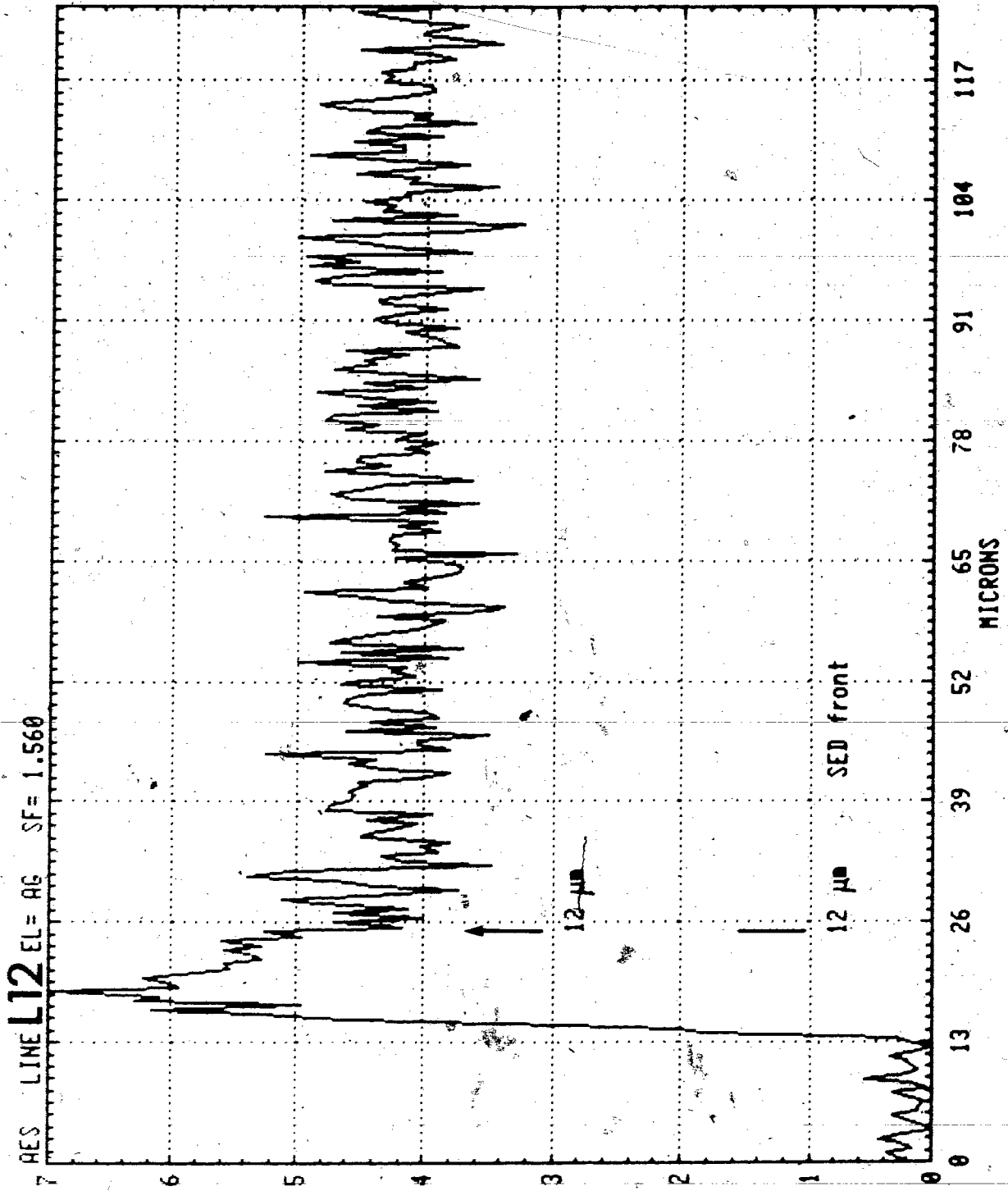
Fig. 4.29

Fig. 4.30   Auger line scan for Ag at d = 9290 A.
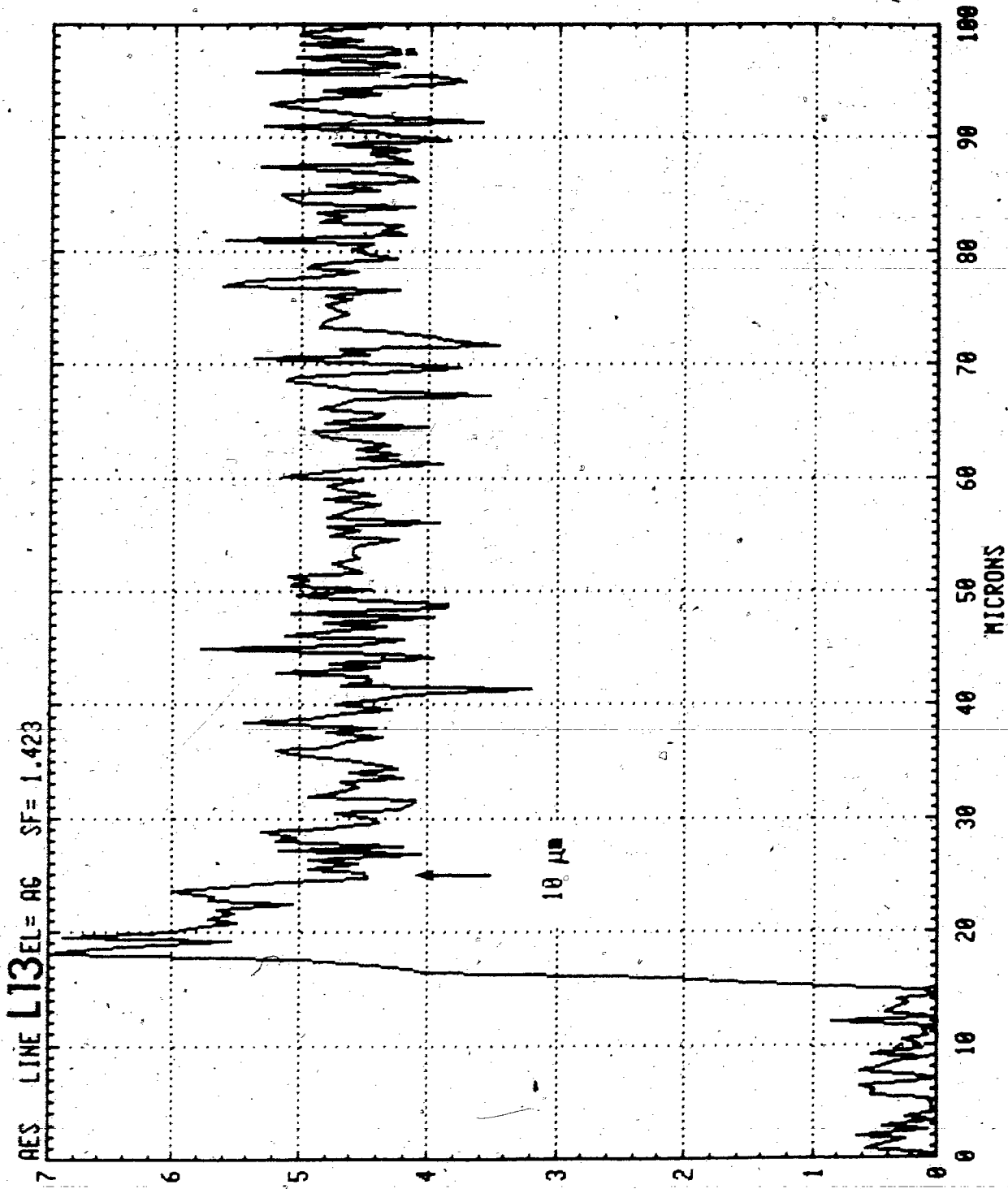
Fig. 4.30

Fig. 4.31   Auger line scan for Ag at d = 10,730 A.

The determination of the background level is
described in section 6.1.
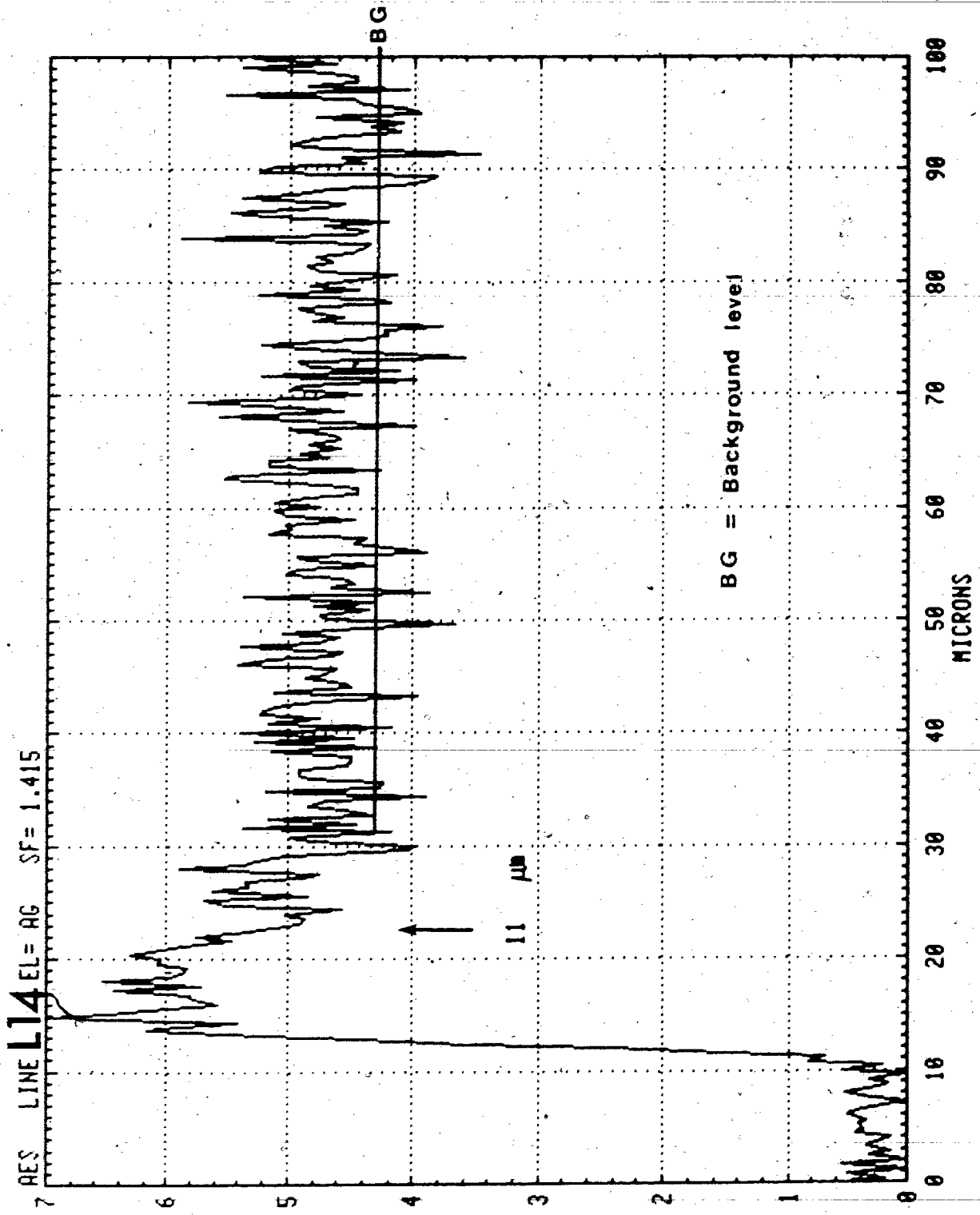
Fig. 4.31

Fig. 4.32   (a) A typical Auger line scan for sulfur

(b) A typical Auger line scan for titanium.

(These two line scans were obtained

simultaneously with the Ag line scan

given in Fig. 4.16.)
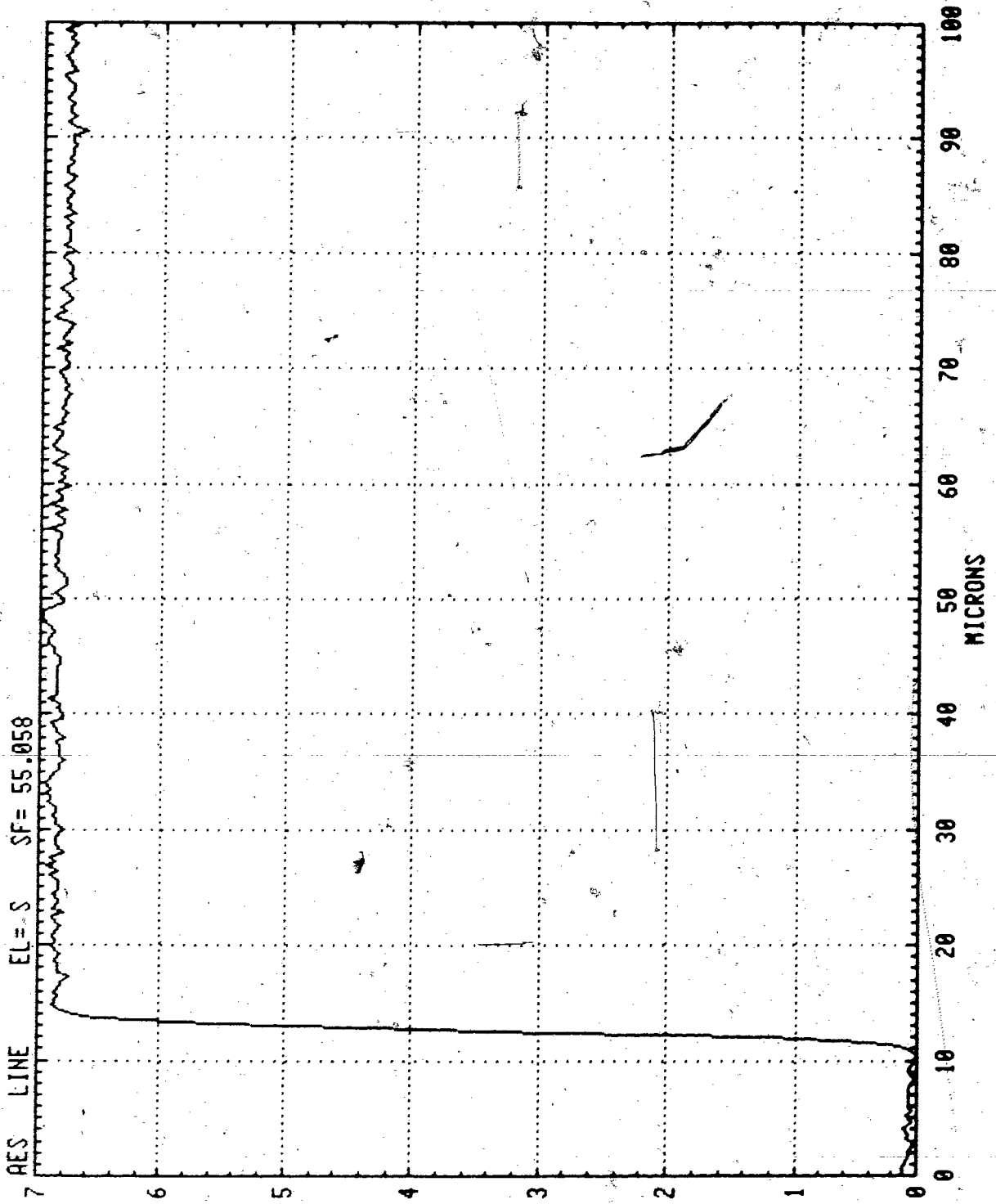
Fig. 4.32a
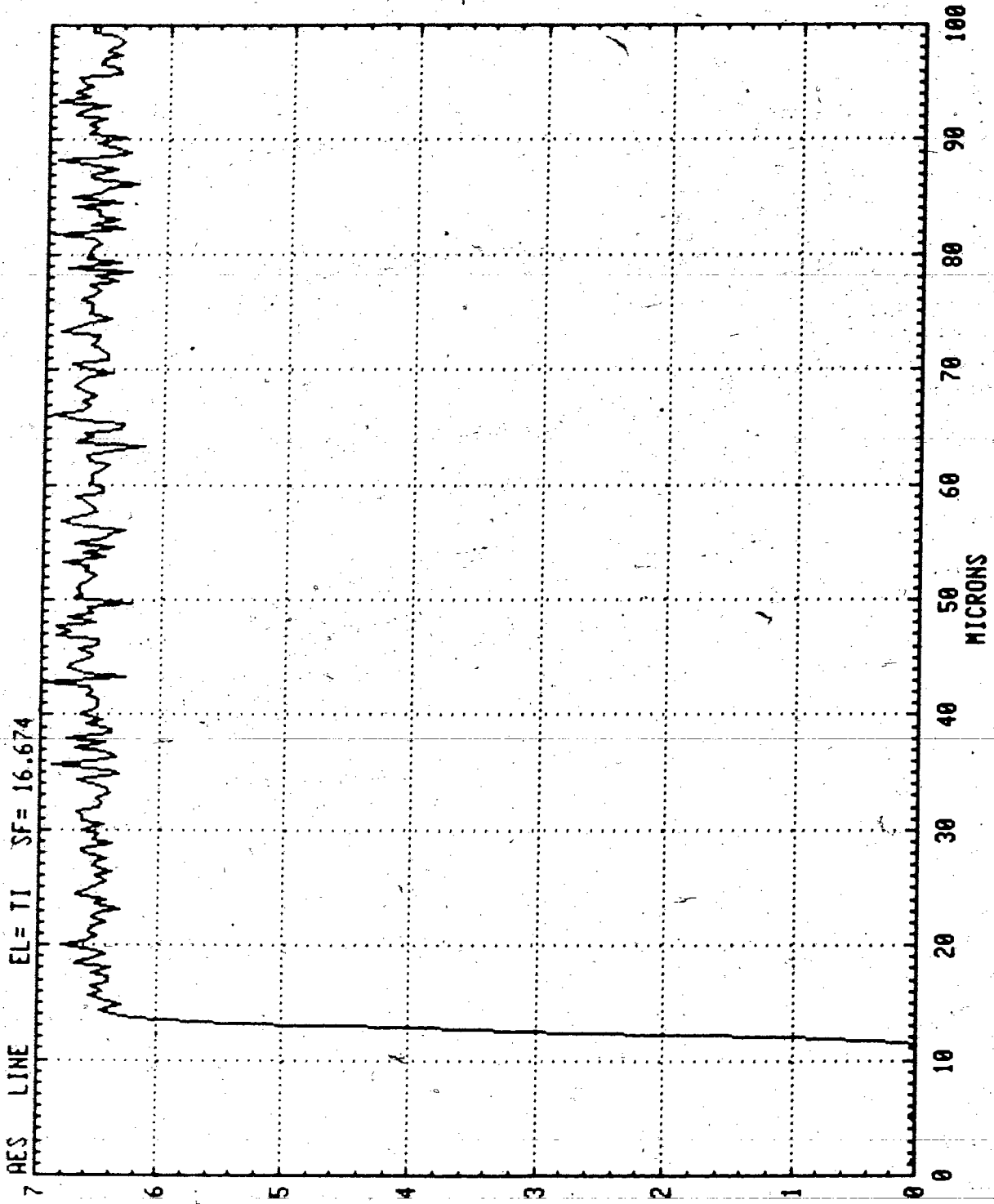
Fig. 4.32b

CHAPTER 5

DETERMINATION OF SPUTTERING RATE FOR TiS₂ AND Ag/TiS₂

5.1 Introduction

The data obtained during a depth profiling experiment consists of the changes in Auger signal intensities of the detected elements as a function of the sputtering time. The procedure used for calibrating the sputtering time scale in terms of the eroded depth is as follows.

Depth profiles can be calibrated for depth only if the sputtering rates of the materials are known. For a given eroded depth z from the surface, the rate of surface erosion is described by an instantaneous sputtering rate $\dot{z}$, where

$$\dot{z} = dz/dt.$$

For a constant sputtering rate,

$$z = \dot{z}t.$$

Therefore, in addition to the zero point, only one other point is necessary to determine the calibration factor $\dot{z}$. A method usually used for obtaining the sputtering rate for given operating conditions of the sputter ion gun is to measure the time required to sputter through a known thickness of a sample (47, p. 147). This method was used to obtain the sputtering rate for pure TiS₂ and Ag/TiS₂ samples.

5.2 Sample preparation

Pure TiS_2 crystals with thicknesses ranging from 1 to 3 μm were peeled from as-grown crystals as described in section 4.2.1. Thickness measurements were done in two ways: (a) using a Wild M20 optical microscope with an interference attachment, and (b) taking a polaroid photograph of the secondary electron image of the cross-section of the crystal using a scanning electron microscope.

The interference method utilizes the principle of the Michelson interferometer. A sample is placed under the Wild M20 optical microscope and focussed using monochromatic light reflected from the sample surface. Selecting a mirror in the interference attachment to match the reflectivity of the sample, interference fringes are obtained. Straight fringes are observed on a smooth and flat surface and a fringe shift is observed at a step. A shift of one fringe is equivalent to a step height of $\lambda/2$ where λ is the wavelength used. Counting the fringe shift between the crystal and the substrate one may obtain the thickness of a sample to an accuracy of ± 0.06 μm. A problem that one might encounter when using the interference method is that if the sample is not in intimate contact with the substrate, the air gap between the sample and the substrate will also cause a fringe shift, adding the gap height to the measured crystal thickness. One way to avoid this effect is to check the fringe shift at several edges of the crystal to see if the data are consistent. In the experiments given in this chapter

the thicknesses were checked by re-measuring them using the
ISI Model DS-130 scanning electron microscope (SEM).

For SEM measurements, a crystal was mounted flat on a
conducting substrate such that a crystal edge which was used
to measure the thickness was projecting out of the substrate
(Fig. 5.1(a)). To prepare the conducting substrate, a square
glass piece coated with a SnO_2 layer was taken and then a gold
layer was evaporated on the top edge surface. The substrate
with the crystal attached was then mounted on a SEM sample
holder keeping the crystal plane vertical and the edge to be
measured horizontal (Fig. 5.1 (b)). An electron beam with an
accelerating voltage of 10 kV was used and the sample
orientation was adjusted such that the electron beam was
perpendicular to the crystal edge. Polaroid photographs of
the SED image of the crystal cross-section at the edge were
then taken. The thicknesses were measured from these
photographs with an accuracy of about ± 0.07 μm.

To find the sputtering rate for pure TiS_2, a crystal
which was mounted on the conducting glass substrate was then
clamped onto a 60° SAM sample holder as explained in section
4.2.3. Next, the SAM sample holder was placed on the specimen
stage in the main chamber of the SAM and the analysis was
carried out as will be explained in the following sections 5.3
and 5.4.

In order to find the sputtering rate of Ag/TiS_2
crystals, first,the thickness of a pure TiS_2 crystal was
measured as explained in this section and then the crystal was

intercalated with Ag following the same steps given in section

4.2.2. The thickness of the intercalated crystal was

calculated assuming an expansion of 6% per stage (42). The

intercalated Ag/TiS_2 crystal was mounted on a piece of

aluminum-coated silicon wafer*, which was then clipped onto a

SAM sample holder and mounted on the specimen stage for

analysis.

5.3 Depth profiling

The same settings used in Auger electronics and argon

ion gun control for the sample analysis in chapter 4 were used

for studying the sputtering rate. Before sputtering was

started, the ion beam was aligned with the center of the TV

monitor. In order to do this, first the beam size was

adjusted to its smallest value and then the ion beam was

mechanically centered using offset adjustments to move the ion

gun. (The beam position is visible on some substrates when

they are briefly sputtered, making it possible to observe and

adjust the beam. A slightly contaminated sample substrate or

silicon wafer is convenient for this purpose.)

Depth profiling was carried out at selected points on

the sample. For Auger analysis, an element (oxygen) from the

*After the first sputtering experiment with pure TiS_2, it was
noticed that the SnO_2 conducting layer was sputtered away
after some time, exposing undesirable non-conducting glass if
part of the substrate was included in the sputtered area.
Since it was necessary to select points for depth profiling
close to the intercalated crystal edge for Ag/TiS_2, these
crystals were mounted on pieces of silicon wafer coated with a
thick aluminum layer. A silicon wafer was used since it
provides a flat surface.

sample substrate was selected in addition to the elements specified from the sample. The reason for selecting an element from the substrate is that when the sample has been completely sputtered through, the signal from the element chosen from the substrate will rise while the signal from the sample elements will drop. Alternative sputtering and Auger analysis was carried out through a number of cycles until the sample was sputtered through its thickness. The settings for the sputter ion gun and the parameters defined for the Auger analysis are given in detail in Appendix 2.

5.4 Results and calculations

5.4.1 Pure TiS_2

An example of the depth profiling analysis is given here. In this example, the thickness of the TiS_2 crystal measured using interference fringes was 3.14 μm. An SED photograph taken from the scanning electron microscope for thickness measurement is given in Fig. 5.2. This photo was taken before any sputtering and the thickness of the crystal measured on the SED photograph is 3.22 μm. The average crystal thickness from the two methods was 3.18 μm.

For comparison, three points on the crystal were selected for depth profiling and profiles for Ti, S and O were obtained. Fig. 5.3 presents the depth profiles during 84 minutes of sputtering time. This figure shows the depth profiles obtained only for one point selected on the crystal;

similar results were obtained for the other points. After sputtering for 84 minutes the thickness of the remaining crystal was measured by taking an SED photograph using the SEM (Fig. 5.4). It is seen from Figs. 5.2 and 5.4 that the crystal has been sputtered through 0.97 μm. (Fig. 5.4 shows some surface irregularities. It has been observed that the irregularities due to sputtering become prominent in TiS_2 after sputtering about 1 μm of the crystal thickness.) The sputtering rate obtained from the depth profiles for pure TiS_2 crystals are given in Table 5.1. Three values for the sputtering rate are given for sample #2. In order to obtain several measurements from one sample, the crystal was first sputtered partly through, then the thickness of the remaining crystal was measured and this procedure was repeated. In sample #2 the crystal was completely sputtered through its thickness in three sputtering-time durations of 96, 36 and 88 minutes. The depth profiles obtained during the final sputtering period (for 88 minutes) are given in Fig. 5.5 to show the drop of the S and Ti signals after the crystal has been sputtered completely through. Optical photographs of sample #2 before and after sputtering are shown in Fig. 5.6.

5.4.2 Intercalated TiS_2

An optical photograph of an intercalated TiS_2 crystal used for depth profiling is shown in Fig. 5.7. For this Ag/TiS_2 crystal, three points were selected for depth profiling, one within the intercalated region, and the other

two points at different distances away from the edge as seen in Fig. 5.8a. The idea was to determine whether any significant differences would be found in the sputtering rates in the three regions with different Ag concentrations. The results obtained for two samples are given in Table 5.2.

Tables 5.1 and 5.2 show no significant difference between the sputtering rates for pure TiS_2 and Ag/TiS_2 crystals. This may be due to the low concentration of Ag in Ag_xTiS_2 crystals, where x for Ag was ≤ 0.2 for the samples used in these experiments. In both Ag/TiS_2 and TiS_2 the sputtering rate was found to be 120 $\pm$ 30 A/min, for the settings used. The observation that the sputtering rates for pure TiS_2 and Ag/TiS_2 are the same (within experimental uncertainty) is important in interpreting the data presented in chapter 4. If the sputtering rates had been significantly different, each line scan would be probing regions at different depths, confusing the data and making interpretation more difficult.

In order to investigate possible structural changes due to sputtering, reflection high energy electron diffraction (RHEED) patterns of the surface of a TiS_2 sample were obtained (by Dr.B. Heinrich) before and after sputtering. In both cases, the surface structure of the TiS_2 crystal showed hexagonal symmetry indicating that atomic mixing due to sputtering was negligible and the crystal retained its single crystal structure. This observation suggests that the TiS_2 samples may have sputtered as TiS_2 molecules or as Ti or S

atoms. But it is still possible to have surface irregularities as steps due to sputtering.

Fig. 5.1   A TiS$_2$ crystal mounted for thickness measurement.

   (a) A crystal mounted on a conducting substrate

   (b) A sample mounted on an SEM sample holder

(a)

Crystal edge used
to measure
thickness

Gold evaporated edge
of the substrate

TiS_2 crystal

Conducting substrate

(b)

Electron beam

TiS_2 crystal
mounted vertically

SEM sample holder
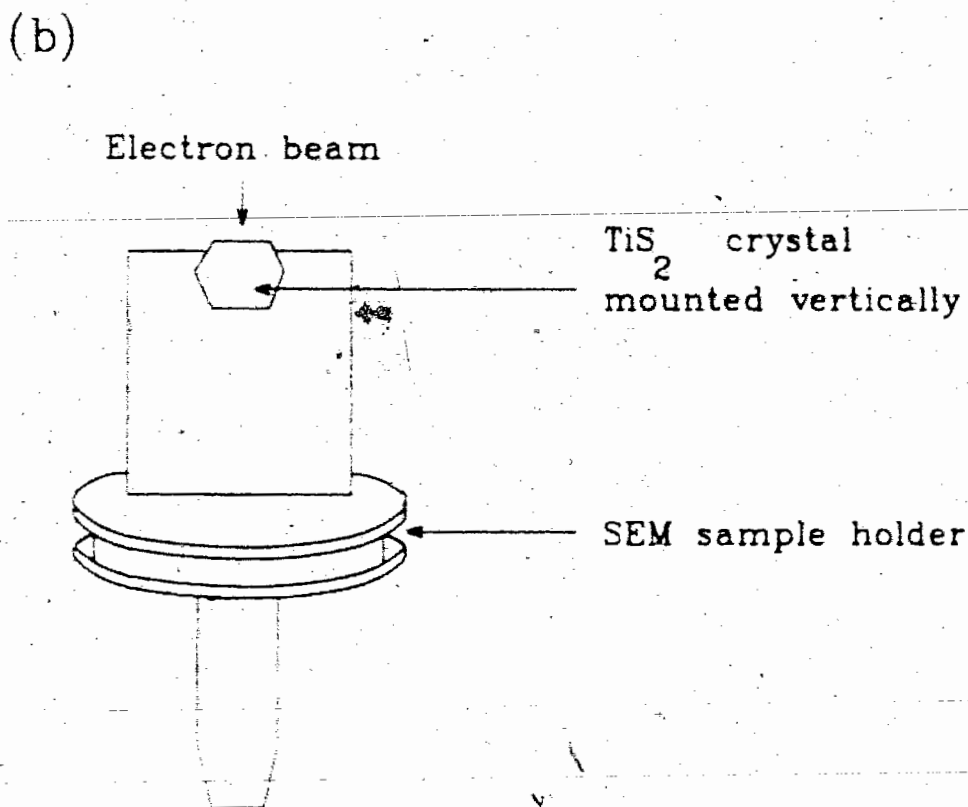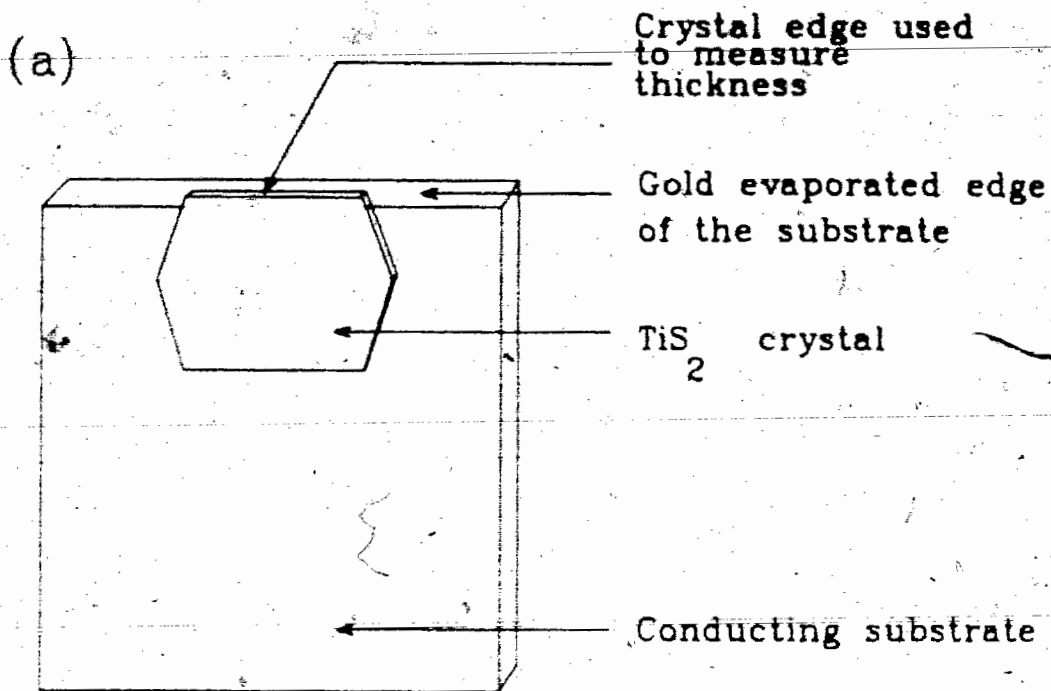
Fig. 5.1

Fig. 5.2   SEM photograph showing the cross-section at

an edge of a pure TiS_2 crystal used in depth

profiling.   This photograph shows the original

crystal thickness before sputtering.

10KV   7.44KX 1.34Μ 0583
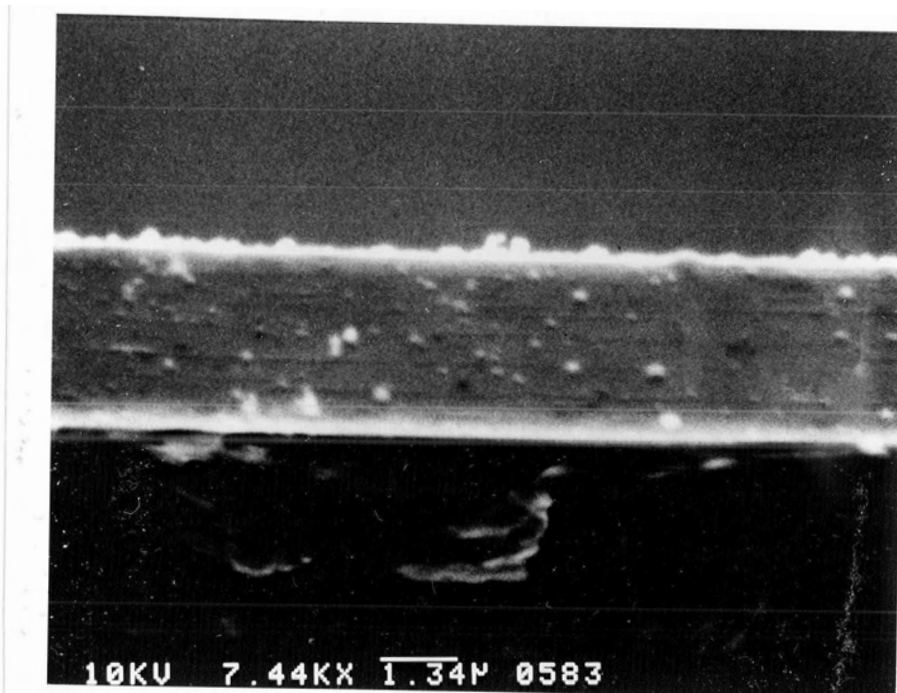
Measured thickness = 3.22   μm

Fig. 5.2

Fig. 5.3 AES depth profile for S, Ti and O on the pure TiS₂ crystal shown in Fig. 5.2.

AES PROFILE

Fig.5.3

C. (%)

SPUTTER TIME (MIN.)
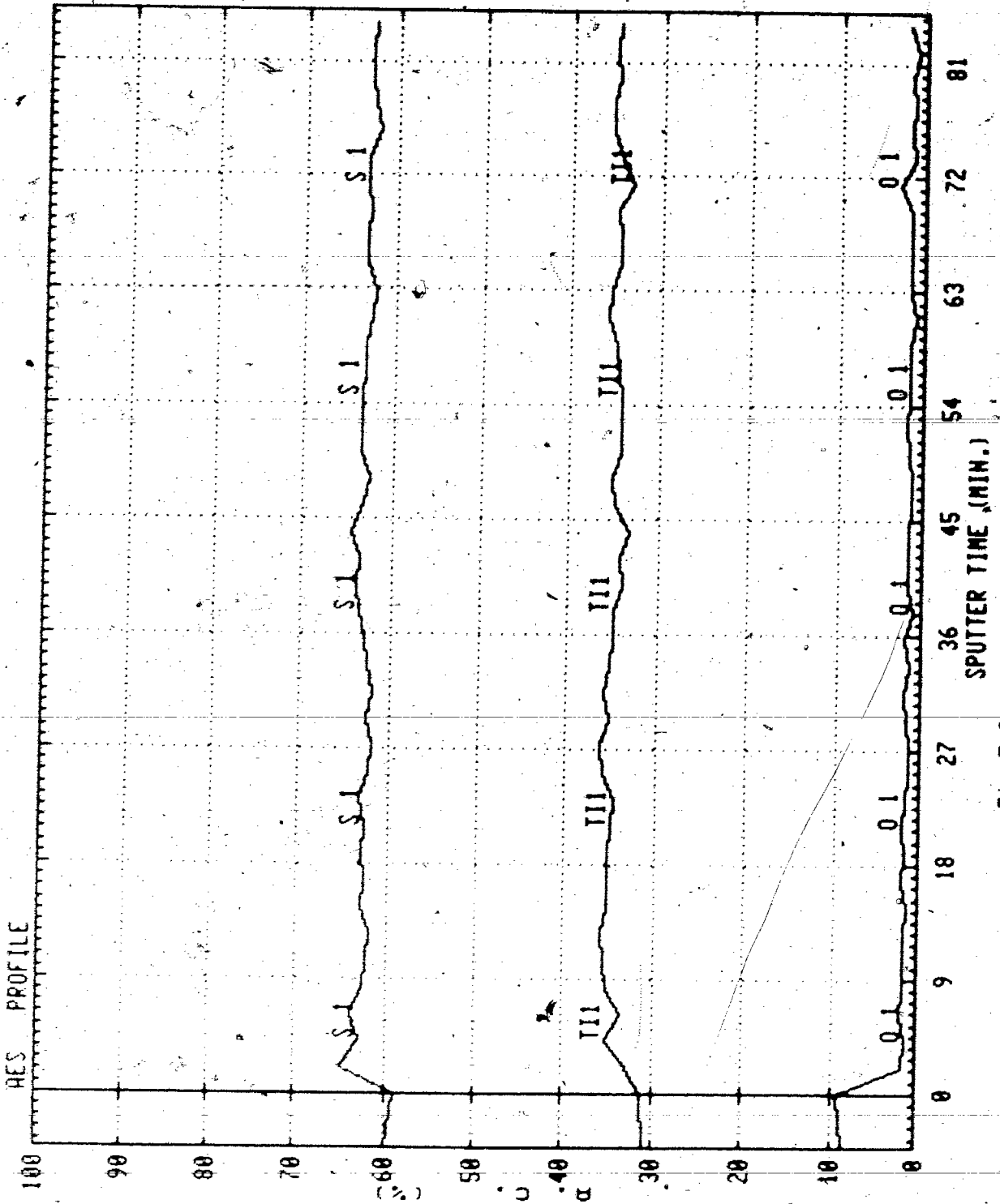
Fig. 5.4 SEM photograph of the cross-section of the TiS_2

crystal at an edge after the depth profiles given

in Fig. 5.3.
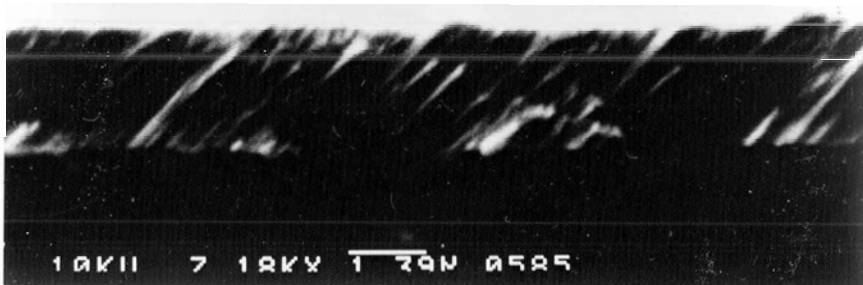
Measured thickness = 2.21 µm

Fig. 5.4

Table 5.1 Sputtering rate for pure TiS_2 crystals.

Table 5.1

Sample #	Sample thickness after sputtering (μm)	Sputtering time (minutes)	Sputtered thickness (μm)	Sputtering rate (A/min)
1 (Initial thickness = 3.18 μm)	2.21	84	0.97	115
2 (Initial thickness = 2.55 μm)	1.41 0.95 0	96 36 88	1.14 0.46 0.95	119 128 108

Average sputtering rate = 120 A/min

Fig. 5.5   Depth profiles for S, Ti and O obtained from

sample #2 in Table 5.1.

This figure shows the drop of the S and Ti signals

from the TiS_2 crystal as the sample is completely

sputtered through its thickness.
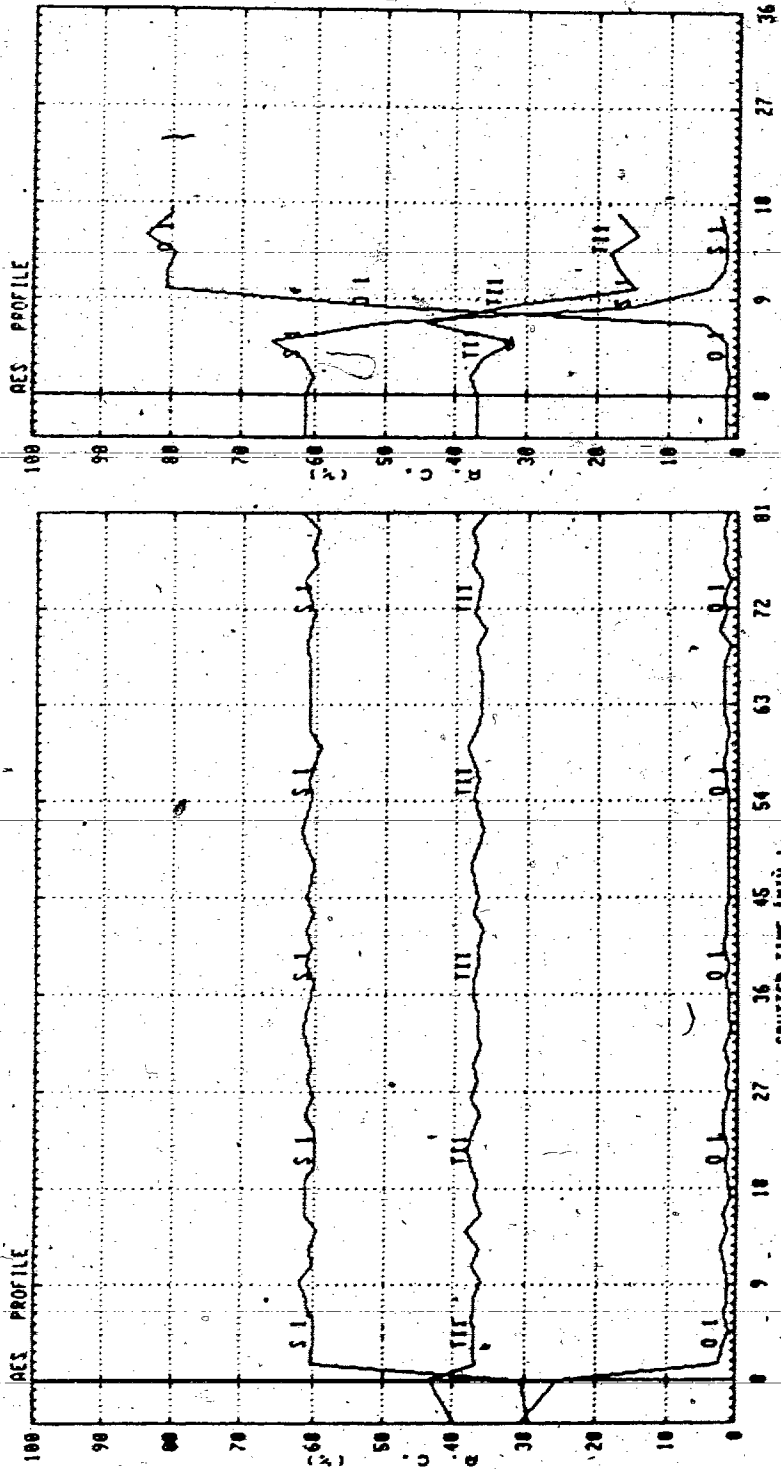
Fig.5.5

Fig. 5.6   Optical photographs showing the pure TiS$_2$ crystal

used in the depth profiles presented in Fig. 5.5

(a) before any sputtering

(b) after sputtering through the crystal.
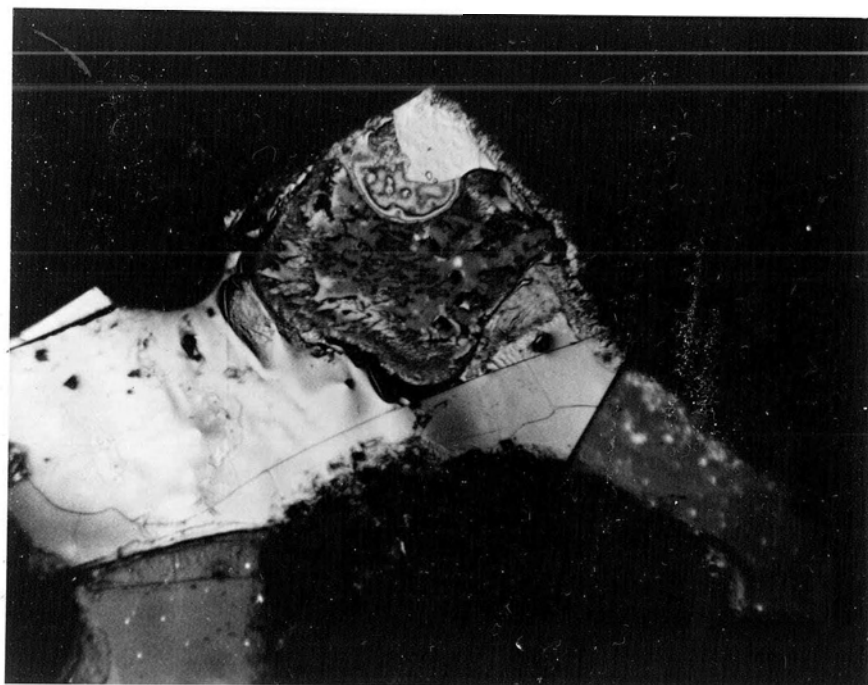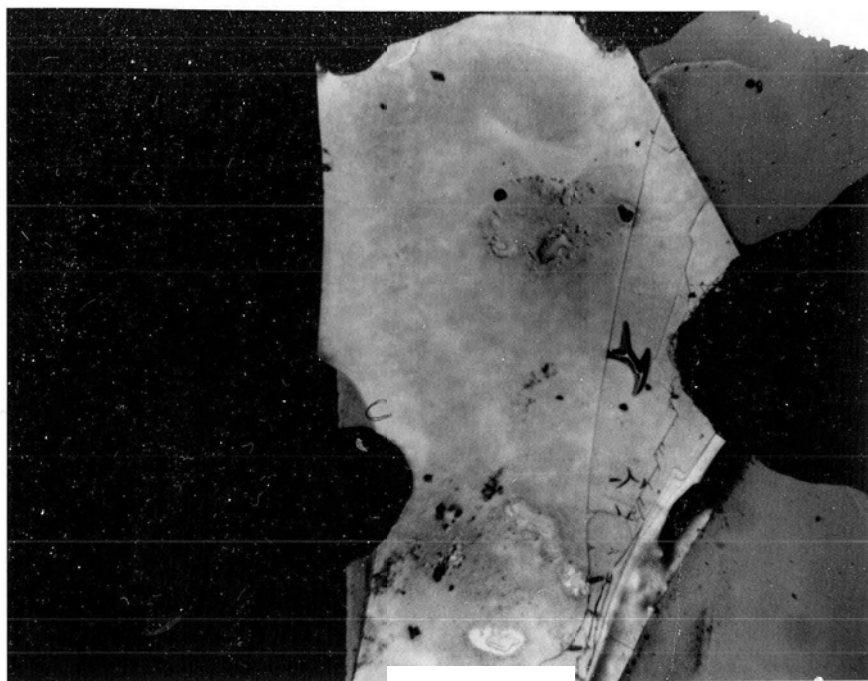
Fig. 5.6

Fig. 5.7   Optical photograph of an intercalated TiS_2

crystal (sample #1, Table 5.2) used in depth

profiling.

Intercalated region

crystal edge

100 μm
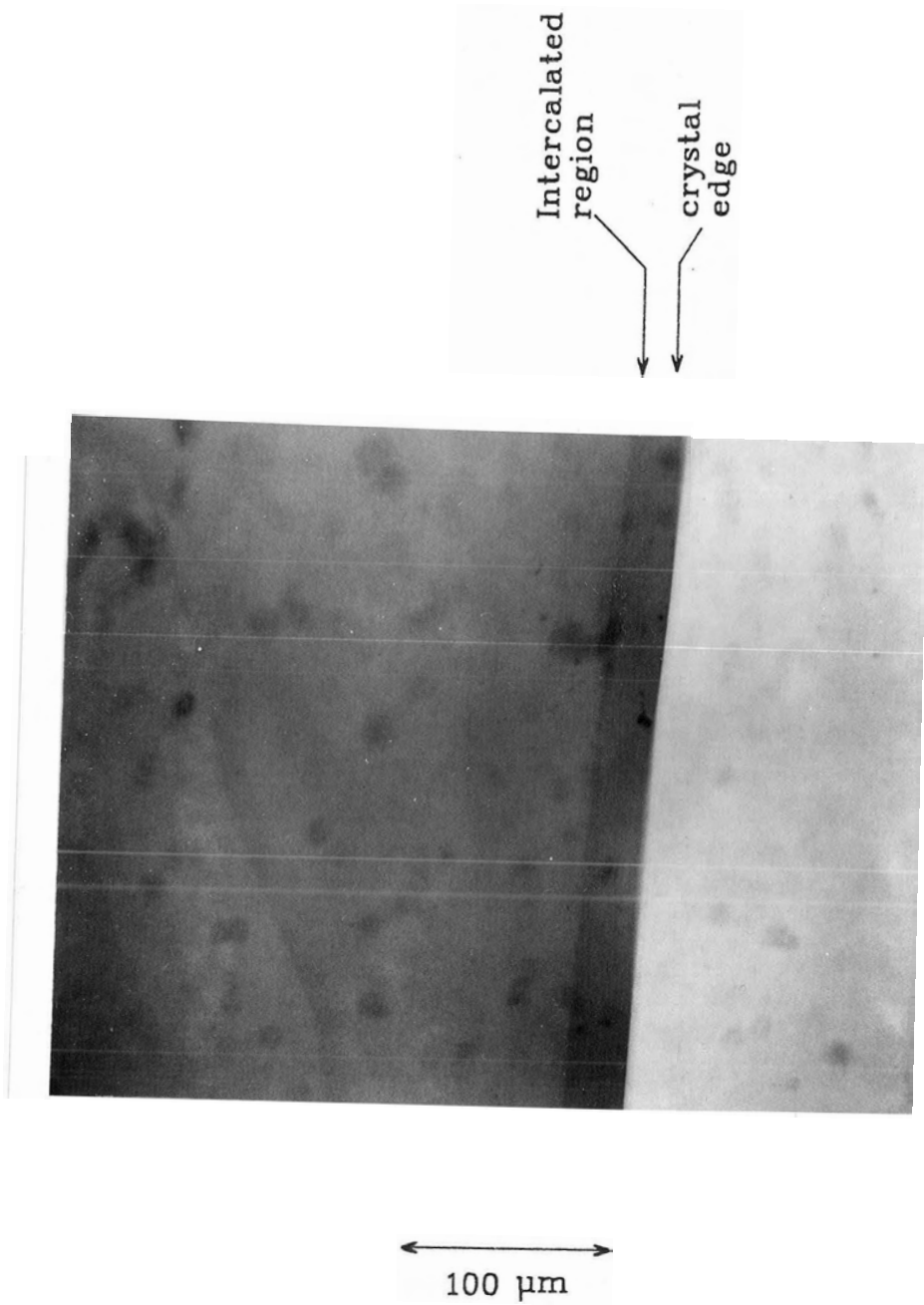
Fig. 5.7

Fig. 5.8 Diagrams showing the positions of the points used

in depth profiling for samples #1 and #2

in Table 5.2.

(a) Sample #1

③

450 μm

② 150 μm

① 15 μm

Optical stage 2 front

Crystal edge

(b) Sample #2

30 μm

15 μm

② ①

400 μm

Optical stage 2 front

Crystal edge
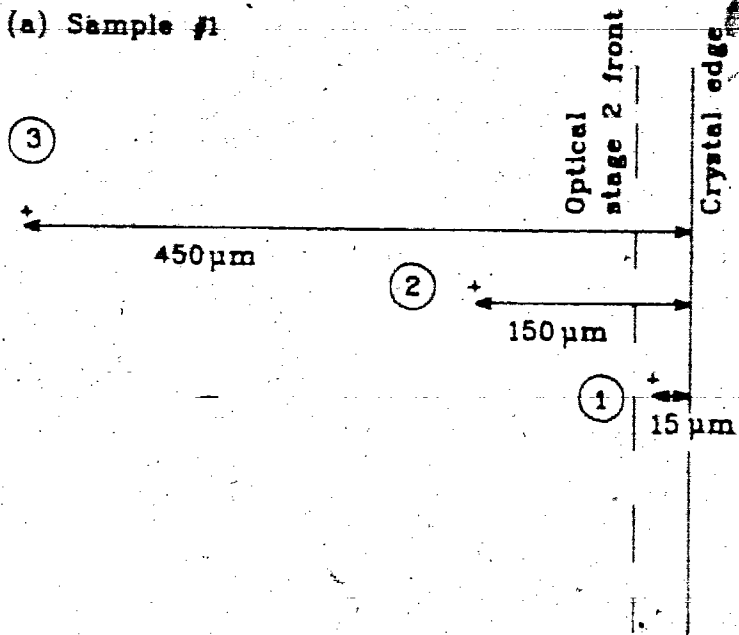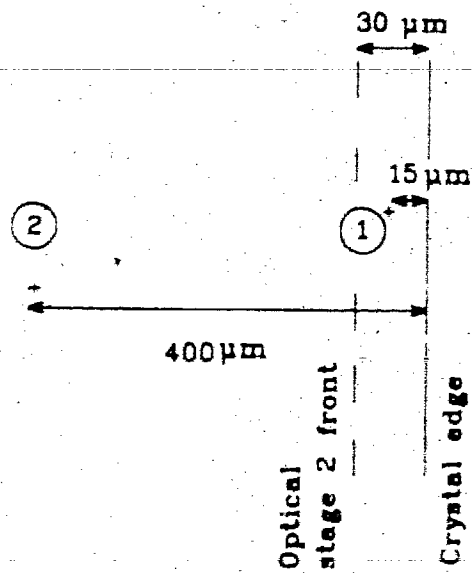
Fig. 5.8

Table 5.2 Sputtering rate for Ag/TiS$_2$ crystals.

The point numbers given for samples #1 and #2

are identified in Fig. 5.8.

The total crystal thicknesses in column 1 are for

pure TiS$_2$ crystals. Lattice expansion of 6% was

added to the thickness at point #1.

Table 5.2

Sample	Point#	Sputtering time (minutes)	Sputtering rate (A/min)
1 (Total thickness = 0.96 μm)	1 2 3	84 80 82	121 120 117
2 (Total thickness = 1.07 μm)	1 2	88 86	128 124

Average sputtering rate = 120 A/min

CHAPTER 6

DATA ANALYSIS AND DISCUSSION

6.1 Development of a 3-dimensional picture of the Ag distribution in a partially intercalated TiS₂ crystal

Using the data presented in section 4.4, a diagram representing the 3-dimensional distribution of silver in a partially intercalated Ag/TiS$_2$ system was constructed as shown in Fig. 6.1. An enlarged view of the region from 0 to 2000 Å of Fig. 6.1 is shown in Fig. 6.2 for clarity. Each line scan given in Fig. 6.1 represents the distribution of intercalated silver in a plane parallel to the basal planes of a Ag/TiS$_2$ crystal, at a given depth. The intercalation front positions are indicated in Fig. 6.1 as they were observed in the line scans and on the SED photographs presented in section 4.4. The front positions detected in the line scans are marked with arrows. Solid bars indicate the front positions seen on the SED photographs or on the SED image display. A broken arrow is used when a front position was not very clear due to a slope in a line scan. The intercalated regions that were faintly visible on SED photographs are indicated with a broken bar.

As shown in Fig. 6.1 the front positions found in the line scans were always observed on the SED photographs. Some

additional fronts seen on the SED photographs were located in transition regions between two intercalated regions found in line scans. The low contrast regions on the SED photographs were observed distinctly only at high magnifications.

To compare the Ag distributions at different depths, the ratios of the average counts of Ag to S in different regions were considered. The ratios, given in Figs. 6.1 and 6.2, were calculated for different regions seen on the line scans with approximately constant Ag concentration. A value given between two arrows is the ratio of (Ag counts)/(S counts) for that particular region after subtracting the background. The statistical errors of Ag/S ratios ranged from ± 0.003 to ± 0.006. Some line scans performed on a pure TiS_2 crystal using the same energy window used for the Ag peak in Ag/TiS_2 gave a Ag/S ratio of about 0.160, and this value was considered as the background level of the Ag signal.

In the course of data analysis another observation was made supporting the instability of high-concentration Ag regions near the surface of a partially intercalated crystal. Fig. 6.3 shows a line scan obtained from a Ag/TiS_2 crystal after sputtering the sample until stage 2 (region A) appeared near the intercalated crystal edge. The regions indicated as A and D in Fig. 6.3 are defined in section 6.2. This line scan was obtained at d = 1730 Å. (The high noise level present in the line scan is due to low data acquisition time.) Then the sample was left without further analysis and the next line scan obtained after about 16 hours at the same depth is shown

in Fig. 6.4. It was noticed that the high amount of Ag observed in the region A in Fig. 6.3 had diffused into the crystal from the edge. The next line scan obtained at a depth d = 1970 Å from the original surface also did not show a high Ag/S ratio near the crystal edge as observed in Fig. 6.3. However, the region A reappeared in the line scan conducted at d = 2450 Å, presented in Fig. 6.5. The line scans obtained afterwards followed the regular pattern as seen in Fig. 6.1. This type of diffusion was observed in some other samples also. The diffusion of Ag as shown in Fig. 6.4 was observed to be insignificant within the data acquisition time for a line scan (1 hour/line). To verify this, a sample was sputtered until the region A appeared and line scans were repeated continuously at the same depth and position. No significant changes in the front positions were observed during this period.

6.2 Data analysis and discussion

From the information in Fig. 6.1, the regions which were intercalated with approximately the same concentration are indicated in Fig. 6.6. The stage 2 (region A) observed near the crystal edge below a depth d = 1130 Å (after L6 in Fig. 6.1) had intercalated to the highest silver content. The average Ag/S ratio in this region was calculated to be 0.081. The region just below the original crystal surface, indicated as region B in Fig. 6.6, showed the next highest Ag concentration. The intercalated region near the crystal edge

in L3, L4 and L5 (region C, Fig. 6.6) showed a lower Ag concentration than that in region A. This indicates that formation of a higher concentration of stage 2 in region C did not occur probably because of motion of Ag from the region near the edge into the interior of the crystal. Although the line scans L3, L4 and L5 were performed only up to a distance of 90 μm from the edge, the crystal at this depth must have intercalated much farther. In many cases the average Ag concentration in region C was the same as that found in region B.

In the line scans from L6 to L11, the second intercalated region from the edge (region D, Fig. 6.6) seemed to have intercalated to an approximately to a constant concentration of Ag with an average Ag/S of about 0.042. After L8, the width of the region D started to decrease with increasing depth, and disappeared completely as the depth reached ~ 8000 A (Fig. 6.1). After the region D had disappeared the region F in L12 showed a lower ratio of Ag/S at a value of 0.013. It seemed that region F had intercalated with Ag to a low concentration. For this sample, the line scans in region F were performed only up to a distance of about 100 μm from the crystal edge. Most probably, the regions far from the crystal edge had negligible amounts of Ag. Line scans performed on other Ag/TiS₂ crystals at low magnifications to probe longer distances showed crystal regions without any significant Ag counts at distances far from the crystal edge. For example, the line scan given in

Fig. 6.7 was conducted at a depth of 3800 Å for a Ag/TiS$_2$

crystal of original thickness 1.2 μm. The crystal was probed

up to about 350 μm from the edge and the region beyond about

250 μm was found to have no significant counts for Ag above

the background level.

The data obtained from one sample indicated that the

Ag distribution given in Fig. 6.6 is symmetrical around the

center of the crystal. The crystal thickness was about 1 μm

and after sputtering through the center of the crystal, the

region D was redetected.

As observed in Fig. 6.6, all intercalation fronts in

the region D form a curved envelope which tends to bend toward

the crystal edge near the surface region (see fronts in L3 to

L6). The reason for this behavior must be, as explained

earlier, increased diffusion of Ag into the interior of the

crystal from the edge region at shallow depths. This type of

behavior was once observed even for region A. In that case

the crystal was intercalated to obtain a broad stage 2 (region

A) of about 100 μm in width, and hence it was possible to

observe the formation of region A as the depth increased. The

region A initially had a narrow width (~ 20 μm) and then the

width of the region increased gradually as the depth

increased, showing the same effect as seen in Fig. 6.6 for the

region D. These observations imply that an intercalated

region with a high Ag concentration tends to be unstable near

the surface region.

From the XRF and optical results in chapter 3, region A

in Fig. 6.6 was considered to be stage 2, most probably with a Ag mole fraction (x = Ag atoms/Ti atoms) of 0.2. In order to give a rough estimate for the Ag concentration in region A using Auger peaks, the Ag and Ti peaks given in Figs. 6.8a and b were considered. The height of the minor Auger peak for Ti(354 eV) which overlapped with the main Ag peak (351 eV) was obtained from Fig. 6.8b. After subtracting the Ti(354 eV) peak height from [Ag(351 eV) + Ti(354 eV)] peak height in Fig. 6.8a the ratio of Ag(351 eV)/Ti(387 eV) was found to be 0.03. The atomic sensitivity factors for Ag and Ti were included in this calculation. (Survey spectra obtained for pure Ag and Ti metals showed that the Ag signal is three times higher than the Ti signal.) The Ag/Ti ratio obtained from Auger analysis is seven times lower than the expected ratio, x = 0.2. This can be explained by considering the different sputtering rates for Ag and Ti. The sputtering rate for Ag has been observed to be seven times higher than that for Ti when pure metal targets are used (51, p170 and p182). The preferential sputtering for Ag may have produced a Ag deficient layer on Ag/TiS$_2$ sample surface. In addition, a slight local diffusion of Ag was observed due to the heating caused by the electron beam. This diffusion may also have reduced the Ag signal.

To compare the amount of Ag intercalated in different regions, the Ag counts for each region were considered relative to the Ag counts for the region A of the same sample. The Ag counts obtained for the region A can be considered as a measure of stage 2 Ag concentration. Consistent results were

found for all the analyzed samples, about 10 altogether, as summarized in Fig. 6.9. The region B always seemed to have intercalated to a Ag content from about 0.6 to 0.7 times that of the region A. The Ag content in the region C was found to be the same as that of the region B in most crystals, however, in a couple of samples it was close to the Ag content in the region D. Relative Ag content in the region D was found to be from about 0.4A to 0.5A, and for the region E from about 0.2A to 0.3A where A is the Ag content in the region A.

When analyzing Ag/TiS_2 samples the distribution of Ag was always observed to be similar to Fig. 6.6. However, it was observed that the first detection of the region C or the region A did not occur exactly at the same depth for all the samples analyzed. The first detection of the region C, as in L3 at 25 µm for the sample in Fig. 6.1, occurred at a depth between about 100 to 700 A for the samples analyzed. This depth interval was estimated considering the depths where line scans were performed. After intercalation the samples were left for at least about a day before the analysis to give enough time to dry the glue (torr seal) used for sample mounting and to allow evaporation of the other solvents used in sample preparation. This time interval between the intercalation and the analysis ranged from about 0.75 day to 3.5 days for all the samples except for one which was analyzed 10 days after intercalation. It was noticed that the first detection of the region C occurred at a depth which was in the lower range of 100 to 700 A (i.e., at shallow depths) for the

samples which were analyzed between about 0.75 to 1 day after
intercalation. In the samples which were analyzed about 2 to
3 days later, the region C started at a depth between about
400 to 700 A. This observation indicated that the silver in
the region C was still moving after intercalation. The region
C in the sample which was analyzed 10 days after intercalation
was also detected first at a depth between 400 to 700 A as for
the samples left for 2 to 3 days. This indicated that the Ag
in the region C had been stabilized by 2 to 3 days after
intercalation. The depth at which the region A started to
appear was estimated to be between about 1000 to 2000 A for
the samples analyzed. In this case, it was difficult to
observe any significant differences between the samples with
various time delays before analysis. One problem associated
with the detection of the starting point of the region A was
the difficulty of observing this narrow region (typically 10
to 35 μm) distinctly in a line scan performed at a low
magnification.

The regions such as B, C, D and E which precede region
A (stage 2) may have been intercalated with mixed phases.
Very low-concentration regions such as F may have formed with
dilute stage 1 silver. It has been observed in a previous
theoretical study (38) that stage 2 intercalation starts with
mixed phases of stage 2, 3 and 4 and that eventually the
crystal intercalates to a well-ordered DH stage 2 structure as
the intercalation is continued (Fig. 6.10). This study has
been carried out for the potassium/graphite system. (Some

details are given on page 7, chapter 1.) The intercalant was
assumed to be made up of small elementary islands. A
collection of elementary islands was considered as a DH island.
Fig. 6.10 shows the formation of stage 2 from a pristine
microcrystal of graphite. A row of rectangles represents the
time evolution of the intercalation process. In the very
beginning of the intercalation process (column a) the islands
are very small and highly unstable. As intercalation proceeds
the islands grow and tend to merge with each other and a stage
2 structure begins to emerge at the crystal edge in contact
with the guest reservoir (column c). Yet the interior of the
crystal shows stage 3 and stage 4-like structures. Eventually
the crystal orders into a Daumas and Hérold stage 2 structure
(column d). Fig. 6.10 indicates that higher mixed stage
phases precede a well-ordered staged structure during
intercalation. The regions D and E in Fig. 6.9 may be the
mixed stage phases that appear to precede well-formed stage 2.

Auger results indicate that Ag in TiS_2 has a high rate
of motion near the crystal surface. The crystal lattice can
easily expand near the basal surfaces, increasing the
diffusion of intercalants through van der Waals gaps. A
highly concentrated stage 2 region was not observed just below
the crystal surface (from 0 to 100 A) probably due to the
rapid diffusion of Ag near the surface. Such a rapid
diffusion of intercalant in the first van der Waals gap has
been observed in the computer simulation shown in Fig. 6.10.
Another study which supports rapid surface intercalation has

been done using electron microprobe analysis of Ag/NbSe₂ crystals with thicknesses of 2 to 60 μm (44). This study revealed two Ag intercalated phases in NbSe₂ with one phase extending a greater distance from the intercalated edge than the other phase. The intercalated region which had moved farther from the edge was found to be localized near the crystal surface to a depth less than·1 μm.

In Ag/TiS₂, it may be possible that a stage 2 region (as region A) had formed in the region C (Fig. 6.9) during intercalation and then the Ag atoms redistributed by the time of the analysis. This depends on both the Ag intercalation rate and the rate of motion of Ag in the region C in the TiS₂ lattice. In the case of stage 1 and stage 2 formation in TiS₂, it is possible to create only a stage 2 region by selecting an intercalation rate lower than the stage 1 to 2 conversion rate (chapter 3).

Another observation made, but not studied in detail during the experiments given in chapter 3, is that the stage 2 front observed optically with reflected light during intercalation either faded or disappeared when the intercalated crystals were reobserved optically after several days. The optical absorption coefficient (α) for TiS₂ is about 7.5 x 10⁵ cm⁻¹ (58, page 111) for white light ($\overline{\lambda}$ = 5500 A), yielding a value of about 130 A for the penetration depth 1/α . This implies that the optically observed region during intercalation is in the region C. Hence, the disappearance of the optical stage 2 front indicates that the Ag in the region

C had been moving even after intercalation was terminated. This supports the Auger results discussed on page 136 regarding the motion of Ag in region C.

The x-ray fluorescence results given in section 3.2.2 for the motion of the stage 2 front in TiS_2 crystals of thickness about 2 μm indicated a stationary behavior of the stage 2 front at room temperature. Repeated XRF line scans performed on stage 2 Ag/TiS_2 crystals indicated the same stage 2 front position. Even though a stable stage 2 region was found in the bulk of a thick crystal, the stage 2 was observed to be unstable in thin crystals of thickness less than around 700 Å (59). In this case, a stage 2 Ag region was observed optically during intercalation and the Ag in the stage 2 region remained mobile even after the intercalation was terminated.

The stage 2 Ag intercalation rate in TiS_2 crystals has been observed to be strongly thickness dependent (41) and the rate varies approximately as $x^{-1/2}$, where x is the crystal thickness. This is consistent with the observations made here that a thick crystal intercalates faster (i.e., longer distances from the intercalated edge) at the basal surfaces than deeper in the crystal, as reported in the Auger analysis in section 4.4. The optically observed stage 2 intercalation rate in Ag/TiS_2 samples given here was about 2 μm/min. Considering the probing distances in line scans in the surface region B (depth < 100 Å), the rate of intercalation in the region B was found to be more than 10 times higher than the

value found with optical measurements. The intercalation
rates found here are in agreement with the values reported in
ref.41.

In the course of the study of the motion of stage 2 Ag
in the TiS_2 lattice it was noticed that the stage 2 Ag has a
high rate of motion in the following three circumstances: (1)
near the crystal surface region in Auger analysis, (2) in the
bulk of a crystal when the crystal is being intercalated
(section 3.3.1) and (3) in the bulk of a crystal during the
stage 1 to stage 2 conversion (section 3.3.2). As mentioned
in section 3.3.3 the driving force for the stage 2 motion in
(2) and (3) can be the interlayer electrostatic repulsion
between the Ag atoms in the stage 1 region. The separation
between stage 2 Ag atoms is twice that of the stage 1 Ag atoms
in the "c" direction while the in-plane Ag atoms in both
stages reside at equal separations. (In case (2), it is
believed that there is a narrow region of stage 1 at the edge
of an intercalating crystal.) In spite of the elastic strains
induced by the distortion of the host lattice during the
formation of a stage 2 region (Fig. 3.11), the observation of
rapid stage conversion indicates that the decrease in Coulomb
energy is greater than the elastic energy expended in forming
the stage 2.

The stage 2 Ag did not show any significant motion in
the bulk of a crystal in the absence of stage 1 Ag. The
electrostatic repulsive forces in the "c" direction between
the stage 2 Ag atoms are probably not strong enough to drive

the Ag atoms through the bulk lattice. It is clear from Fig. 3.11 that in order to move an island from a stage front into the empty crystal region it is necessary to create new bends in the host layers. The number of bends to be created increases with the depth from the crystal surface. In other words the elastic energy that has to be overcome during the motion through the van der Waals layers is less near the crystal surface. As observed in the Auger analysis it seems that the electrostatic repulsive forces between the stage 2 Ag is sufficient to move stage 2 Ag in the surface region of TiS_2 crystals.

Two modes of intercalation have been proposed for graphite systems in a previous study (60). The first type is characterized by the absence of an intercalate concentration gradient in the intercalated region which implies that Fick's law is not applicable. In the first type, the intercalation is observed as a sharp intercalation front advancing into the crystal. This suggests that diffusion is much faster than the accompanying stress relaxation and that the intercalation process is interface-controlled. The second type of concentration profiles have been characterized by a gradual decrease of the intercalate concentration from the intercalated edge to the interior. In this case the profile does not exhibit a sharp front and appears to resemble one based on Fick's law diffusion. The intercalation mode associated with Ag/TiS_2 samples where sharp fronts are observed at boundaries between intercalated regions seems to

be interface-controlled.

Combining both Auger and XRF results it seems that the intercalation front which separates the empty and intercalated regions in a partially intercalated TiS$_2$ crystal has a shape similar to Fig. 6.11. The surface region within a depth of about 100 Å from the original crystal surface intercalates continuously with a more or less constant intercalant concentration. The steepness of the intercalation front which separates the empty and the intercalated regions of a crystal is reduced by regions such as D, E and F. It seems that mixed-stage phases such as D and E precede a well-ordered stage. Since stage ordering is expected to improve with a longer intercalation time or a higher molar fraction of intercalants (38), the fraction of stage 2 in the mixed-stage phases such as D and E would probably increase with longer intercalation time. However, it seems that in any partially intercalated system the intercalated distance from the crystal edge decreases with increasing depth from the basal surface. The broad intercalation fronts observed in XRF scans (Fig. 3.6) seem to be due to this behavior. The island model presented in Fig. 3.11 assumed a well-ordered stage 2 structure without any mixed-stage phases. Since the crystals used in the XRF analysis had been intercalated for relatively longer times, the proposed island model can be assumed to be valid perhaps except in the region very near the basal surfaces (~100 Å). In addition, stage disorder may be observed, to some extent, at the stage 2-empty crystal

intercalation front., The result presented in Fig. 6.11 is expected to be applicable for other partially intercalated systems.

6.3 Suggestions for future work

The deintercalation of Ag/TiS$_2$ occurs in stages (6). When a stage-1 crystal deintercalates, the edge region first starts converting into stage 2 from stage 1. The depleted region proceeds farther into the crystal from the edge as deintercalaltion continues. An XRF scan obtained from a partially deintercalated crystal showed a broad deintercalation front at the boundary between the stage 2 and stage 1 regions. It would be of interest to study a partially deintercalated crystal using Auger analysis to observe the variation of the distribution of intercalants in the host structure.

Fig. 6.1 A diagram representing the 3-dimensional

distribution of Ag in a partially intercalated

Ag/TiS$_2$ system.

The front positions are marked with arrows and bars

as they were observed in line scans and on SED

photographs presented in section 4.4. The numbers

given here are the ratios of (Ag counts)/(S counts)

for regions indicated with arrows.
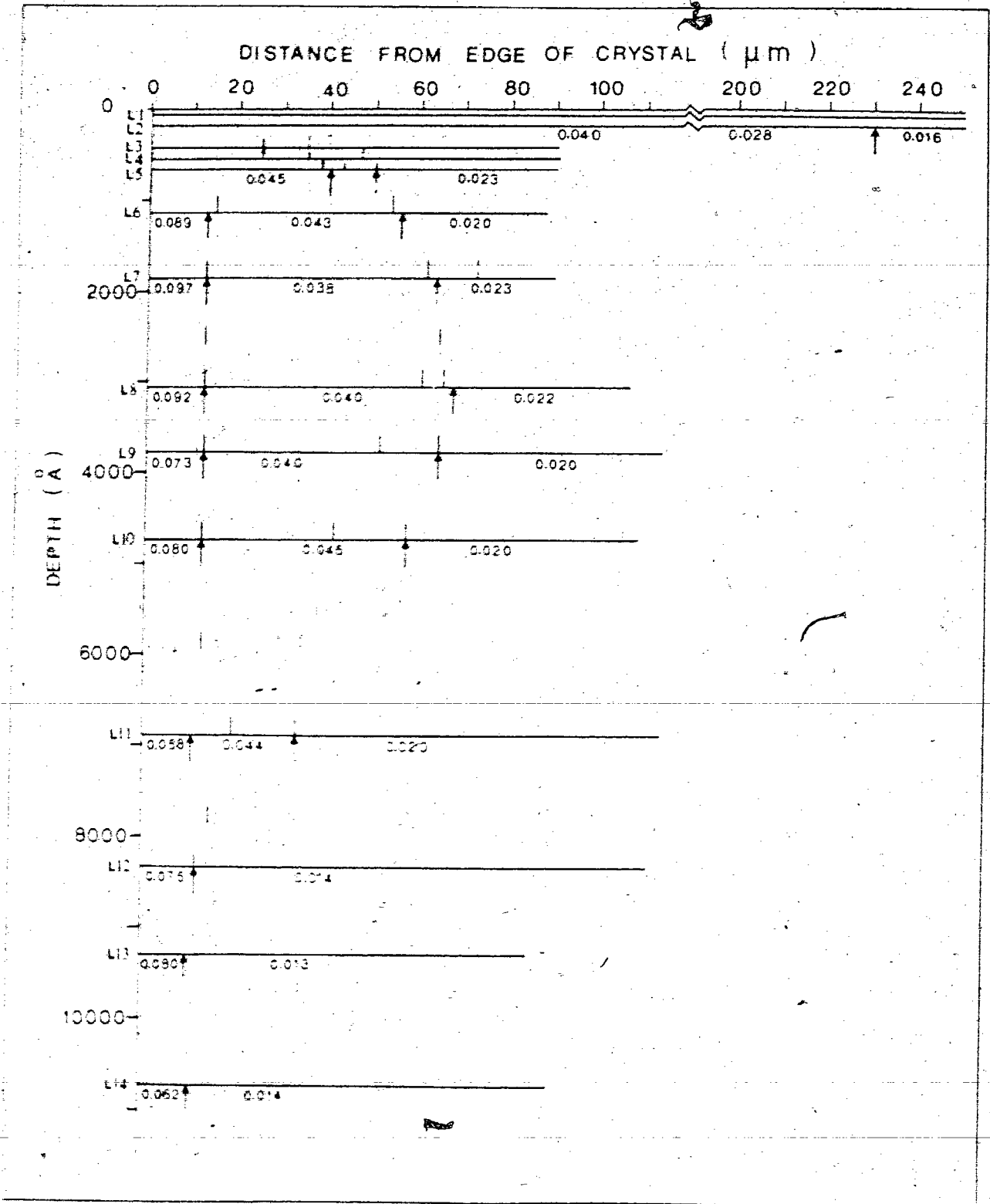
Fig. 6.1

Fig. 6.2   An enlarged view of the region from 0 to 2000 A
           of Fig. 6.1.

145b
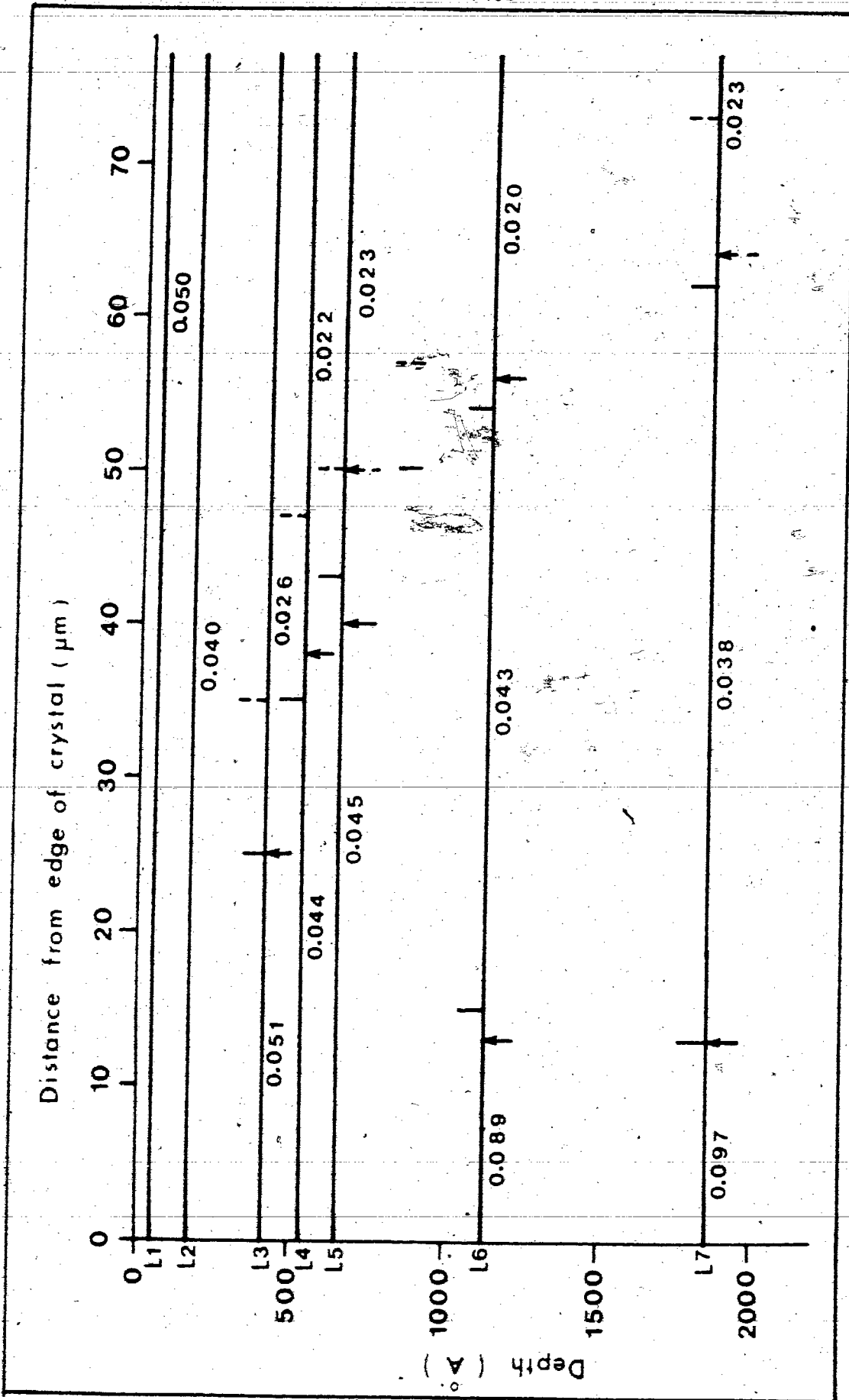
Fig. 6.2

Fig. 6.3   Auger line scan obtained on a Ag/TiS$_2$ crystal

at d = 1730 A showing both regions A and D.
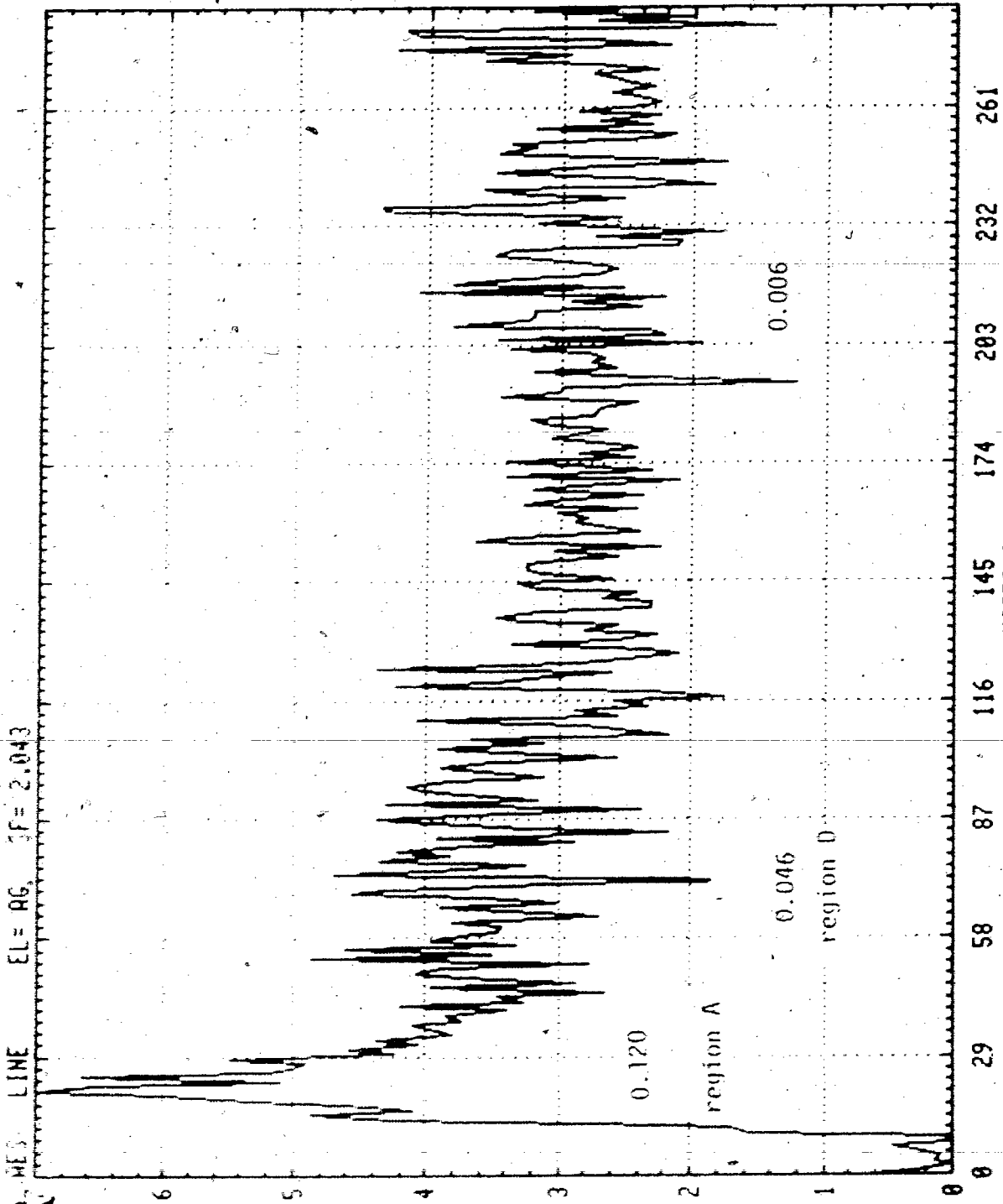
Fig. 6.3

Fig. 6.4 Auger line scan performed on the same sample

as in Fig. 6.3 after about 16 hours.

Ag in the region A had diffused into the crystal.
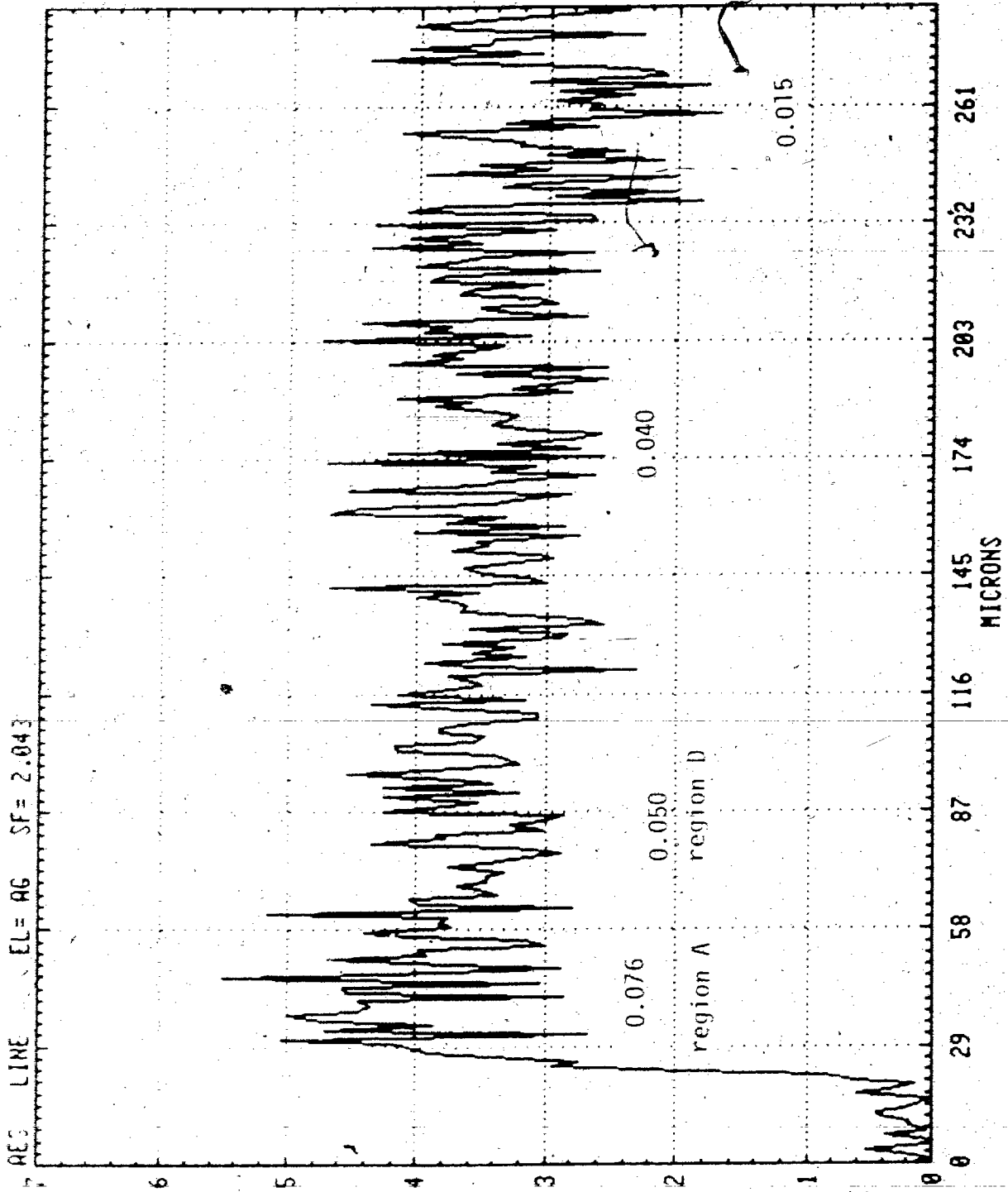
Fig. 6.4

Fig. 6.5   Auger line scan conducted on the same sample
as in Figs. 6.3 and 6.4 at d = 2450 A.
The regions A and D reappeared after sputtering.
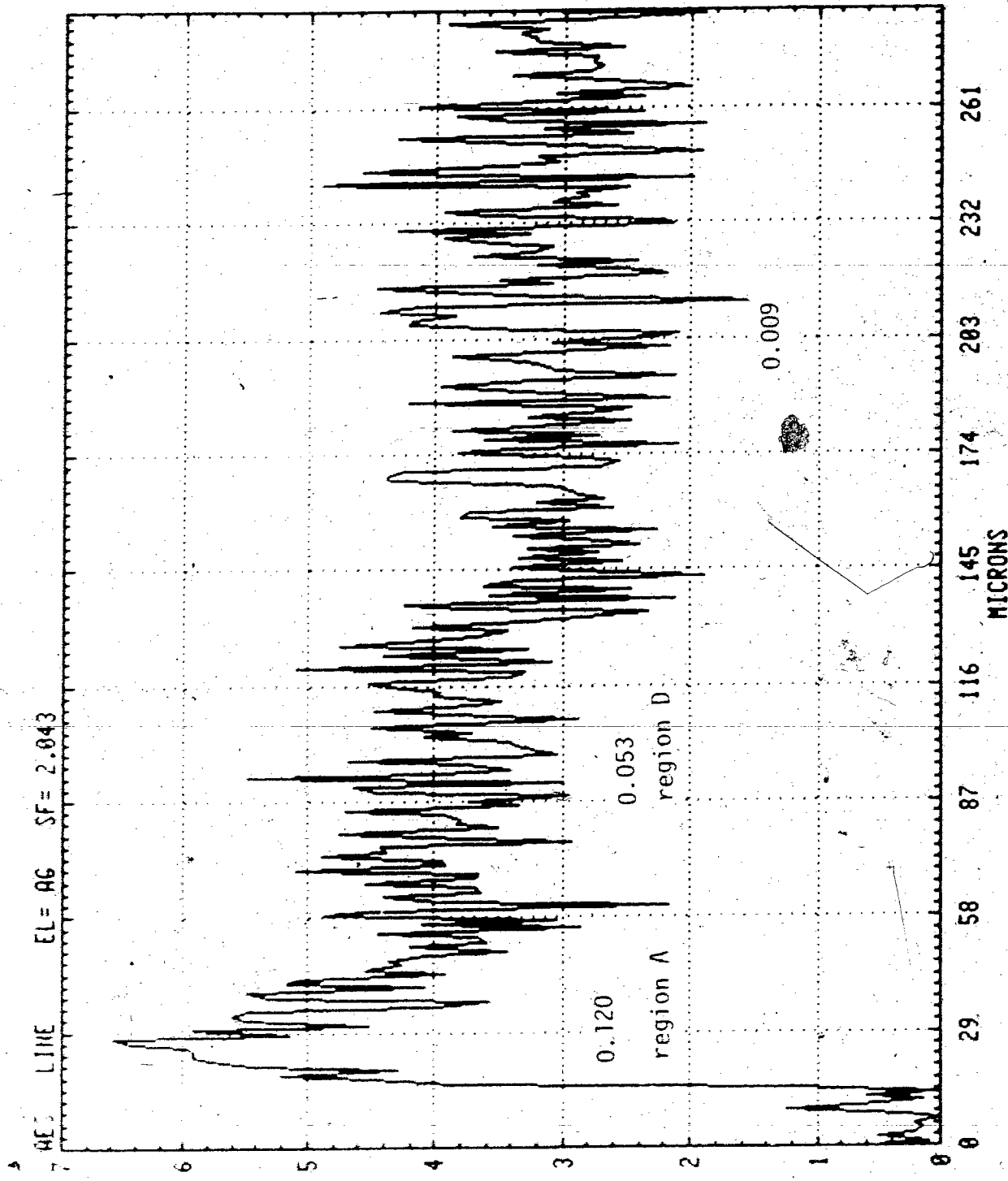
Fig. 6.5

Fig. 6.6   A figure showing regions with approximately the
same Ag concentration, constructed from Fig. 6.1.
The region A is stage 2.
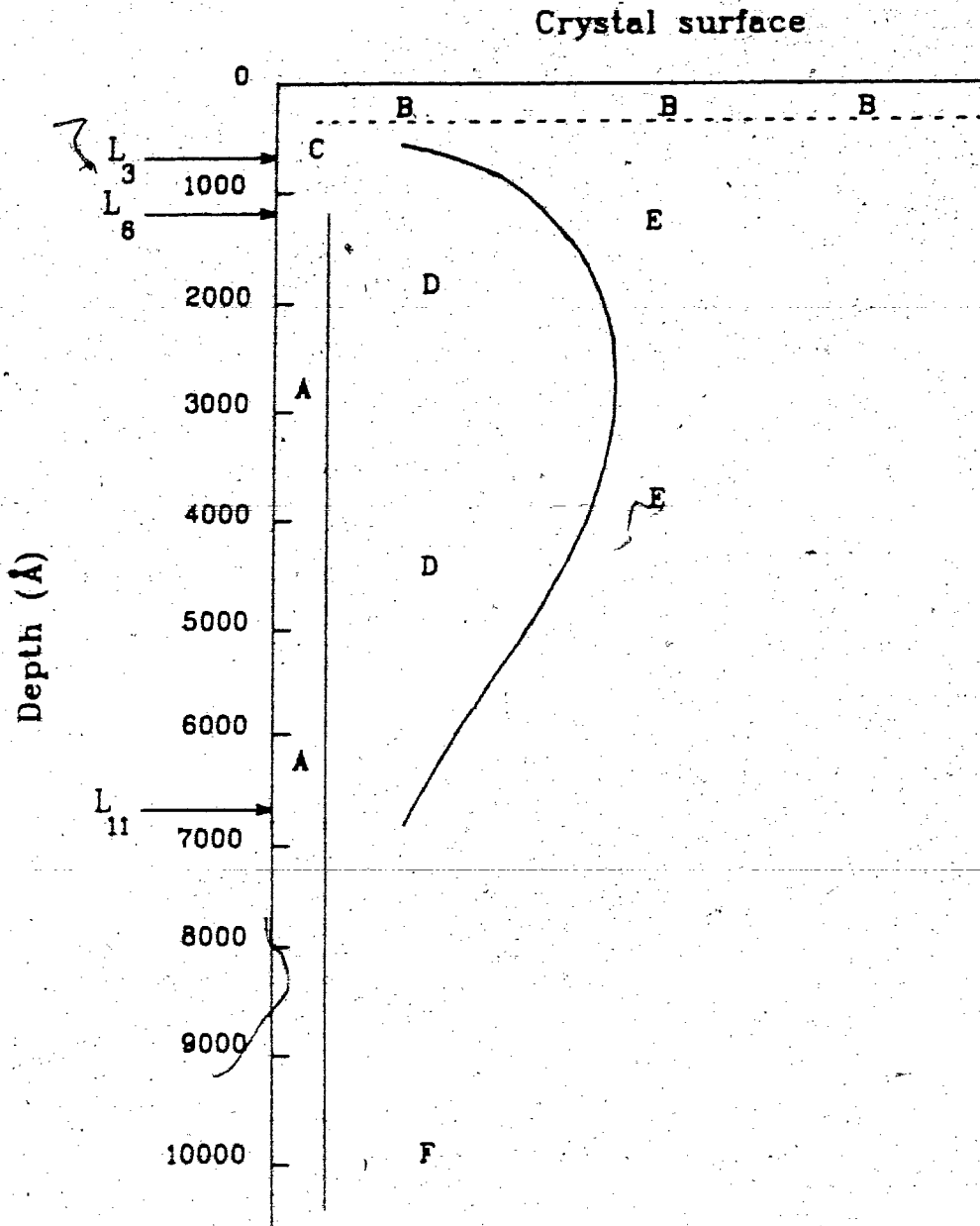
Fig. 6.6

Fig. 6.7   An Auger line scan performed at a low magnification

analyzing over a long distance.

The amount of Ag in the region beyond ~300 μm is

insignificant.
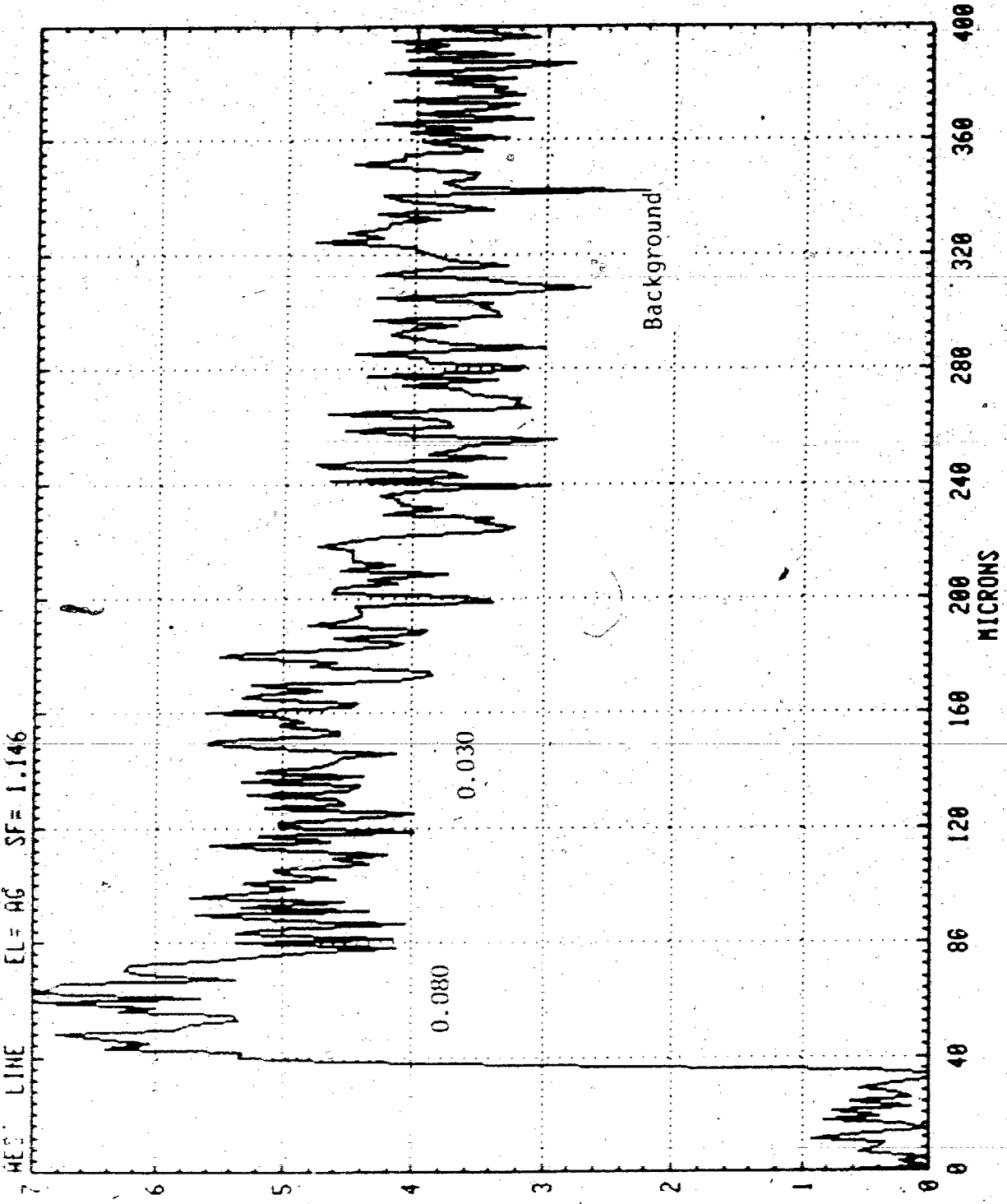
Fig. 6.7

Fig. 6.8   (a) Auger survey spectrum for a Ag/TiS$_2$ sample

(region A).

Ag and Ti peaks are shown.

(b) Auger survey spectrum for a pure TiS$_2$ sample.

Ti peaks are shown.

(Peak energy values given here are from standard

spectra. In Figs. 6.8a and b the peak energies

for Ag and Ti are shifted by 5 eV and 6 eV,

respectively.)

$$\frac{Ag(351) \text{ peak height}}{Ti(387) \text{ peak height}} = \frac{0.3}{3} = 0.1$$
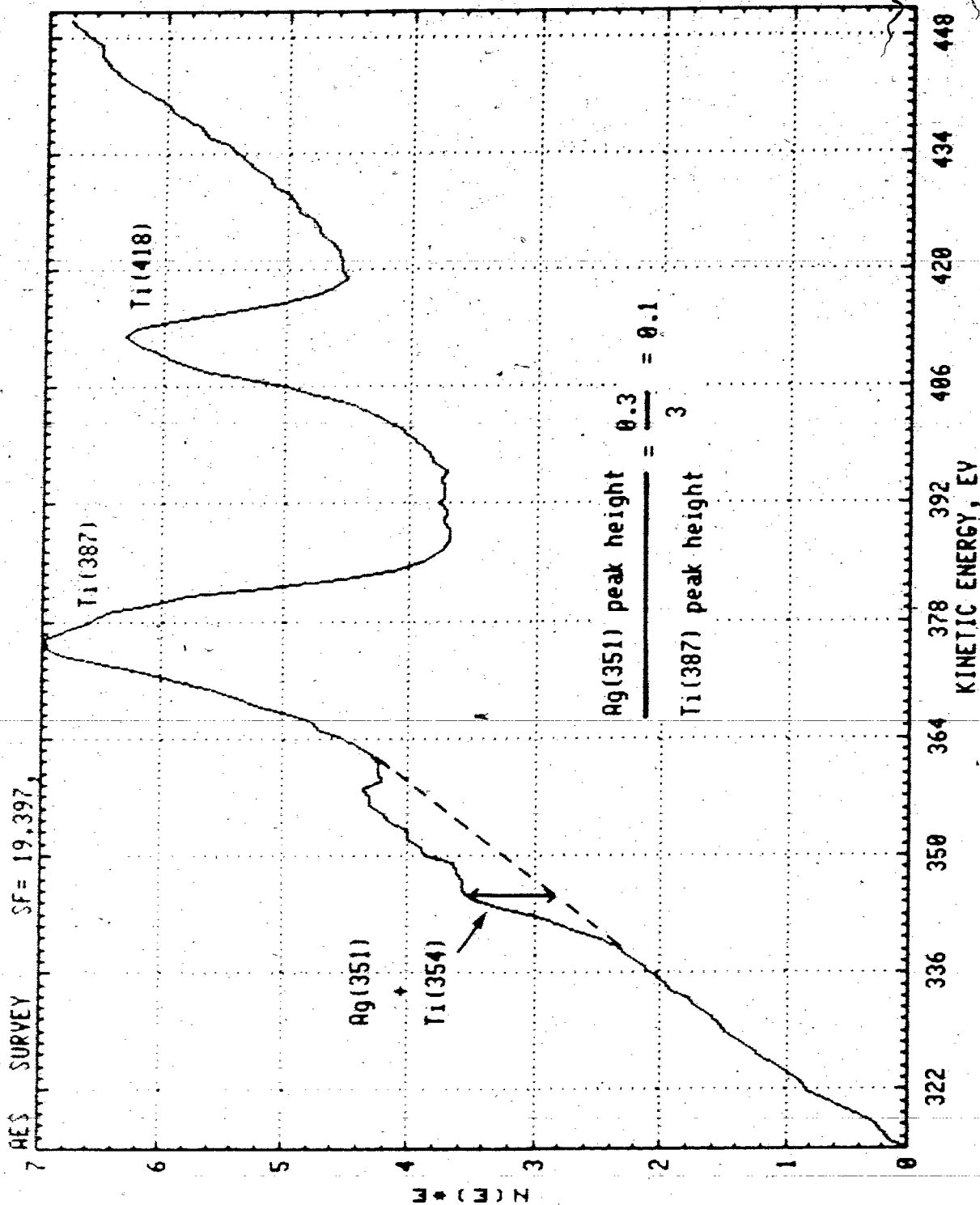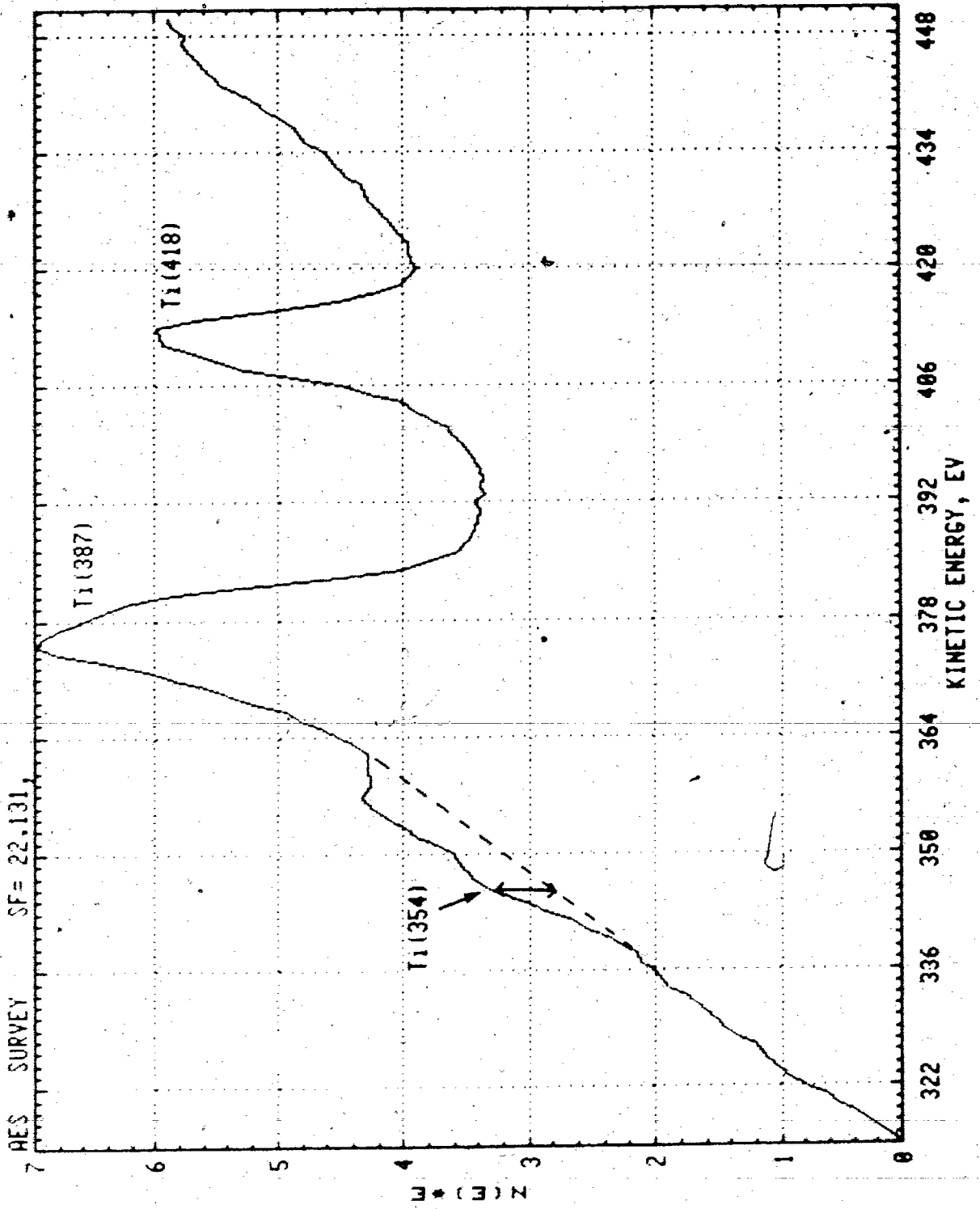
Fig. 6.8a

Fig. 6.8b

Fig. 6.9   A figure showing intercalated Ag content

in different regions in Ag/TiS$_2$ relative to the

region A.

152b
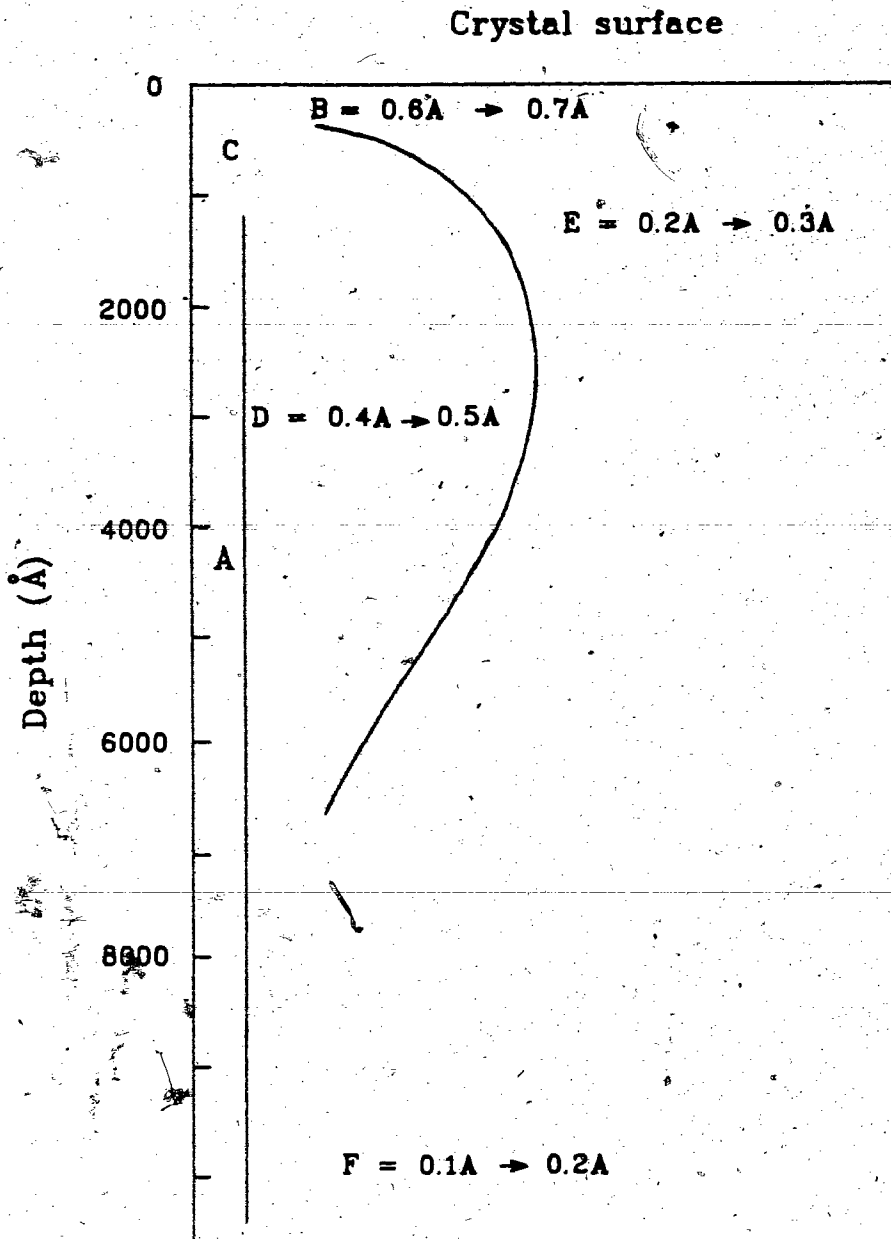
Fig. 6.9

Fig. 6.10   Three dimensional Monte-Carlo computer simulation

of intercalation of a pristine host to stage 2.

Each column represents a stack of van der Waals gaps

at a different time.   Time increases from left to

right.   The intercalate is shown as black areas

in van der Waals gaps 1 to 10 of the crystal.   The

gap 1 is next to a basal surface and the gap 10 is

near the crystal center.   The intercalate enters into

the crystal from a reservoir at the left of each gap.

(Courtesy of Dr.G. Kirczenow)
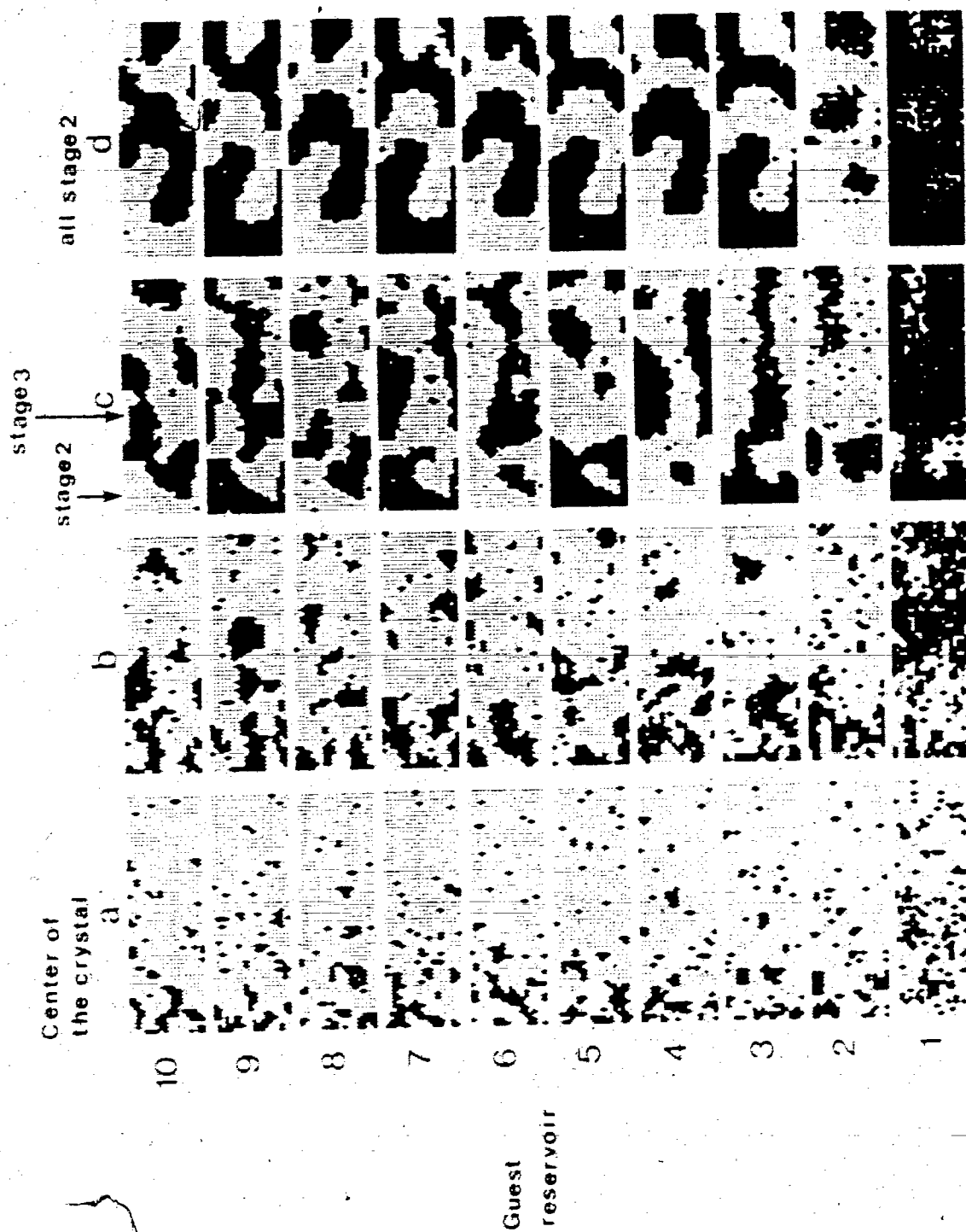
Fig. 6.10

Fig. 6.11 Schematic cross-sectional view of the shape of

the intercalation front which separates the empty

and the intercalated regions in a partially

intercalated Ag/TiS$_2$ crystal. The vertical

scale (c-direction) is greatly exaggerated.

Crystal surface

C

B

E

D

A

Empty crystal region

Intercalated
crystal
edge

Stage 2 front
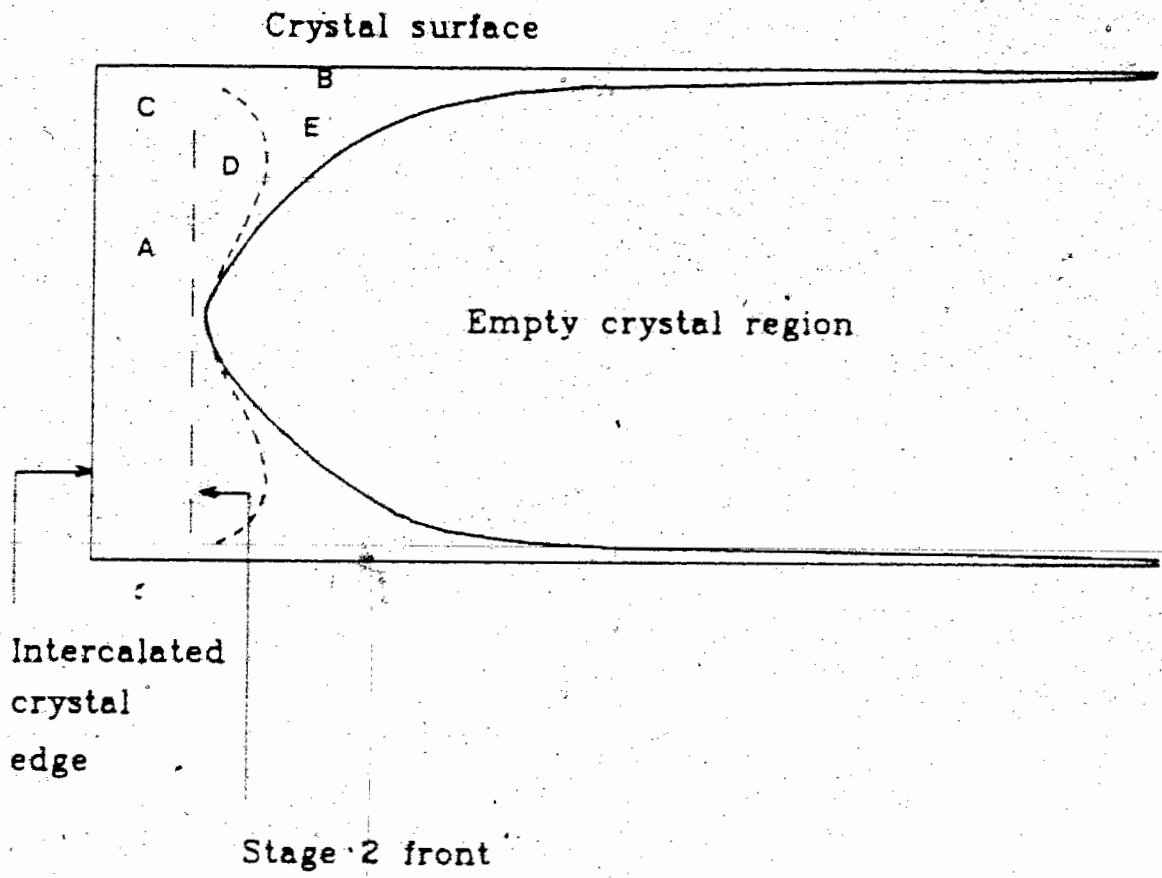
Fig. 6.11

CHAPTER 7

CONCLUSIONS

The motion of intercalated Ag in TiS_2 was studied using an optical microscope, a scanning electron microscope, radioactive tracers and a scanning Auger electron microscope. Both optical and XRF studies done on a partially intercalated Ag/TiS_2 crystal showed three regions, identified as stage 1, stage 2 and an empty crystal region. The XRF study showed that Ag in the stage 1 region converted into stage 2 Ag rapidly at room temperature. In addition, no motion of the stage 2 front was observed at room temperature after the stage 1 to stage 2 conversion was completed.

The radioactive tracer results indicated that Ag in the stage 2 region can move through the bulk of a TiS_2 crystal during the stage 1 to 2 conversion and also when a crystal is being intercalated. The electrostatic repulsion between the stage 1 Ag atoms in the "c" direction seems to be responsible for the stage 2 Ag motion in the bulk of the TiS_2 lattice.

The Auger results showed that Ag has a high rate of motion near the crystal surface. The analysis carried out on partially intercalated stage 2 TiS_2 crystals indicated that Ag had intercalated across the crystal surfaces while the bulk of the crystals intercalated only up to a short distance. A stage 2 region with a high Ag concentration was observed to be

unstable near the crystal surface. Mixed-stage phases were observed to precede a well-ordered stage 2 phase.

APPENDIX 1

Parameters specified for Auger line scans

In Auger line scans, the electron beam is stepped point by point along a selected line and the difference between the Auger peak height and the background level is measured.

Table Al.la presents the parameters specified for data acquisition in order to obtain Auger peaks for Ti, Ag and S. The lower limit and the range define the energy "window" for which data is to be acquired. The last four parameters yield the data acquisition time. Longer data acquisition time was used for Ag by selecting a higher number of sweeps since the Ag signal is weaker than those of Ti and S.

After obtaining the Auger peaks, the peak energies and the base energies for Ti, Ag and S were specified as shown in Table Al.lb. The base energies define the background level.

Once the peak amplitudes for the elements were selected, the number of points per line, dwell time per point and the total data acquisition time per line were defined to continue the line scan. The number of points in each line was selected as 250 and the dwell time for each point was chosen to be 20 ms. The data acquisition time per line was usually selected as 60 minutes.

Table A1.1   (a) The parameters specified for data acquisition

in obtaining Auger peaks in a line scan.

(b) The peak and the base energies specified for

Auger peaks in a line scan.

Table A1.1

(a)

ELEMENT NAME	T1	Ag	S
LOWER LIMIT (eV)	367	336	130
RANGE (eV)	20	25	20
VOLTS/STEP	0.50	0.50	0.50
TIME/STEP (ms)	100	100	100
SWEEPS	1	10	1

(b)

ELEMENT NAME	T1	Ag	S
PEAK ENERGY (eV)	378	346	144
BASE ENERGY (eV)	387	355	153
2ND BASE ENERGY (eV)	367	336	0.00
SWEEPS	1	10	1

APPENDIX 2

Parameters specified for depth profiling

Table A2.1a and b present the parameters selected in depth profiling. The energy "window" for each element is given by the lower limit and the range while the data acquisition time is specified by the last four parameters in Table A2.1a. The parameters specified for sputtering and the settings for the sputter ion gun are shown in Table A2.1b. Analysis was carried out with alternative sputtering; each cycle included an Auger analysis of the sample at specified points followed by sputtering. This cycle was carried out until the sample was completely sputtered through its thickness. The sputtering time per cycle is given by sputter time /number of cycles.

In this particular example given in Tables A2.1a and b, two points were selected for depth profiling, the elements Ti, S and O were selected for Auger analysis and the sample was sputtered for two minutes in every cycle. The values given for the last six parameters in Table A2.1b were used for analyzing all samples.

Table A2.1 Parameters specified for depth profiling.

Table A2.1

(a)

ELEMENT NAME	O	TI	S
LOWER LIMIT (eV)	495	367	130
RANGE (eV)	20	20	20
VOLTS/STEP	0.50	0.50	0.50
TIME/STEP (ms)	100	100	100
SWEEPS	1	1	1

(b)

SPUTTER TIME (MIN)	60
NUMBER OF CYCLES	30
NUMBER OF POINTS	3
ION VOLTAGE (kV)	3.0
CONDENSER SETTING	970
OBJECTIVE SETTING	750
X RASTER (mm)	2.0
Y RASTER (mm)	2.0
ARGON PRESSURE (millipascals)	10
EMISSION CURRENT (mA)	25

References

1. M.S. Dresselhaus and G. Dresselhaus, Adv. Phys., $\underline{30}$, 139 (1981).

2. Physics and Chemistry of Materials with Layered Structures, F.A. Lévy, vol.1 to 6, D. Reidel Publishing Company, Holland (1976).

3. J.A. Wilson and A.D. Yoffe, Adv. Phys., $\underline{18}$, 193 (1969); R.H. Friend and A.D. Yoffe, Adv. Phys., $\underline{36}$, 1 (1987).

4. R. Clarke and C. Uher, Adv. Phys., $\underline{33}$, 469 (1984).

5. M.S. Whittingham and R.R. Chianelli, J. Chem. Ed., $\underline{57}$, 569 (1980).

6. D. Kaluarachchi and R.F. Frindt, Phys. Rev. B, $\underline{31}$, 3648 (1985).

7. R.O. Carlson, J. Phys. Chem. Solids, $\underline{13}$, 65 (1960).

8. N. Daumas and M.A. Hérold, C.R. Acad. Sci., Ser.C, $\underline{268}$, 373 (1963).

9. R. Clarke, N. Wada and S.A. Solin, Phys. Rev. Lett., $\underline{44}$, 1616 (1980).

10 M.E. Misenheimer and H. Zabel, Phys. Rev. B, $\underline{27}$, 1443 (1983).

11. C.D. Fuerst, J.E. Fischer, J.D. Axe, J.B. Hastings and D.B. McWhan, Phys. Rev. Lett., $\underline{50}$, 357 (1983).

12. R. Nishitani, Y. Uno and H. Suematsu, Phys. Rev. B, $\underline{27}$, 6572 (1983).

13. J.M. Thomas and G.R. Millward, Mat. Res. Bull., $\underline{15}$, 671 (1980).

14. References 1-4 and 15-26 given in S.E. Ulloa and G. Kirczenow, Comments Cond. Mat. Phys., $\underline{12}$, 181 (1986).

15. R. Levi-Setti, G. Crow, Y.L. Wang, N.W. Parker, R. Mittleman and D.M. Hwang, Phys. Rev. Lett., $\underline{54}$, 2615 (1985).

16. M. Matsura, Y. Murakami and K. Takeda, Synth. Met., $\underline{12}$, 427 (1985).

17. H. Mazurek, M.S. Dresselhaus and G. Dresselhaus, Carbon, $\underline{20}$, 297 (1982).

18. S. Flandrois, J.M. Masson, J.C. Rouillon, J. Gaultier and C. Hauw, Synth. Met., 3, 1 (1981).

19. G. Timp and M.S. Dresselhaus, J. Phys. C, 17, 2641 (1984).

20. D.M. Hwang, X.W. Qian and S.A. Solin, Phys. Rev. Lett., 53, 1473 (1984).

21. A. Erbil, A.R. Kortan, R.J. Birgeneau and M.S. Dresselhaus, Phys. Rev. B, 28, 6329 (1983).

22. F. Baron, S. Flandrois, C. Hauw and J. Gaultier, Solid State Comm., 42, 759 (1982).

23. D. Kaluarachchi and R.F. Frindt, Phys. Rev. B, 28, 3663 (1983).

24. S.A. Safran, Phys. Rev. Lett., 44, 937 (1980).

25. S.A. Safran and D.R. Hamann, Phys. Rev. B, 22, 606 (1980).

26. J.R. Dahn, D.C. Dahn and R.R. Haering, Solid State Comm., 42, 179 (1982).

27. S.E. Millman and G. Kirczenow, Phys. Rev. B, 26, 2310 (1982)

28. S.E. Millman, G. Kirczenow and D. Solenberger, J. Phys. C, 15, L1269 (1982).

29. S.E. Millman and G. Kirczenow, Phys. Rev. B, 28, 3482 (1983).

30. G. Kirczenow, Phys. Rev. Lett., 49, 1853 (1982).

31. P. Hawrylak, K.R. Subbaswamy and G.W. Lehman, Solid State Commun., 51, 787 (1984).

32. S.A. Safran, Synth. Met., 2, 1 (1980).

33. G. Kirczenow, Phys. Rev. Lett., 52, 437 (1984).

34. G. Kirczenow, Phys. Rev. B, 31, 5376 (1985).

35. P. Hawrylak and K.R. Subbaswamy, Phys. Rev. Lett., 53, 2098 (1984).

36. G. Kirczenow, Synth. Met., 12, 143 (1985).

37. G. Kirczenow, Phys. Rev. Lett., 55, 2810 (1985).

38. G. Kirczenow, to be published in Can. J. Phys. (1987).

39. M.S. Whittingham, J.A. Panella, Mat. Res. Bull., 16, 37 (1981).

40. H.P.B. Rimmington and A.A. Balchin, J. Crystal Growth, 21, 171 (1974).

41. G.A. Scholz, P. Joensen, J.M. Reyes and R.F. Frindt, Physica, 105B, 214 (1981).

42. G.A. Scholz and R.F. Frindt, Mat. Res. Bull., 15, 1703 (1980).

43. A.G. Gerards, H. Roede, R.J. Haange, B.A. Boukamp and G.A. Wiegers, Synth. Met., 10, 51 (1984/85).

44. J.T. Folinsbee, M.H. Jericho, R.H. March and D.A. Tindall, Can. J. Phys., 59 (1981).

45. M. Patriarca, M.A. Voso, B. Scrosati, F. Bonino and M. Lazzari, Solid State Ionics, 6, 15 (1982).

46. G.A. Wiegers, H.J.M. Bouwmeester and A.G. Gerards, Solid State Ionics, 16, 155 (1985).

47. Practical Surface Analysis, D. Briggs and M.P. Seah, John Wiley and Sons (1983).

48. Methods of Surface Analysis, A.W. Czanderna, Elsevier Publishing Company, N.Y., (1975), Chapters 1, 2, 5 and 7.

49. SAM - 595 Instruction Manual, Perkin-Elmer Corporation (1981).

50. Handbook of Auger Electron Spectroscopy, L.E. Davis, N.C. MacDonald, P.W. Palmberg, G.E. Riach, R.E. Weber, Perkin-Elmer Corporation, Minnesota, 2nd Ed. (1978).

51. Topics of Applied Physics, V.47, Sputtering by Particle Bombardment, I.R. Behrisch, Springer (1981).

52. J.W. Coburn, Thin Solid Films, 64, 371 (1979).

53. A. Benninghoven, Thin Solid Films, 39, 3 (1976), page 9.

54. Practical Scanning Electron Microscopy, I. Goldstein and H. Yakowitz, Plenum Press, N.Y. (1975).

55. Instruction Manual for ISI-Model-DS-130 Scanning Electron Microscope.

56. G.A. Scholz and R.F. Frindt, J. Electrochem. Soc., 131, 1763, (1984).

57. M.S. Whittingham, Prog. Solid State Chem., $\underline{12}$, 41 (1978).

58. Physics and Chemistry of Materials with Layered Structures, F.A. Lévy, vol.4, D. Reidel Publishing Company, Holland (1976).

59. P. Joensen (personal communications).

60. K.K. Bardhan and D.D.L. Chung, Carbon, $\underline{18}$, 303 (1980).